

STRUCTURAL FRAMEWORK ANALYSIS IN THE
MISSISSIPPI CANYON PROTRACTION AREA,
CENTRAL GULF OF MEXICO: IMPLICATIONS FOR
CO₂ SEQUESTRATION

By

SEYI SHOLANKE

Bachelor of Science in Geology

Texas A&M University

College Station, Texas

2017

Submitted to the Faculty of the
Graduate College of the
Oklahoma State University
in partial fulfillment of
the requirements for
the Degree of
MASTER OF SCIENCE
July, 2020

STRUCTURAL FRAMEWORK ANALYSIS IN THE
MISSISSIPPI CANYON PROTRACTION AREA,
CENTRAL GULF OF MEXICO: IMPLICATIONS FOR
CO₂ SEQUESTRATION

Thesis Approved:

Dr. Jack Pashin

Thesis Adviser

Dr. Jim Puckette

Dr. Mohamed Abdelsalam

ACKNOWLEDGEMENTS

I am grateful to my advisory committee chair, Dr. Jack Pashin, for his guidance, patience and support throughout the course of this work. I would also like to thank the members of my advisory committee, Dr. Jim Puckette and Dr. Mohamed Abdelsalam for their invaluable advice and incredible support.

A special thank you to my mentors, friends, staff, faculty and colleagues at Oklahoma State University for their support and encouragement throughout my graduate experience.

I would like to thank the U.S. Department of Energy National Energy Laboratory for providing funding for this project through the Southern State Energy Board under cooperative agreement DE-FE0031557.

Lastly, I'm very thankful to my family for their love and support throughout my education.

Name: SEYI SHOLANKE

Date of Degree: JULY, 2020

Title of Study: STRUCTURAL FRAMEWORK ANALYSIS IN THE MISSISSIPPI
CANYON PROTRACTION AREA, CENTRAL GULF OF MEXICO:
IMPLICATIONS FOR CO₂ SEQUESTRATION

Major Field: GEOLOGY

Abstract: Geologic factors such as faults and salt tectonics have implications for the reliability of CO₂-Enhanced Oil Recovery (CO₂-EOR) and CO₂ sequestration targets in deep water reservoirs of the Gulf of Mexico. Salt-tectonic faults within withdrawal basins that serve as primary targets for CO₂ -EOR, can be either conduits or barriers for fluid flow. To understand the impacts of salt-related faults and other salt tectonic structures on potential CO₂ storage in deep water reservoirs, this study focuses on 1) identifying fields with CO₂-EOR potential and associated storage, and 2) characterizing salt systems, faults, folds, minibasins and associated hydrocarbon traps and CO₂ sinks. The analysis focuses on salt tectonics to develop an understanding of its potential impact on the stratal geometry of candidate reservoirs for carbon sequestration. The structural and stratigraphic framework within the study area was analyzed by integrating wireline logs, biostratigraphic information, and 3-D seismic data.

The structural framework in the Mississippi Canyon area comprises an array of growth faults and decollements that separate distinct depositional objectives. Salt canopies, diapirs, rollers, allochthonous sheets, pillows, withdrawal synclines, anticlines, and roho structures have been interpreted and mapped. Basinward dipping listric growth faults have also been identified. Listric normal faults cut siliciclastic seal and reservoir strata. Faults above salt canopies are extensional, and remnant salt rollers are present in roho complexes. Sets of growth faults superimposed on salt sheets were identified. The Mississippi Canyon protraction area contains laterally continuous sandstone reservoirs that are overlain by thick and regionally correlated sections of shale, and sandstone that form effective seals. Minibasins are potential storage objectives that result from salt withdrawal. Other objectives are salt seals in the footwalls of some faults and strata that are truncated below allochthonous salt wings.

TABLE OF CONTENTS

Chapter	Page
I. INTRODUCTION	1
Statement of purpose.....	1
Hypothesis.....	2
Objectives	3
Significance.....	5
 II. GEOLOGICAL BACKGROUND	6
Gulf of Mexico geological setting	6
Regional setting	7
I. Structural setting	9
II. Regional salt tectonics	12
III. Sedimentation and stratigraphy.....	12
IV. Depositional history and paleogeography.....	13
V. Geological constraints that can impact CO ₂ -Enhanced Oil Recovery (EOR) and carbon sequestration	16
a. Slope gradient	16
b. Fault	17
c. Salt	17
d. Gas	17
e. Shallow water flow	18
 III. METHODOLOGY	19
Description of available data	19
Structural framework analysis	22
Seismic recognition of salt in the Mississippi Canyon protraction area.....	24
Seismic attributes.....	27
I. Variance	27
II. Root-mean-squared (RMS) Amplitude.....	27
III. Structural smoothening	27

Chapter	Page
IV. RESULTS	28
Bathymetry maps	28
Structural framework features observed within the study area.....	30
I. Growth fault families	30
II. Allochthonous salt	30
III. Salt welds.....	30
IV. Withdrawal synclines and minibasins.....	31
Salt tectonics	31
I. Distribution of salt within study area A	31
a. Salt body A1 morphology	31
b. Salt body A2 morphology	31
c. Salt body A3 morphology	32
II. Distribution of salt within study area B	39
a. Salt body B1 morphology	41
d. Salt body B2 morphology	41
e. Salt body B3 morphology	41
f. Salt body B4 morphology	41
Observed structural styles of salt minibasins.....	44
Major fault distribution	44
I. Major fault distribution within study area A	45
II. Major fault distribution within study area B	46
Identification of fields for potential tertiary hydrocarbon recovery/carbon sequestration projects.....	47
I. Identification of fields within study area A	47
II. Identification of fields within study area B.....	48
Seismic profiles across identified fields	50
I. Fields within study area A	50
a. Field A1: MC 763-805-851	50
b. Field A2: MC 764-808	51
c. Field A3: MC 809-810	52
d. Field A4: MC 809-810-853-854.....	53
II. Fields within study area B.....	54
a. Field B1: MC 725-726	54
b. Field B2: MC 771a.....	55
c. Field B3: MC 771b.....	56

Chapter	Page
d. Field B4: MC 728-772	57
e. Field B5: MC 773	58
f. Field B6: MC 687-730-731	59
Well log (Gamma ray and Resistivity log) interpretation.....	60
I. Well logs within study area A.....	60
II. Well logs within study area B	64
Field analysis summary information: Study area A.....	70
Field analysis summary information: Study area B.....	71
CO ₂ storage assessment	72
I. Storage objective: Alpha.....	73
II. Storage objective: Beta	74
V. CONCLUSION.....	89
REFERENCES	92

LIST OF TABLES

Table	Page
1. List of fields evaluated and associated well logs used within study area A	49
2. List of fields evaluated and associated well logs used within study area B	49
3. Field analysis summary: Study area A.....	70
4. Field analysis summary: Study area B.....	71
5. Potential storage areas: Storage objective Alpha.....	80
6. CO ₂ Storage resource: Storage objective Alpha	81
7. Potential storage areas: Storage objective Beta	86
8. CO ₂ Storage resource: Storage objective Beta.....	87

LIST OF FIGURES

Figure	Page
1. Estimated reserves of deep water fields in the Mississippi Canyon (MC) protraction area	2
2. Northern Gulf of Mexico deep water bathymetry map.....	4
3. Regional shaded bathymetric map of the Gulf of Mexico, with protraction boundaries.....	8
4. Tectonostratigraphic provinces within the study area	10
5. Distribution of shallow salt in the Gulf of Mexico	11
6. Generic deposystem/paleogeography of a typical Cenozoic Gulf of Mexico depositional episode.....	15
7. Study area map.....	20
8. Location of wells used for reservoir characterization within the study area	21
9. Salt features in a seismic profile	26
10. Seafloor bathymetry map of focus area A	28
11. Seafloor bathymetry map of focus area B.....	29
12. Distribution of salt bodies and associated minibasins within Study area A: Seismic variance attribute time slice at Z= -4332.00 ms	33
13. Variance attribute time slice (Study area A) at Z= -4332.0 ms with structural boundaries of salt bodies more visible.....	34
14. Time structure map: Top of salt bodies within study area A.....	35
15. Seismic profile (seismic amplitude) through crossline 787 illustrating salt body A1, crestal faults and channel complexes	36
16. Seismic profile (RMS amplitude) through crossline 787 illustrating salt body A1 and proximal gas accumulations	37
17. Seismic profile (seismic amplitude) through inline 4708 illustrating salt body A1, salt body A2 and salt body A3	38
18. Distribution of shallow salt within study area B.....	40
19. Seismic profile through crossline 1136 illustrating salt bodies B1, B2 and B3	42
20. Seismic profile through crossline 1680 illustrating salt body B4	43
21. Structural styles of minibasins observed in the Mississippi Canyon protraction area.....	44
22. 3-D visualization of major faults in study area A	45
23. 3-D visualization of major faults in study area B	46
24. Map of study area A illustrating oil fields (red bubbles) that have been evaluated	47

Figure	Page
25. Map of study area B illustrating oil fields (red bubbles) that have been evaluated	48
26. Location of well logs used in this study.....	49
27. Seismic profile cross-section across field A1: MC 763-805-851	50
28. Seismic profile across field A2: MC 764-808	51
29. Seismic profile across field A3: MC 809-810	52
30. Seismic profile across field A4: MC 809-810-853-854.....	53
31. Seismic profile across field B1: MC 725-726.....	54
32. Seismic profile across field B2: MC 771a	55
33. Seismic profile across field B3: MC 771b.....	56
34. Seismic profile across field B4: MC 728-772.....	57
35. Seismic profile across field B5: MC 773	58
36. Seismic profile across field B6: MC 687-730-731	59
37. Interpreted geophysical well log from well MC 807-1.....	60
38. Interpreted geophysical well log from well MC 764-1.....	61
39. Interpreted geophysical well log from well MC 765-1.....	62
40. Interpreted geophysical well log from well MC 809-1.....	63
41. Interpreted geophysical well log from well MC 682-1.....	64
42. Interpreted geophysical well log from well MC 771-1 (below 24,000 ft).....	65
43. Interpreted geophysical well log from well MC 771-1 (above 15,200 ft)	66
44. Interpreted geophysical well log from well MC 772-1.....	67
45. Interpreted geophysical well log from well MC 773-1.....	68
46. Interpreted geophysical well log from well MC 731-1.....	69
47. Effect of burial depth on CO ₂ density.....	72
48. CO ₂ density as a function of temperature and pressure	73
49. Location of assessed storage objectives within study area A	75
50. Depth structure map of reservoir horizon (channel sands in well MC 773-1) within storage objective Alpha	76
51. Depth structure map of reservoir horizon (channel sands in well MC 773-1) within storage objective Alpha, with adjacent overhanging salt body.	77
52. RMS attribute map of reservoir horizon (channel sands in well MC 773-1) within storage objective Alpha	79
53. Depth structure map of reservoir horizon (amalgamated sands in well MC 731-1) within storage objective Beta..	82
54. Depth structure map of reservoir horizon (amalgamated sands in well MC 731-1) within storage objective Beta	83
55. RMS attribute map of reservoir horizon (amalgamated sands in well MC 731-1) within storage objective Beta	85

CHAPTER I

INTRODUCTION

Statement of purpose

Subsurface geologic storage of CO₂ can be instrumental in offsetting greenhouse gas emissions safely and over the long term (Gentzis, 2000; Bachu, 2001; McKee, 2003; Baines and Worden, 2004). As part of a U.S Department of Energy project, a seismic-based assessment of the structural and associated stratigraphic elements within sections of the Mississippi Canyon protraction area was performed to identify suitable areas for carbon sequestration associated with enhanced oil recovery. The study area (Fig. 1) is ideal because the existing pipeline infrastructure and pathways can be followed for CO₂-enhance oil recovery (CO₂-EOR) projects. Also, established pipelines can be repurposed to transport CO₂ to prospective geologic locations. Additionally, the ownership of offshore blocks is clearly delineated and uniform, that is, access rights are more easily defined in comparison to with that of onshore blocks. To ensure containment of injected CO₂ within a defined storage complex, it is paramount to understand the effects of structural salt emplacement and structural geometry on potential storage. For example, faults can be either conduits or barriers for fluid flow (Weber et al., 1978; Bouvier et al., 1989; Gibson, 1994). The containment of fluids, such as CO₂, is governed by trap geometry and the integrity of fault seals in combination with topseals, and the presence of salt (Alexander and Handschy, 1998; Davies et al., 2003; Davatzes et al., 2005).

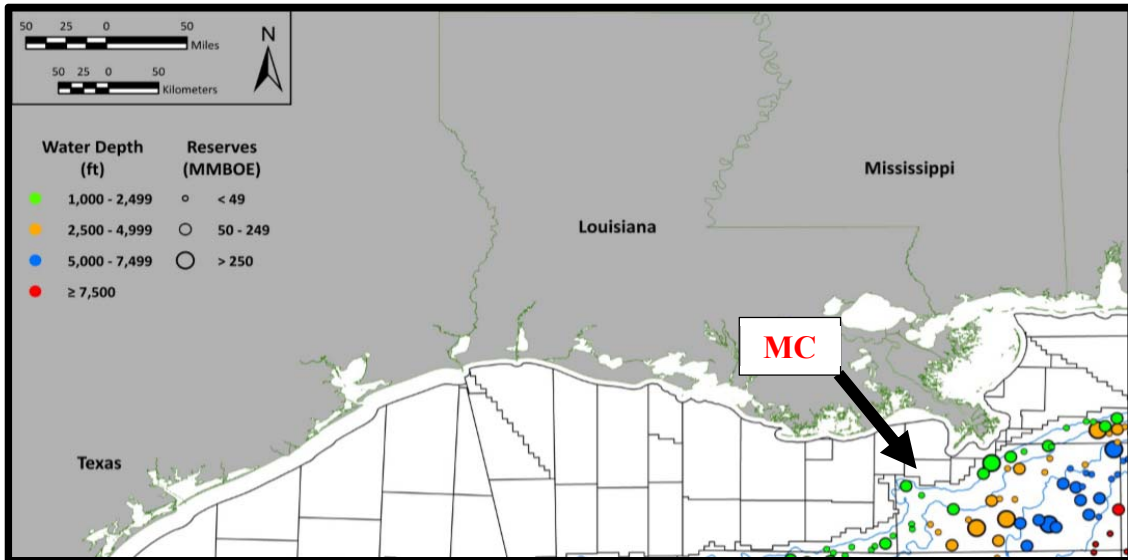


Figure 1. Estimated reserves of deep water fields in the Mississippi Canyon (MC) protraction area (after BOEM OCS Report, 2014).

To understand the sealing capacity of potential storage targets within the Mississippi Canyon protraction area, 3D seismic reflection data and well log data have been used to analyze geological structures. In order to understand the impacts of subsurface geological features on CO₂ migration, this study focuses on salt-related structural geometry and the effects of salt tectonics on minibasins within the central Gulf of Mexico. Results show that the Mississippi Canyon area is characterized by a mixture of channel-levee complexes and widespread sheet sands (lobe deposits) that make up reservoirs that are overlain by thick and regionally correlated sections of tight mudrock that form effective seals. In addition, salt seals are common in this area, and oil reservoirs include major subsalt accumulations in the Pliocene-Pleistocene section.

Hypothesis

A central hypothesis of this research is that ineffective seals below salt, along faults, above salt, and adjacent to salt bodies, may pose risk for fluid migration, and so careful structural analysis is required to delineate potential objectives adjacent to salt bodies and associated structures.

Additionally, it is hypothesized that multiple sandstone formations within the Mississippi Canyon protraction area have viable CO₂-enhanced oil recovery (EOR) potential and storage resource and are effectively sealed.

Objectives

The focus area is situated about 125 to 155 miles southeast of New Orleans, Louisiana, within the Mississippi Canyon protraction area, on the Louisiana continental slope. The study area constitutes a 60-block area covering approximately 540 mi². The water depths within the study area range from approximately 3,600 ft to 6,530 ft below mean sea level. The bathymetry of the seafloor (Fig. 2) is characterized by irregularities that include seafloor valleys and surface manifestations of buried salt structures.

The main objective of this research is to assess the major structural elements within minibasins that can serve as prospective storage sinks associated with CO₂-enhanced oil recovery, by 1) identifying and interpreting the general structural framework of the study area, 2) defining trapping mechanisms and seal potential by mapping reservoir and seal distributions, and 3) identifying and mapping shallow salt bodies within the study area. The goal of this research is to identify opportunities for CO₂-enhanced oil recovery associated with long-term storage of CO₂ in the oil reservoirs.

The pertinent questions for this study are as follows:

- 1) How does salt tectonics affect the structural geometry of potential storage sinks?
- 2) How does the structural framework within the study area affect the security of long-term CO₂ storage?

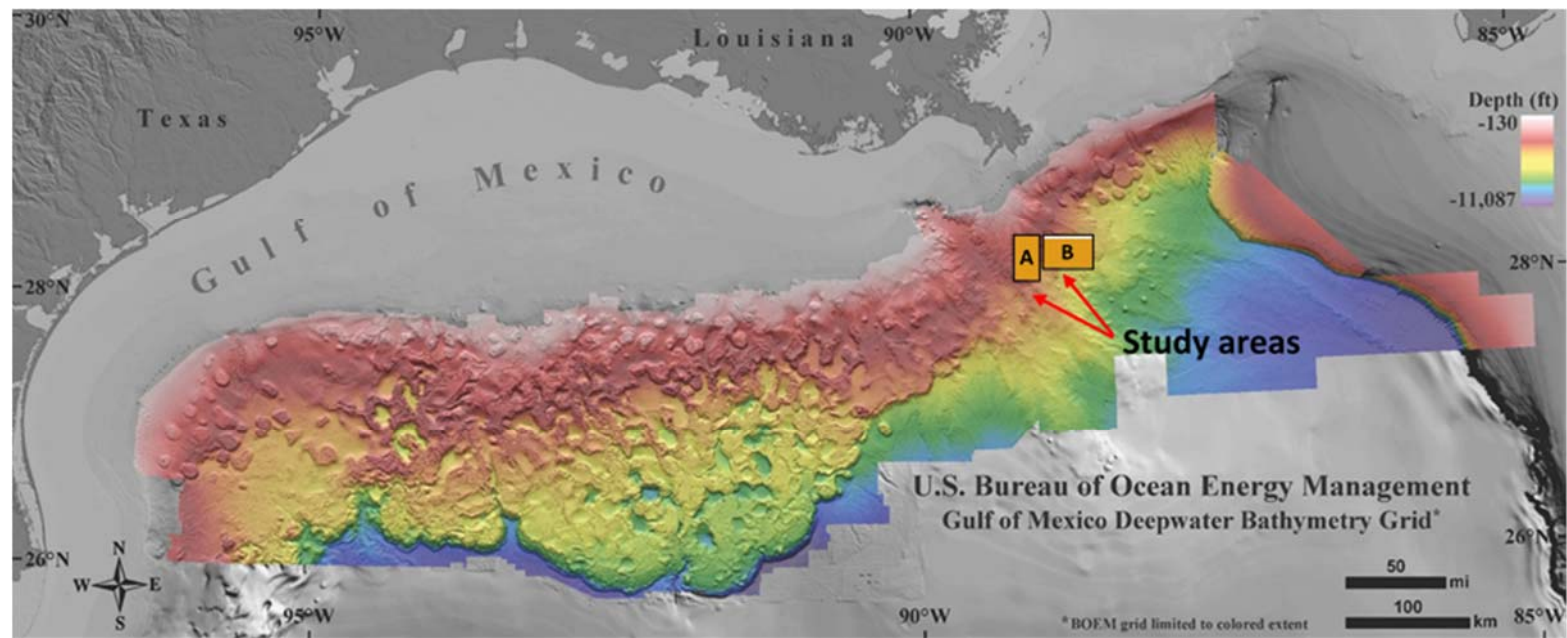


Figure 2. Northern Gulf of Mexico deep water bathymetry map (source: U.S. Bureau of Ocean Energy Management). The orange rectangles outline the seismic survey used in this study.

Significance

This study evaluates the CO₂ storage potential within minibasins in the Mississippi Canyon protraction area, and is part of a larger investigation sponsored by National Energy Technology Laboratory (NETL) of the U.S. Department of Energy (DOE) that aims to predict CO₂ storage resource and identify opportunities for development in the Gulf of Mexico. Additionally, offshore carbon sequestration projects are significant because they occur in areas with clear and uniform mineral ownership and avoid issues relating to the protection of underground sources of drinking water. The Gulf of Mexico contains many viable deep water oil fields (Fig. 1) with potential for CO₂-EOR, and the Mississippi Canyon protraction area is estimated to have about 1,143 million barrels of remaining oil in place (BOEM OCS Report, 2014). With declining production within the Mississippi Canyon protraction area, production practices such as waterflooding and CO₂-EOR will need to be implemented to increase recovery and to prolong the life of the reservoirs (Vidas et al., 2012).

CHAPTER II

GEOLOGICAL BACKGROUND

Gulf of Mexico geological setting

The breakup of the supercontinent Pangea in the Mesozoic initiated the formation of the Gulf of Mexico (Buffler and Sawyer, 1985; Salvador, 1987). In the late Triassic, the Gulf of Mexico Basin formed by the rifting and drifting of the North American, South American, and African Plates (Pindell, 1985; MacRae, 1993). The Gulf of Mexico Basin formed due to the extension and isostatic adjustment of the crust as the Yucatan block rotated counterclockwise relative to North America (Pindell, 1985; Sandwell et al., 2014). The development of the extensive transitional crust of the Gulf of Mexico basin developed during the Triassic/Jurassic rifting (Buffler, 1989) during the breakup of Pangea. Subsequent episodic flooding in the Middle Jurassic (Salvador, 1991) and arid climate resulted in the formation of thick evaporite deposits, which include the Louann Salt (Salvador, 1991). This salt was deposited atop transitional crust, and the subsequent formation of oceanic crust led to the separation of the Louann salt into northern and southern sections (Salvador, 1991). Thermal subsidence and the formation of oceanic crust resulted in the modern Gulf of Mexico basin, in which over 10,000 ft of Jurassic and Cretaceous sediment was deposited (Lopez, 1989). From the Eocene onward, rapid sediment accumulation in the western and central Gulf of Mexico led to the mobilization of the Louann Salt. The mobilization of the salt as a result of sediment loading resulted in the development of regional growth faults on the Texas-

Louisiana shelf-slope system (Worall and Snelson, 1989). Since the Late Paleocene and Early Eocene, allochthonous salt bodies have migrated seaward (Worral and Snelson, 1989). Thus, the primary structural framework of the Gulf of Mexico basin resulted from the interaction of the following parameters: rapid sedimentation and the deformation, mobilization, and remobilization of the Jurassic-age Louann Salt.

Regional setting

The study area is positioned in the Mississippi Canyon protraction area (Fig. 3) on the continental slope offshore of Louisiana. The central Gulf of Mexico Basin is structurally complex because of the extensive salt tectonics (Buffler, 1991). Indeed, the Mississippi Canyon protraction area hosts a more comprehensive range of salt structural styles than any other part of the Outer Continental Shelf (OCS) (Buffler, 1991). The province is characterized by a hill and basin morphology (Fig. 3) that developed as a result of turbidite sedimentation and the mobilization of underlying salt (Martin and Bouma, 1978). The seafloor gradient ranges between 1° and 2°, although it can exceed 20° in sections with salt bodies, faults, and withdrawal basins (Coleman et al., 1986). The geology of the study area constitutes a thick Mesozoic-Cenozoic sedimentary fill (>15,000 m; 50,000 ft) containing varied allochthonous salt systems, extensional and contractional faults, and outer fan fold belts (Rowan et al., 1999). Structural features that contribute to the complex structural setting in the study area include basement faults, allochthonous salt systems, anticlines, growth fault families, surface failures, decollements, and salt welds that separate a broad range of structural and depositional objectives. Welds form where nearly complete evacuation of salt has occurred. (Rowan et al., 1999).

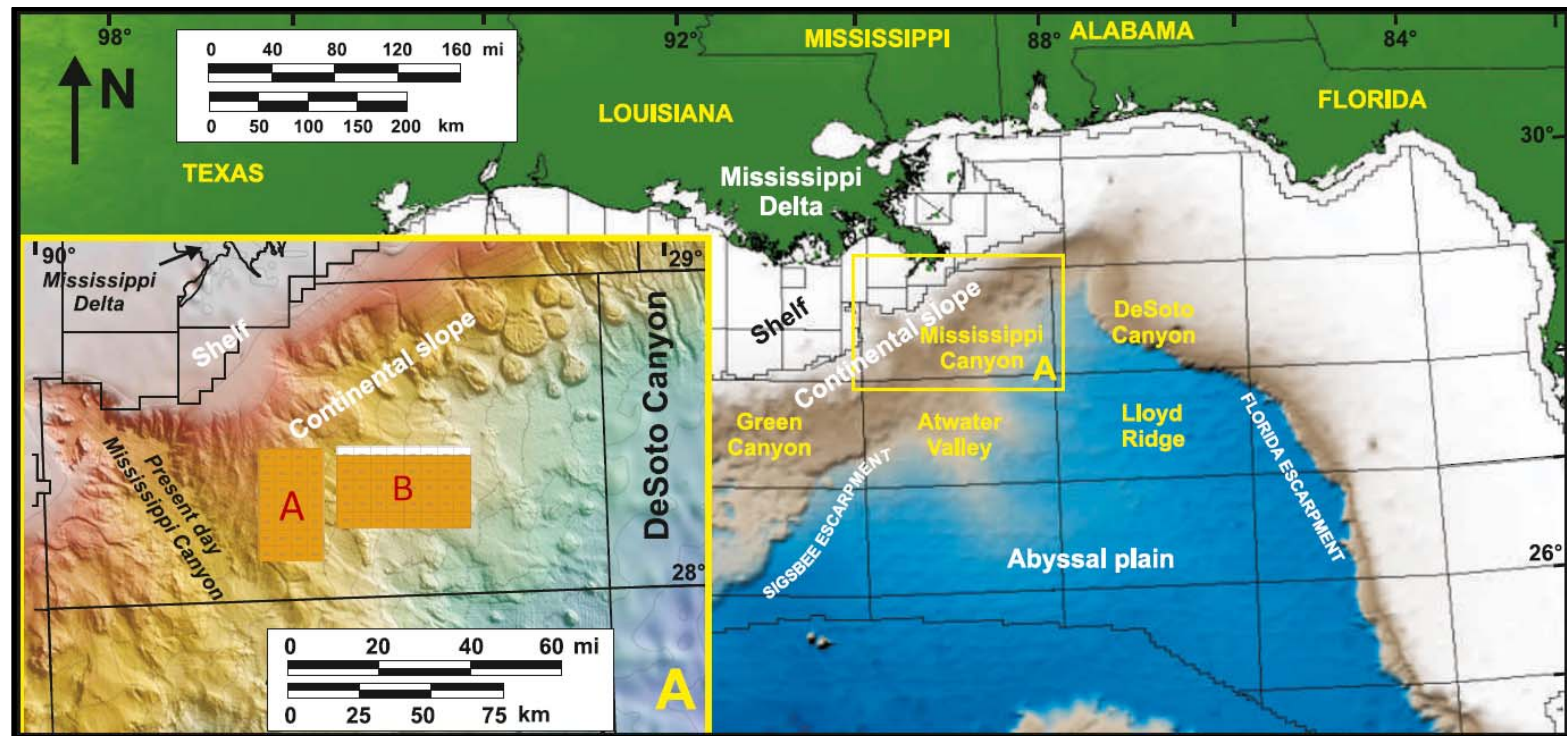


Figure 3. Regional shaded bathymetric map of the Gulf of Mexico, with protraction boundaries (Weimer and Bouroullc, 2012). The orange rectangles outline the seismic survey used in this study.

I. Structural setting

The study area is positioned in a transition zone characterized by the following tectonostratigraphic regions in the northern Gulf of Mexico (Diegel et al., 1995): a salt dome/minibasin region, a Plio-Pleistocene detachment region, and a tabular salt/minibasin region (Fig. 4). Jurassic age salt accumulations are present beneath the upper continental slope. However, the emplacement of late Mesozoic and Cenozoic sediments superimposing the Jurassic age salt led to the seaward mobilization of the salt, which caused deformation and intrusion of salt to higher stratigraphic levels. The salt mobilization produced depressions where the salt withdrew, and diapirs through which salt migrated upward through shallower sediment. As a result, the middle and lower continental slope is made up of intraslope basins, submarine valleys, and submarine canyons (Martin, 1978). Additionally, bodies of allochthonous salt intercalated with younger sediment (Fig. 5) are common (Nelson and Fairchild, 1989). Allochthonous salt bodies are expressed as sheet- and tongue-like bodies that overlie stratigraphically younger strata (Seni, 1994; Wu et al., 1990a, b). The thickness of these salt bodies ranges from approximately 2,000 to 11,000 ft. The increase in horizontal salt body thickness, which increases overburden load, leads to the compaction of underlying sediment, and in places there has been later-stage deformation and intrusion of the strata above the top of the horizontal salt body, including uplift (Nelson and Fairchild, 1989). Bathymetric highs resulting from salt-tectonic uplifts in this area signify that the feeder stocks of salt are sourced from deep in the subsurface and are potentially still actively supplying salt to younger structures (Wu et al., 1990b). The multi-stage horizontal and vertical emplacement of salt bodies is a primary structural parameter that controls the dispersal of sediment in the Mississippi Canyon protraction area (Worall and Snelson, 1989). Vertical salt migration/uplifts (diapirs or sill-like sheets) obstruct the downslope transport of sediment, while structural depressions associated with withdrawal basins serve as sediment conduits. Accordingly,

thick accumulations of sediment are preserved within salt withdrawal basins, and stratal geometry records the growth of these basins.

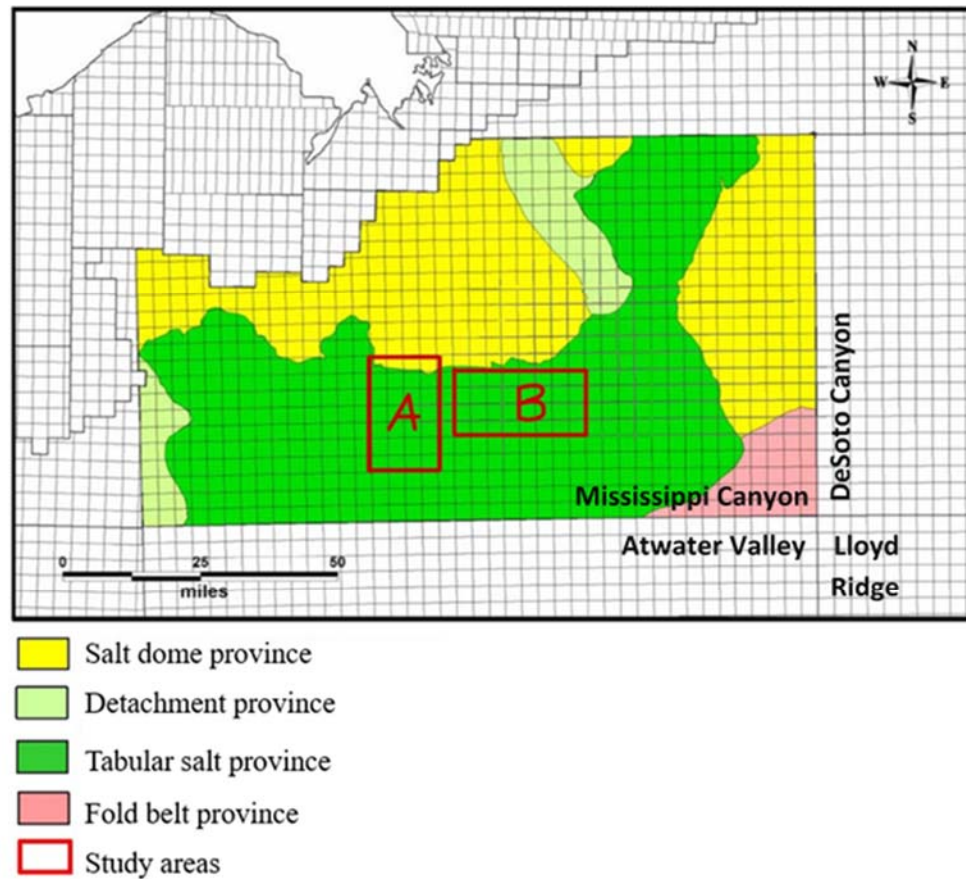


Figure 4. Tectonostratigraphic provinces within the study area (provinces from Diegel, 1995). The red rectangles outline the seismic survey used in this study.

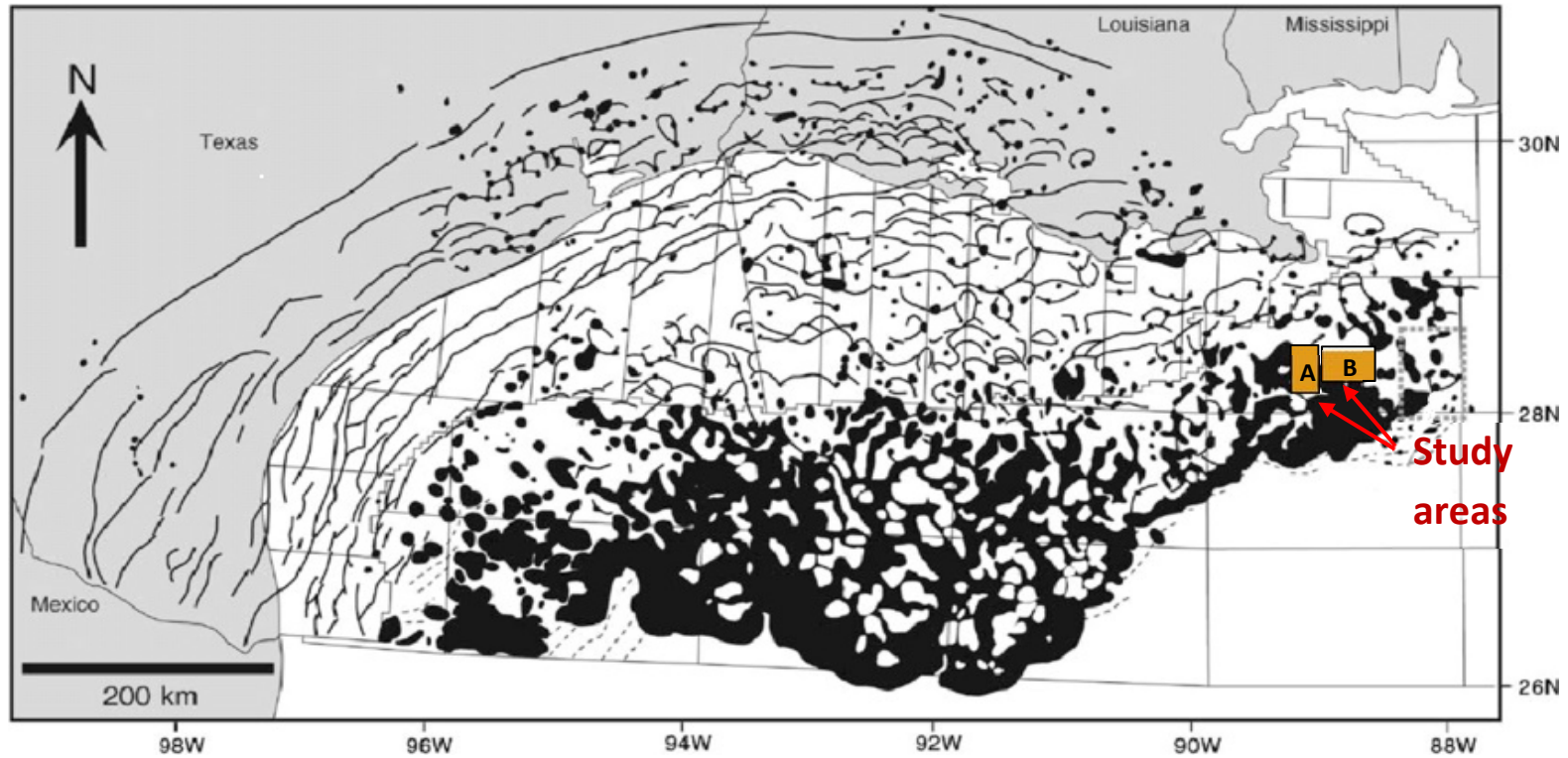


Figure 5. Distribution of shallow salt (Black areas) in the Gulf of Mexico (After, Diegel, 1995). The orange rectangles outline the seismic survey used in this study.

II. Regional salt tectonics

Extensional spreading caused by gravitational processes, including sediment loading, is the main primary mechanism for the emplacement of extensive allochthonous salt bodies in shallower strata (Fig. 5) on the continental slope in the Mississippi Canyon protraction area (Wu et al., 1990b). Following the initial emplacement of shallow salt, loading by younger sediment leads to the formation of salt domes, pillows and sills (Hudec et al., 1995). Additionally, regional, and less commonly, counterregional faults form in the sediment cover as the allochthonous salt is remobilized (Nelson and Fairchild, 1989).

The remobilization of allochthonous salt sheets on the Louisiana continental slope and subsequent burial occurred due to intrusion of salt close to sediment-water interface (Fletcher et al., 1995). Turbidite systems accumulated in concert with the basinward withdrawal and migration of allochthonous salt offshore of Louisiana (Talbot, 1994; Schuster, 1995). Roho systems atop subhorizontal allochthonous salt bodies are characterized by major listric growth faults (McGuinness and Hossack, 1993; Schuster, 1995).

III. Sedimentation and stratigraphy

The Mississippi Canyon protraction area is basinward of the Mississippi bird-foot delta and is also located to the north of the Eastern Mississippi Fan (Dixon and Weimer, 1998). However, the Mississippi Canyon protraction area is along the course/direction of sediment discharge from the modern Mississippi River (Coleman et al., 1983). Fine grained sediments are evident in the upper slope section and are characterized by a progradational stratal geometry (Dixon and Weimer (1998).

The turbidite systems in the study area comprise sheet sands, channel-levee complexes, overbank deposits, mass transport complexes (MTC), and condensed sections (Dixon and Weimer (1998). The first three depositional features are related to turbidity currents, whereas mass transport

complexes include debris flows and slides related to mass movement associated with slope failure (Dixon and Weimer (1998). These features make up most of the lowstand systems tract (LST), that are separated by high-amplitude, laterally continuous stratigraphic markers/reflectors that are indicative of condensed sections that are deposited during sea level rises and highstands (Roberts and Coleman, 1988). The lowstand systems tracts are characterized by mass-movement or turbidite deposits (Dixon and Weimer (1998). However, a small fraction of most sequences is related to transgressive and highstand sedimentation (Dixon and Weimer (1998). These depositional systems are represented by condensed sections (Dixon and Weimer (1998). The highstand systems tracts and condensed sections are composed of clay rich, hemipelagic deposits. These condensed sections form extensive regional seals that overlap sand-prone turbidite sections that include the major petroleum objectives (Dixon and Weimer (1998).

IV. Depositional history and paleogeography

The stratigraphy of the north-central Gulf of Mexico is characterized by a series of depositional episodes (Galloway, 1989). The recorded depositional episodes have been defined using a genetic stratigraphic sequence model (Galloway, 1989), which consists of sandy and shaly facies of fluvial, deltaic, coastal, shelf, slope, and basin depositional systems. The recorded systems are make up the physical topography/geography of the northern-central Gulf of Mexico (Galloway et al., 2000). Eighteen distinct northern Gulf of Mexico Cenozoic depositional episodes have been recognized (Galloway et al., 2000) and grouped into the following four main evolutionary phases:

- 1.) Paleocene-Middle Eocene Laramide compression-related episodes.
- 2.) Late Eocene-Oligocene episodes that began with crustal uplift and volcanism.
- 3.) Miocene episodes that record the eastern North American uplands
- 4.) Pliocene-Quaternary episodes that record the western interior drainage basins.

Large deltaic systems with sandy slope aprons at the North American continental margin (Fig. 6) include sandy turbidite systems (channel, lobe, and sheet facies), that pass basinward onto the adjacent continental rise and abyssal plain (Galloway et al., 2000). However, shelf-fed slope aprons (Fig. 6) are commonly rich in mud that provides thick seals for the major deep-water reservoirs (Winker and Buffler, 1988). These reservoirs are located in transition zones between contemporaneous deltaic and beach-shelf systems, and are characterized by a broad range of structural and erosional features (Galloway et al., 2000). Laterally extensive features, such as slide deposits, represent catastrophic failures that occurred as a result of salt-tectonic tilting, sediment loading, and salt withdrawal (Dixon and Weimer, 1998). The depositional systems consist of a complex mix of channels, growth faults, and thick sections of mixed delta front, turbidite and debris flow facies (Galloway et al., 2000). Additionally, sandy to muddy sediment wedges that contain deep-water faunas, are associated with thick primary salt or salt canopies that contribute to salt-related subsidence and tilting (Dixon and Weimer, 1998). Throughout the Cenozoic, thick reservoir-quality sand bodies were deposited on the continental slope and the adjacent rise (Dixon and Weimer, 1994; Galloway et al., 2000).

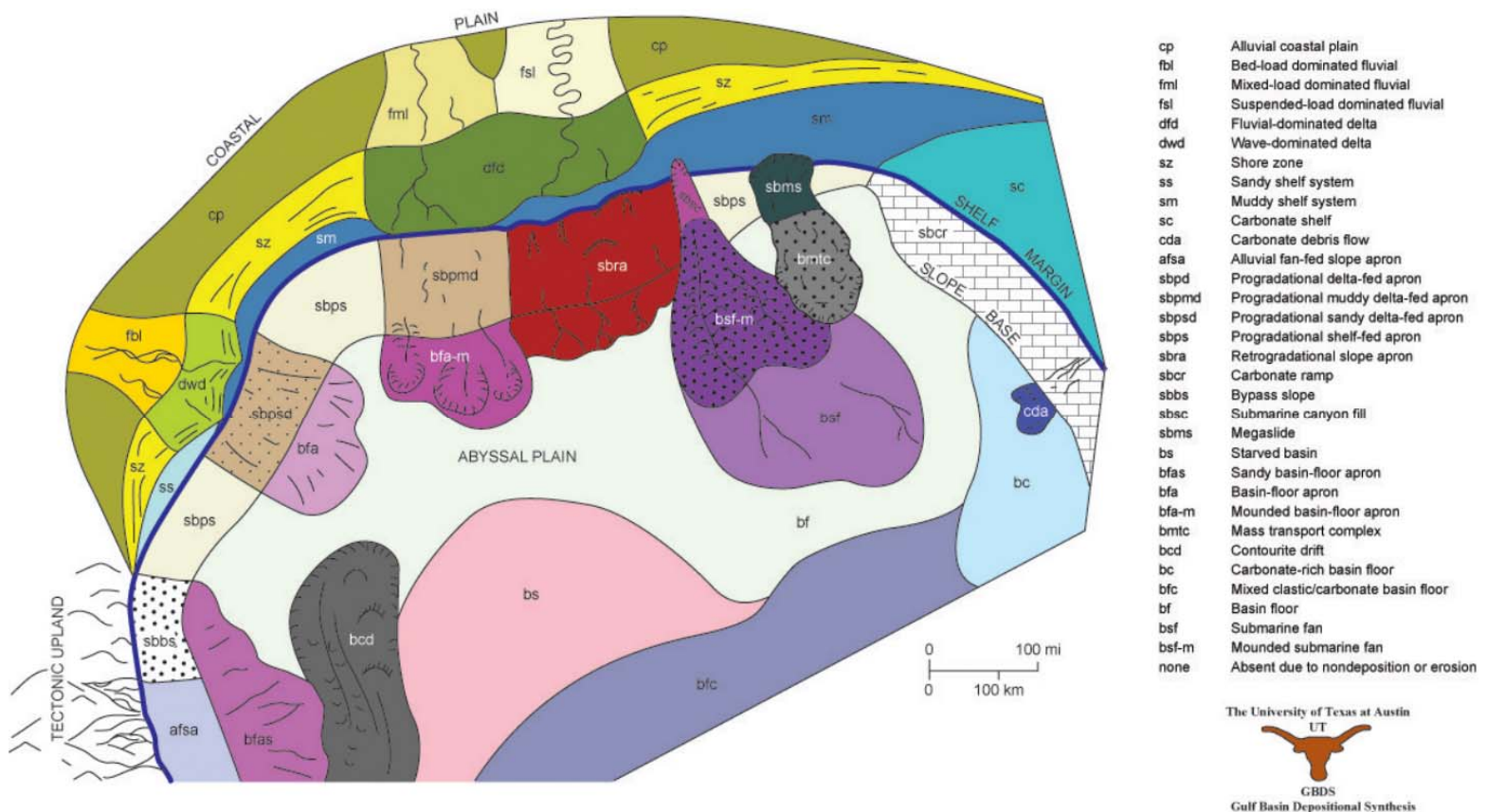


Figure 6. Generic depositional systems and paleogeography of a typical Cenozoic Gulf of Mexico depositional episode (Galloway et. al., 2009).

The sediment on the continental slope is Cretaceous to Recent in age (Lehner, 1969). At first, turbidity flows and hemipelagic deposits accumulated in topographic depressions, and were then reworked by mass-transport events (Beard et al., 1982; Stuart and Caughey, 1977; Woodbury et al., 1978; Behrens 1985; Bouma 1981). Stratigraphic dewatering facies in the Gulf of Mexico can primarily be divided into three lowstand depositional systems: basin floor fans, slope fans, and progradational complexes (Sangree et al., 1988). Depositional sequences associated with the Mississippi fan were deposited between the Miocene to Recent (Weimer, 1989).

V. Geological constraints that can impact CO₂-EOR and carbon sequestration

The subsurface geology within the deep-water Gulf of Mexico poses geologic constraints that can affect the potential for enhanced oil recovery and associated carbon sequestration. Such constraints can also be limiting factors pertaining to the recovery and production of deep-water petroleum plays. Identified potential constraints that can impact CO₂-EOR and carbon sequestration within the focus area include but are not limited to the following: a) slope gradient, b) faults, c) salt, d) gas, and e) shallow water flow. The identification of the impact of the geologic framework and geologic processes is paramount to the identification of potential storage objectives.

a. Slope gradient

Steep slopes along and around faults, salt withdrawal basins, and salt structures can be too steep to drill a well for CO₂-enhanced oil recovery (Baines and Worden, 2004). Slope stability is considered a geologic constraint because of its possibly adverse effect on seafloor structures and infrastructure (Baines and Worden, 2004). Slope failures usually have different size and frequency, and their occurrence is dependent on the associated geologic, geotechnical and geomechanical factors (Baines and Worden, 2004). Approximate slope stability parameters can be inferred from the relative amplitude of the seafloor from the seismic data (Bouvier et al., 1989).

b. Faults

Faults along the rims of diapiric uplifts, and along the margins of salt withdrawal basins are typically extensional (Swiercz, 1992). These faults serve to alleviate stress caused by the relatively rapid emplacement of salt into shallower strata (Swiercz, 1992). Additionally, with the mobilization of salt, faults grow contemporaneously, and the rate of growth tends to decrease through time (Rowan et al., 1999). Faults can act as conduits for the upward migration of fluids such as hydrocarbons and CO₂. Faults are readily observed, identified and interpreted in seismic surveys by offset reflectors (Rowan et al., 1999). Fluid charging, migration along the fault plane, and potentially leaking windows along the fault planes, are recognized in seismic profiles as high amplitudes along or close to faults (Rowan et al., 1999).

c. Salt

The structural deformation caused by salt mobilization, in addition to the salt-related pressure compartments, can have a major impact on carbon sequestration projects. In the Mississippi Canyon protraction area, the migration of salt in multiple directions exerts a primary structural control on how sediment is distributed in the basin (Martin, 1978; McGuiness and Hossack, 1993). Diapirs that result from the upward vertical migration of salt, restrict the downslope transport of sediment (Martin, 1978; McGuiness and Hossack, 1993) and as a result can help build potential CO₂ storage objectives. However, structural depressions around the diapirs can act as conduits for the transport of sediment downslope (Peel et al., 1995). The withdrawal basins developed as a result of salt expulsion, and can act as sediment traps (Peel et al., 1995).

d. Gas

Faults can act as conduits for gas to migrate updip (Mildren et al., 2002). Within seismic profiles and time slices, gas compartments can be identified as bright spots, which are indicated by a high amplitude signal on seismic reflectors (Kim et al., 2020). Also, these bright spots typically

have an associated wavelet phase inversion to indicate the presence of gas (Kim et al., 2020). Furthermore, the deeper the gas zones, the higher the possibility that the pressure is greater than normal hydrostatic pressure. Subsequently, increased formation pressure, in some cases, can cause the formation of gas in solution. Gas in solution may not be easily recognized in seismic; however, it can be problematic if the pressure is not relieved (Kim et al., 2020). Also, if there is no reliable seal, gas can escape from a reservoir.

e. *Shallow water flow*

Shallow water flow sands are also called shallow overpressured sands or flowing water sands. These are recognized by water leaking through wellbore casing, which poses difficulty for well development in the deepwater Gulf of Mexico (Alberty et al., 1997). These overpressured sands are typically between low permeability shale units. Also, overburden above the sands or seals can increase associated pore pressure within the sands, and can cause pore fluids, including gas, to escape (Alberty et al., 1997). Within the digital seismic data, shallow water flow sands are recognized as high amplitude bright spots within reflectors. However, in some cases, these overpressured sands may not have high amplitude signatures (Byrd et al., 1996). Well log data can help to improve the recognition of overpressured sand sections, by identifying sand-rich facies in the Mississippi Canyon area within channel-levee deposits (Burman and Norton, 1998). Additionally, overpressured sands can also be present in salt withdrawal basins. The Mississippi Canyon protraction area has cases of shallow water flows. The most pertinent water flow events are in the Mensa basin, specifically within blocks 686, 687, 730, and 731 (Burman and Norton, 1998).

CHAPTER III

METHODOLOGY

Description of available data

This study used public 3D seismic reflection data, geophysical well logs, checkshot surveys and additional data available from the Bureau of Ocean Energy Management (BOEM). The seismic data from the focus areas within the Mississippi Canyon protraction area (Fig. 7) are of good quality and provide clear imaging from the surface to the Jurassic salt or pre-salt rocks. The offshore wells in the region (Fi. 8) have been logged, and the logs are available in raster form. The well logs are diverse and include SP-resistivity logs, gamma ray logs, neutron-density porosity logs, and sonic logs. Study area A covers approximately 252 mi², and study area B covers approximately 288 mi². Thus, approximately 540 mi² is the total area studied within the Mississippi Canyon protraction area. The seismic survey (Fig. 7) within study area A is characterized by an equal inline and crossline spacing of 87.5 ft., with a sampling interval of 4 ms. However, the seismic survey (Fig. 7) within study area B is characterized by inline and crossline spacing of 175.09 and 175.05 ft, respectively. Both seismic surveys were acquired under permit L88-163 by the United States Department of the Interior: BOEM Public Data Release, and were held proprietary for 25 years as required under 30 CFR 551.14. The projection for the seismic data is UTM 16 USFT, with a Clark-1866 ellipsoid, under the North American Datum 27.

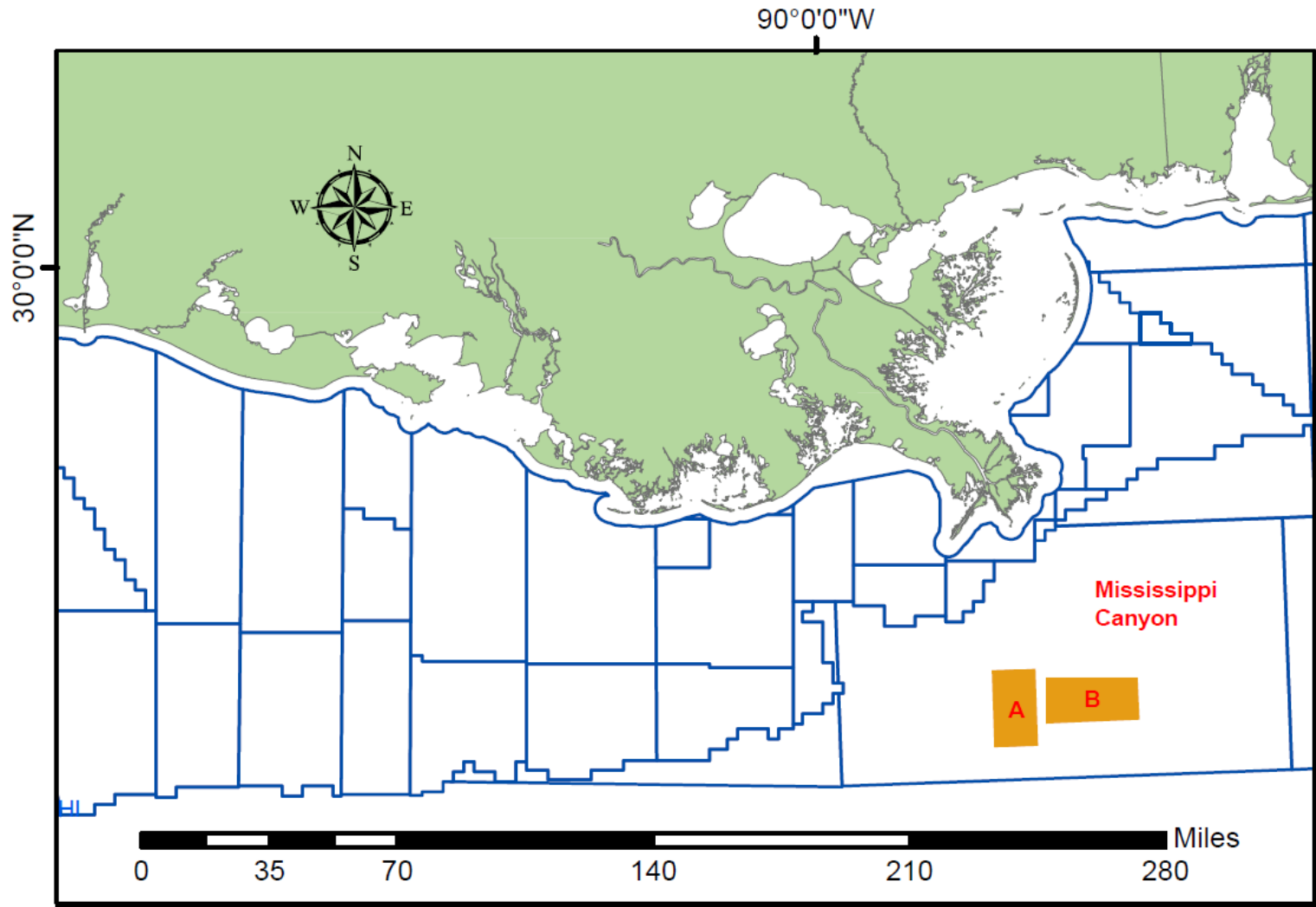


Figure 7. Study area map (after protractions map from the Bureau of Ocean Energy Management database).

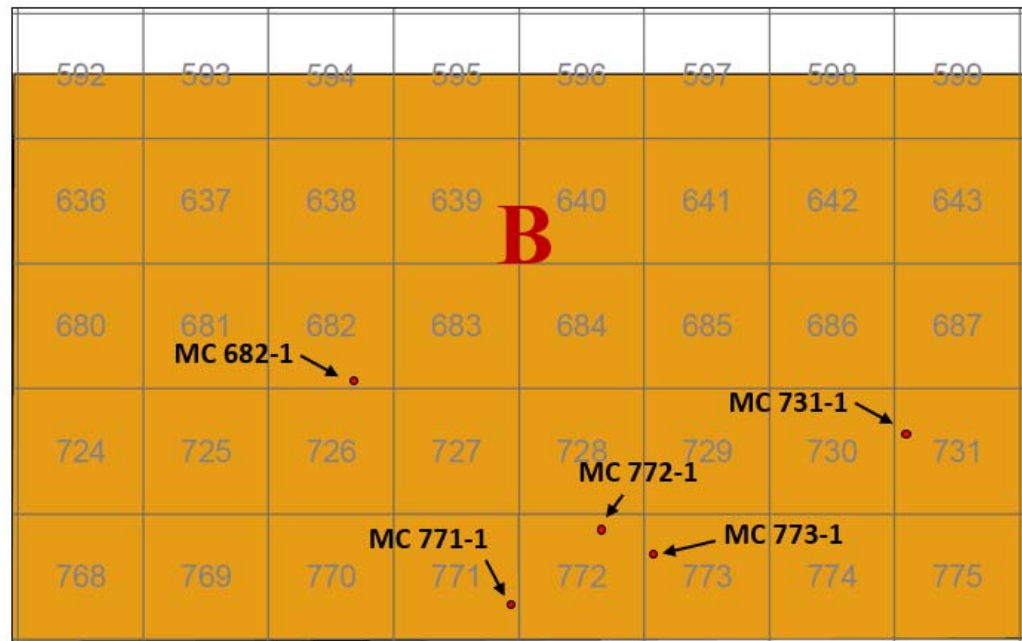
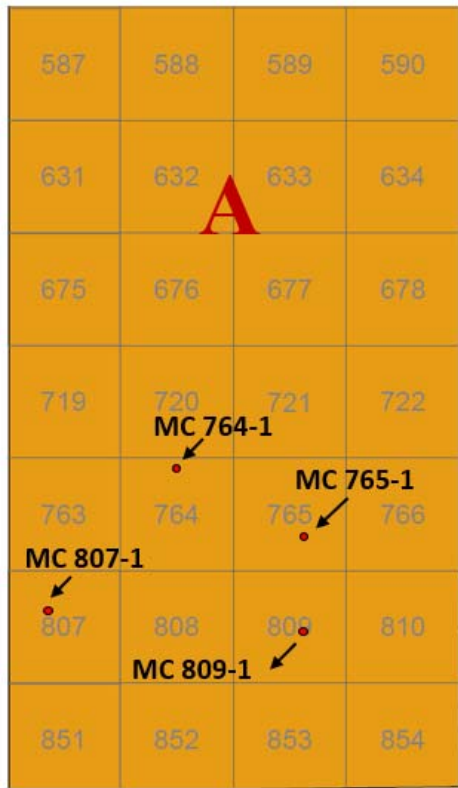


Figure 8. Location of wells used for reservoir characterization within the study area based on protraction maps from the Bureau of Ocean Energy Management database.

Additional supporting data, such as biostratigraphic reports (Waterman, 2000), which aid in the identification and correlation of stratigraphic units, are available for many wells. Also, checkshot surveys are available for many wells, and these surveys help constrain time-depth relationships in seismic reflection surveys. Furthermore, an extensive range of bathymetric surveys, geographic grids, lease maps, well location databases, and infrastructural databases are available through the BOEM database and were used to support this study.

Structural framework analysis

Analysis of the data focuses on the identification and interpretation of salt structures and the associated seismic facies and stratigraphic analysis. The identification and analysis of salt within the seismic record is relatively easily defined based on seismic signature and drilling records. The seismic facies analysis was carried out based on fundamental interpretation techniques (Vail and Wornhardt, 1991).

Well log raster images were interpreted using basic well log interpretation procedures (Asquith et al., 2004). Seismic data analysis was conducted using Petrel and Kingdom 2d/3dPAK software. The seismic data constitute 3D surveys of high quality, and thus, stratigraphic markers were mapped, and geologic structure characterized. The interpretation methodology followed standard procedures for picking stratigraphic markers, identifying faults, and defining hanging-wall and footwall bed cutoffs at intersections with faults (Brown, 2011). The seismic interpretation focused on reservoir characterization, geologic mapping, and volumetric estimation. With further reservoir data analysis, a more comprehensive characterization of target reservoirs was performed, and candidate sinks, and seals identified. Porosity was estimated from geophysical well logs, and a lower limit of 15% porosity was used to characterize intervals as a potential storage reservoir. Identified sandstone intervals were selected to calculate porosity. Asquith et al., (2004) defined porosity as the ratio of the pore volume to the bulk volume of the rock. The porosity of sandstone

is the primary variable that was used to gauge reservoir storage potential. According to Asquith et al. (2004), the porosity of a sandstone formation can be calculated using sonic logs (equation 1), density logs (equation 2) and neutron-density (ND) porosity logs (equations 3, 4),

$$\phi_{Sonic} = \frac{\Delta t_{log} - \Delta t_{ma}}{\Delta t_f - \Delta t_{ma}} \quad \text{Equation 1}$$

$$\phi_{Density} = \frac{\rho_{matrix} - \rho_{bulk}}{\rho_{matrix} - \rho_{fluid}} \quad \text{Equation 2}$$

$$\phi_{ND} = \frac{\phi_D + \phi_N}{2} \quad \text{Equation 3}$$

$$\phi_{ND(gas\ bear)} = \sqrt{\frac{\phi_N^2 + \phi_D^2}{2}} \quad \text{Equation 4}$$

where ϕ is the percent porosity, Δt_{log} ($\mu\text{s}/\text{ft}$) is the zone transit time from the log, Δt_{ma} ($\mu\text{s}/\text{ft}$) is the matrix transit time (sandstone=55.5 $\mu\text{s}/\text{ft}$), and Δt_f is the pore fluid transit time (fresh water=189 $\mu\text{s}/\text{ft}$, salt water= 185 $\mu\text{s}/\text{ft}$); ρ_{matrix} (g/cm^3) is the density of the grain matrix (sandstone = 2.65 g/cm^3), ρ_{bulk} (g/cm^3) is the density of the fluid (fresh water = 1 g/m^3 , salt water = 1.15 g/cm^3); ρ_{bulk} (g/cm^3) is the bulk density of the formation from log.

For carbon sequestration, it is imperative to consider seal integrity. Thus, potential risks from faults, salt, and lateral stratigraphic changes, were taken into consideration. Structure contour, isopach, and isochron maps for potential target zones were developed based on the stratigraphic markers, fault planes, and bed cutoffs. The net reservoir thickness within fields were derived from

the addition of the thickness of each reservoir interval within a formation. A quantitative estimate was generated for each target reservoir zone within fields selected for further analysis. The volumetric approach of Goodman et al., (2011) and NETL (2012) for saline formations and oil and gas reservoirs was used to generate quantitative estimates for potential CO₂ storage within target reservoir zones.

$$G_{CO_2} = A_t h_g \phi_{tot} \rho E_{saline} \quad \text{Equation 6}$$

Where A_t is the reservoir area; h_g is the net formation thickness; ϕ_{tot} is the total porosity; ρ is the CO₂ density; E_{saline} is the CO₂ storage efficiency factor.

E_{saline} , the storage efficiency factor, is defined as the ratio of the pore space occupied by injected CO₂ to the total pore space (Goodman et al., 2011; NETL, 2012). It is quantified by implementing Monte Carlo analysis governed by geological parameters such as reservoir area, gross formation thickness, and average porosity. Established results based on Monte Carlo analysis assert that E_{saline} can span from 7.40 to 24.00% in well-characterized siliciclastic reservoirs, with 7.40% at P10, 14.00% at P50, and 24.00% at P90 (Goodman et al., 2011).

Seismic recognition of salt in the Mississippi Canyon protraction area

The structural geometry of the study area is influenced strongly by salt bodies. The salt bodies were observed and identified on the seismic surveys in the following ways (Fig. 9):

- 1.) High amplitude reflector seismic feature that indicates sediment-salt interface: This is caused by the high-impedance contrast between a higher velocity salt body and bordering sediments

(Jenyon, 1986). The high-amplitude reflector can be identified as a single seismic reflector or a seismic doublet. Salt has very low to no porosity, and for this reason, salt doesn't compress easily when subjected to overburden or surrounding pressure (Yorston and Fox, 1985).

2.) Seismic transparency indicating loss of acoustic contrast within the salt body: The seismic velocity (which depends on the density of the formation/medium) of salt (~4,500m/sec) doesn't change much with depth because the density of salt is relatively consistent in the subsurface (Jenyon, 1986). Therefore, in seismic data, salt character is observed as a zone of low amplitude clear reflections, or recognized simply as a seismic wipeout region.

3.) Deformation-related seismic character of subsalt and supra salt sediment. Deformation of sediment around salt can show seismic response in the following ways (Nelson, 1991):

- a) The presence of velocity pull-up or pull-down up reflectors in sub-salt sediments;
- b) Crestal faults above the top of salt; and
- c) Highly deformed suprasalt sediment.

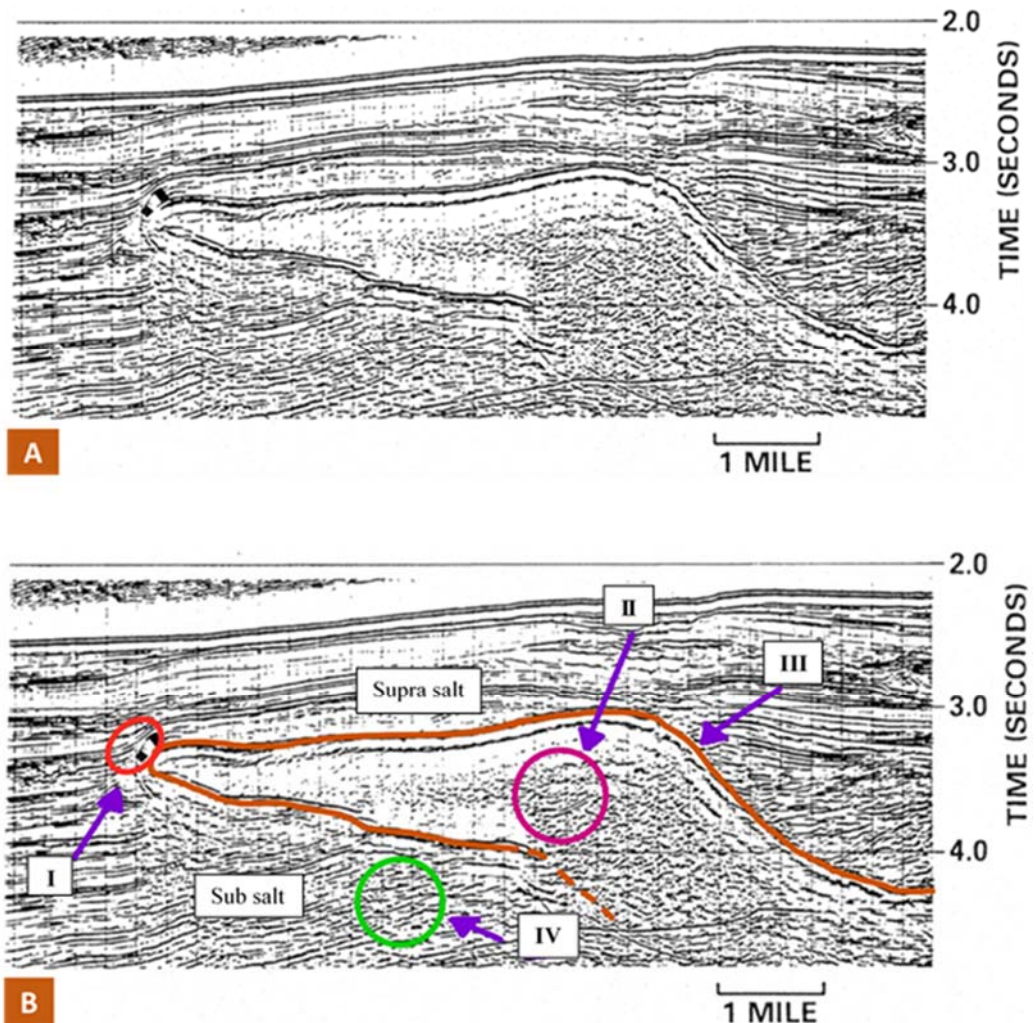


Figure 9. Salt features in a seismic profile (after Nelson, 1991).

A = uninterpreted seismic section;

B = interpreted seismic section;

I = Sediment deformation from lateral salt mobilization;

II = Acoustic wipeout in salt body;

III = Top of salt indicated by a high amplitude reflector;

IV = Pull up seismic character under salt body.

Seismic attributes

Seismic attribute analysis uses the recognition of differences in amplitudes within seismic surveys to identify and track geologic features (Redini et al., 2017). This methodology helps to improve the seismic data quality in order to better image structural features such as faults, and other stratigraphic features (Weimer and Davis, 1996). Seismic amplitudes can be very instrumental in the identification of discontinuities and continuities within the seismic reflector packages, and geological features/restrictions, such as channel sands, gas accumulations, and unconformities (Chopra and Marfurt, 2007) that can influence carbon sequestration and CO₂-EOR projects.

- I. Variance: Variance seismic attribute can help to improve the visibility of major faults, salt bodies and minibasins because it measures the coherency and continuity of amplitudes horizontally (Vav Bemmel and Pepper, 2000). Variance is also useful for delineating channels and salt boundaries (Vav Bemmel and Pepper, 2000).
- II. Root-mean-squared (RMS) Amplitude: The RMS attribute can be used to recognize hydrocarbon indicators (bright spots) and gas chimneys (Satyavani et al., 2008; Chopra and Marfurt, 2007, 2008). RMS amplitude computations amplify high amplitude seismic sections and weaken of low amplitude seismic sections (DeAngelo and Wood, 2001). Shale intervals are usually characterized by low amplitude while sandstone intervals are characterized by high amplitudes (Chopra and Marfurt, 2007, Azevedo and Pereira, 2009).
- III. Structural smoothening: Structural smoothing improves the appearance of continuity within parallel seismic reflectors and packages. It also enhances faults by generating a volume with better resolution characterized by less visibility of background noise (Redini et al., 2017)

CHAPTER IV

RESULTS

Bathymetry maps

Bathymetric contours (Fig. 10; Fig. 11) were generated using the Petrel software. The sea floor horizon was mapped by picking the peak seismic reflector along a 60-line by 60-line grid, and utilizing the auto-fill feature in the Petrel software to fill the seismic volume.

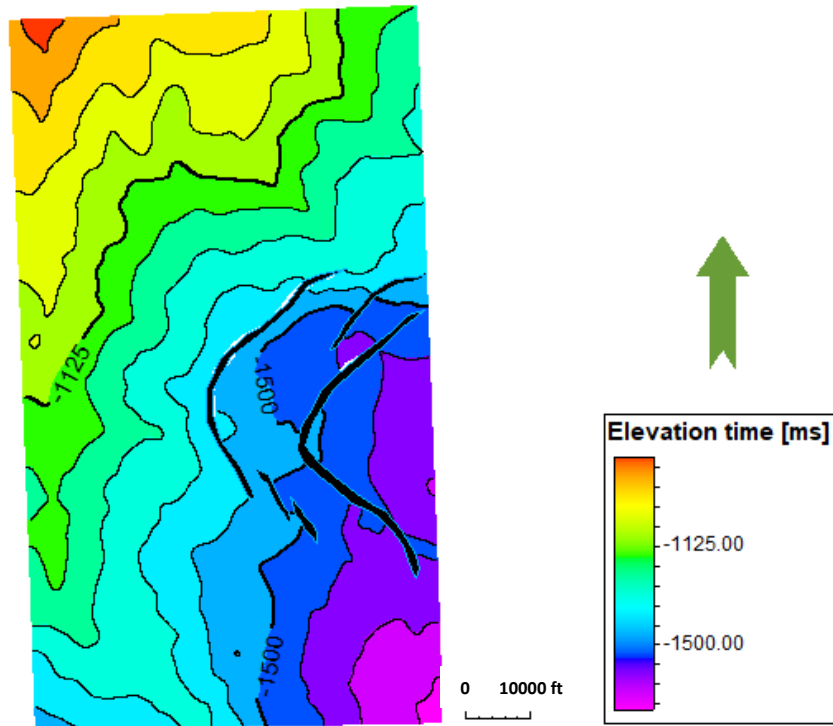


Figure 10. Seafloor bathymetry map of focus area A (see Figure 3 for location). Black polygons represent faults.

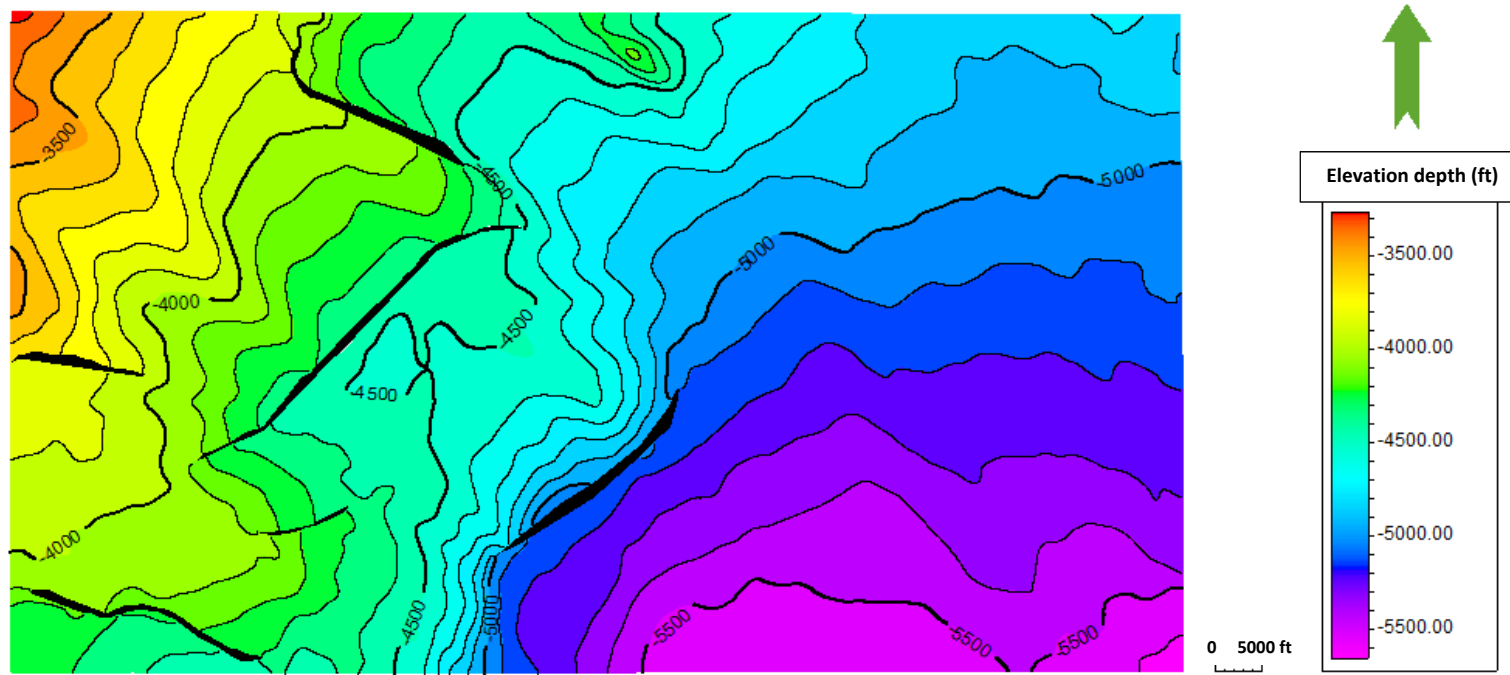


Figure 11. Seafloor bathymetry map of focus area B (see Figure 3 for location). Black polygons represent faults.

Structural framework features observed within the study area

Several complex assemblages of tectonic structures were observed and identified with the seismic profiles and seismic time slices. The array of structures and related features observed and identified include:

I. Growth fault families

Growth faults by definition are faults that grow contemporaneously with sedimentation (Rowan et al., 1999). Within the study area, these growth fault families have been inferred to have resulted from gliding due to gravity and subsequent spreading along detachment surfaces located in salt and the adjacent sections (Figs. 13-18). Additionally, the decollements separate distinct structural objectives.

II. Allochthonous salt

Parautochthonous Louann salt is buoyant and ductile, and the salt was expelled basinward and up section as overburden accumulated (Rowan et al., 1999). Within the study area, salt canopies, diapirs and salt tongues were observed (Figs. 15-18). Additionally, the presence of salt is interpreted to strongly affect the accumulation of deep-water marine facies as salt migrates upward in section.

III. Salt welds

Welds are identified at locations where the complete or nearly complete evacuation of salt bodies such as diapirs, stocks, tongues, or canopies has occurred (Rowan et al., 1999). Welds are important features because they are used to infer the former locations of allochthonous and autochthonous salt (Figs. 17-18).

IV. Withdrawal synclines and minibasins

Within the study area, salt bodies are interpreted to have risen from the Louann Salt, i.e., the original parautochthonous salt body. These diapirs result in the development of withdrawal syncline structures, mini basins and turtle structures (Fig. 36).

Salt tectonics

I. Distribution of salt bodies within Study area A

Salt is present in the southern (salt body A1), center (salt body A2), and northern (salt body A3) parts of study area A (Fig. 12; Fig. 13). The top of the salt bodies are above 12,000 feet. Very deep salt bodies and salt that is not mappable are not identified. The salt mapped may be part of a large salt body beyond the scope of the seismic survey. Thus, directional trend for this salt body is unknown. The structural geometry and morphology of the three salt bodies is presented below. The salt bodies mapped within this study area are within the counterregional salt system/tabular salt minibasin objective (Diegel, 1995).

a. Salt body A1 morphology

Salt body A1 is located in the southern section of study area A. Within the study area, salt body A1 spans approximately 33 mi². The top of salt body A1 is located within two way travel times of 2,930 and 5,150 ms (Fig. 14), and the thickness of sediment overlying Salt body I ranges from approximately 3,500 to 5,000 ft. Figure 15, Figure 16, Figure 17 illustrates the structural geometry of Salt body A3.

b. Salt body A2 morphology

Salt body A2 is in the center of study area A and extends from the western boundary to the eastern boundary of the seismic survey. This salt body spans an area of approximately 77 mi².

Figure 21 shows the structural geometry of salt body A2 and its associated suprasalt sediments, and associated minibasins. The top of salt body A2 is easily identified at time slices ranging from approximately 2,970 to 6,140 ms (Fig. 14). Figure 17 illustrates the structural geometry of Salt body A2.

c. *Salt body A3 morphology*

Salt body A3 is located along the northern boundary of study area A, and it covers approximately 22 mi². The top of salt body A3 is present between seismic time slices at 2,270 to 3,410 ms (Fig. 14). Figure 17 illustrates the structural geometry of Salt body A3.

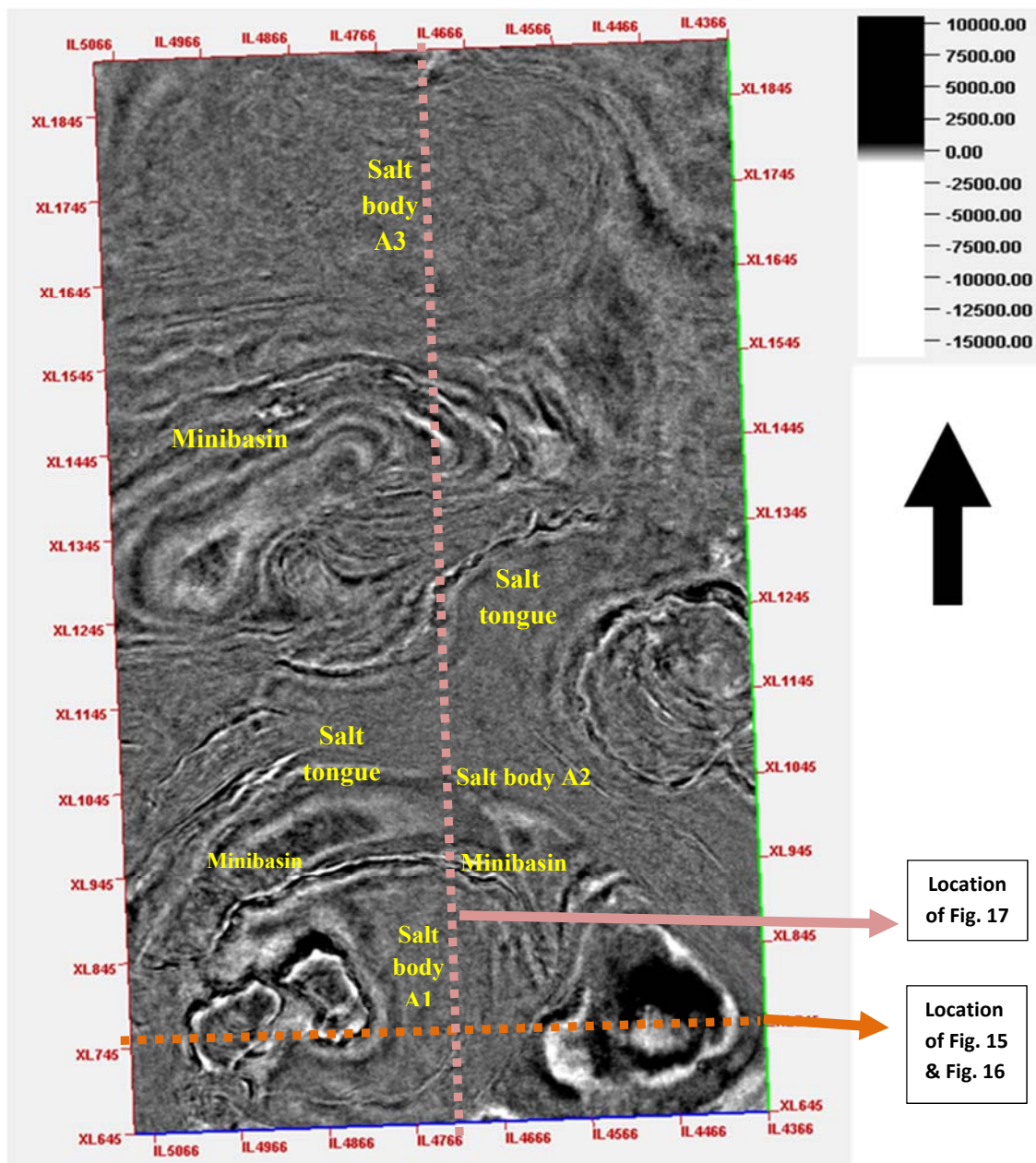


Figure 12. Distribution of salt bodies and associated minibasins within Study area A: Seismic variance attribute time slice at $Z = -4332.00$ ms. Salt bodies and minibasins are evident.

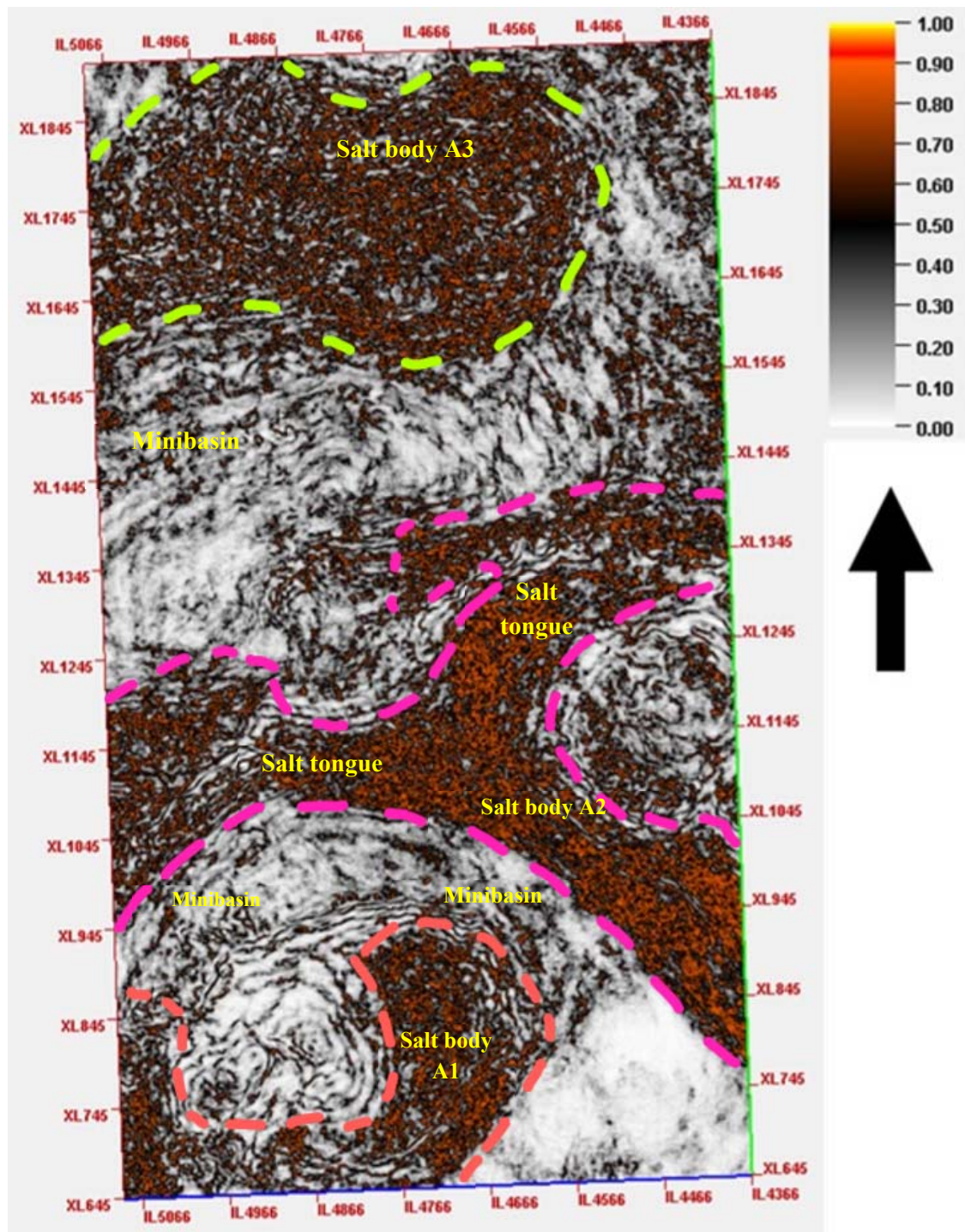


Figure 13. Variance attribute time slice (Study area A) at Z=-4332.0 ms with structural boundaries of salt bodies more visible.

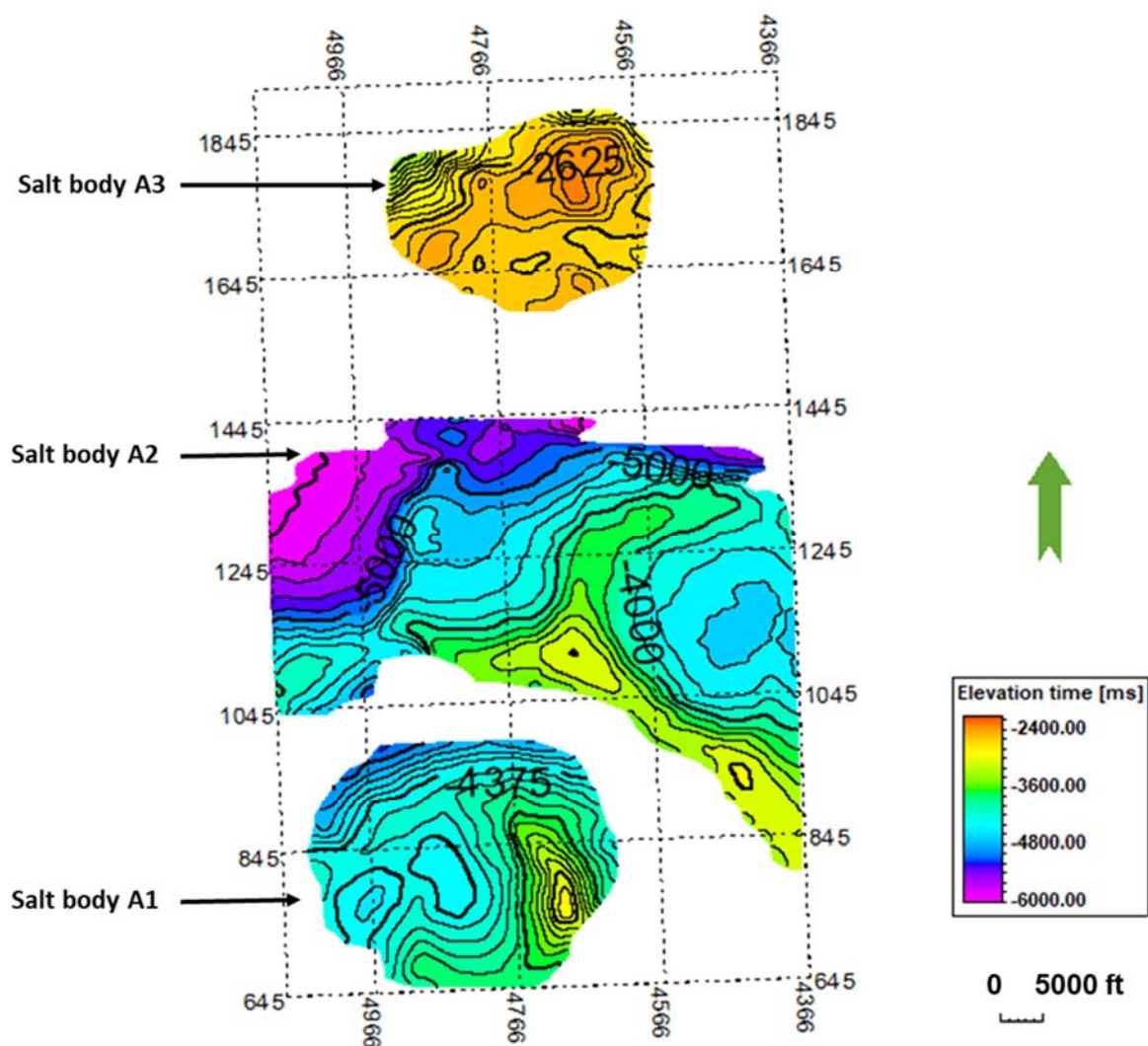


Figure 14. Time structure map: Top of salt bodies within study area A.

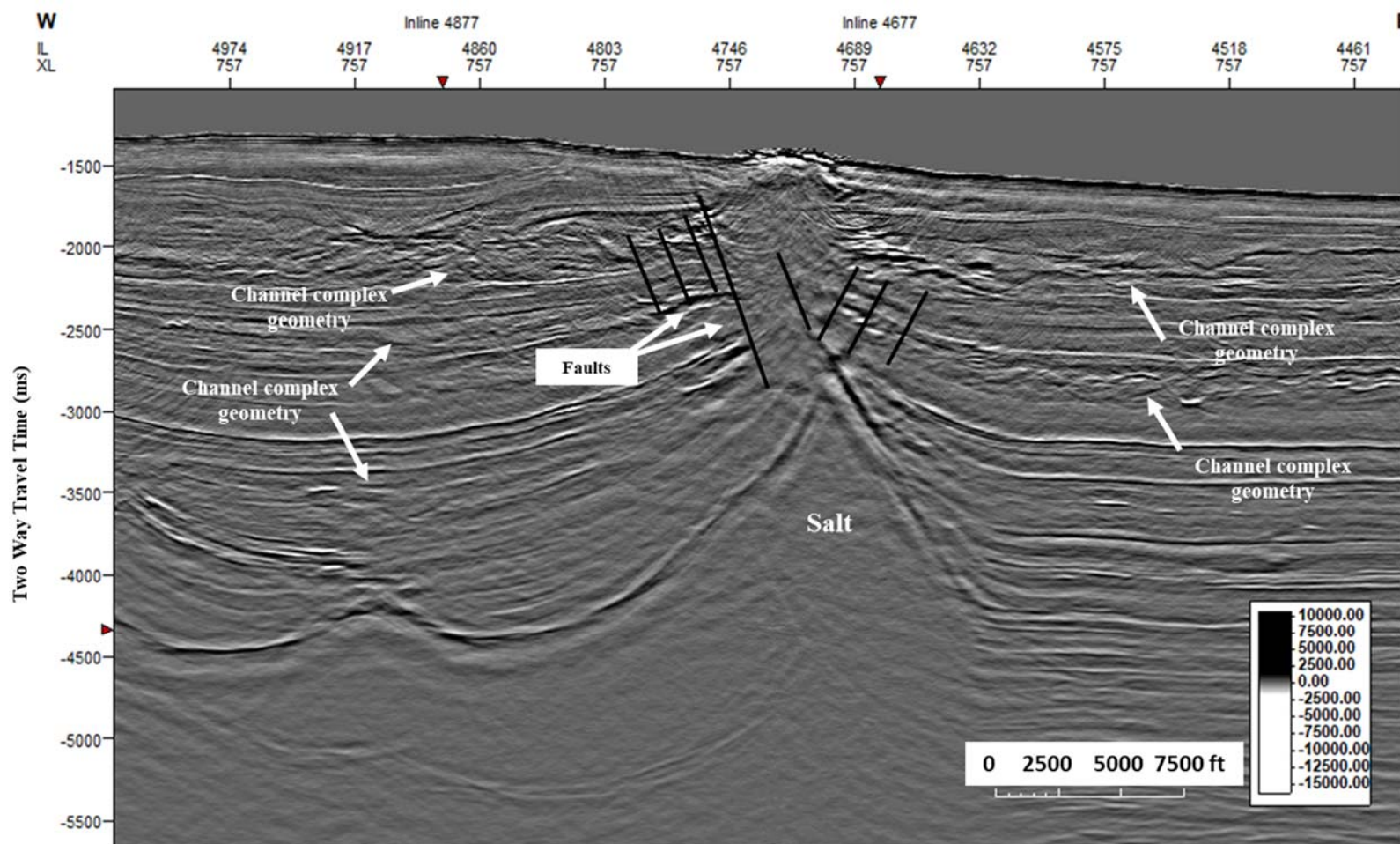


Figure 15. Seismic profile (seismic amplitude) through crossline 787 illustrating salt body A1, crestal faults and channel complexes.

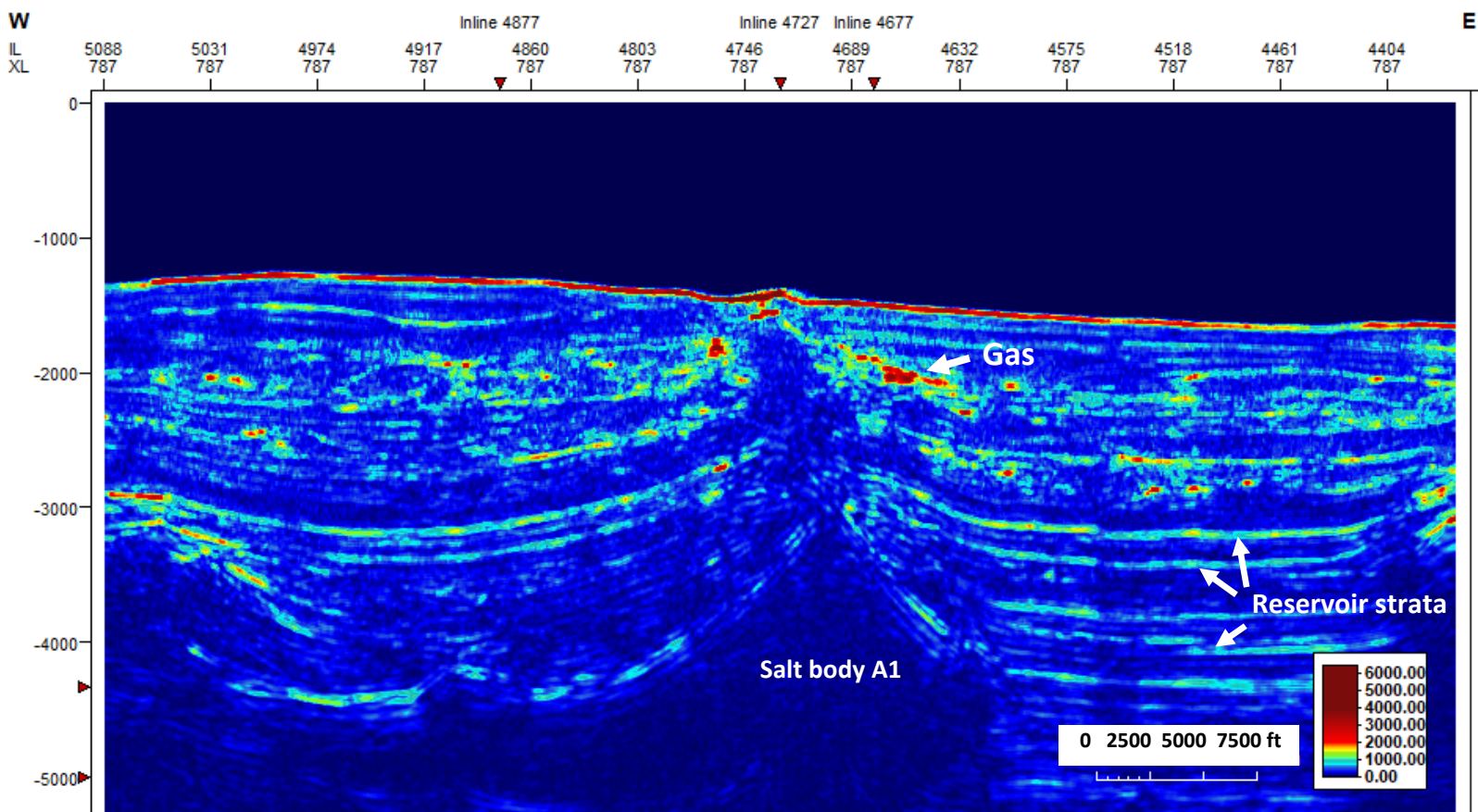


Figure 16. Seismic profile (RMS amplitude) through crossline 787 illustrating salt body A1 and proximal gas accumulations. Gas accumulations are identified by high seismic amplitude phases.

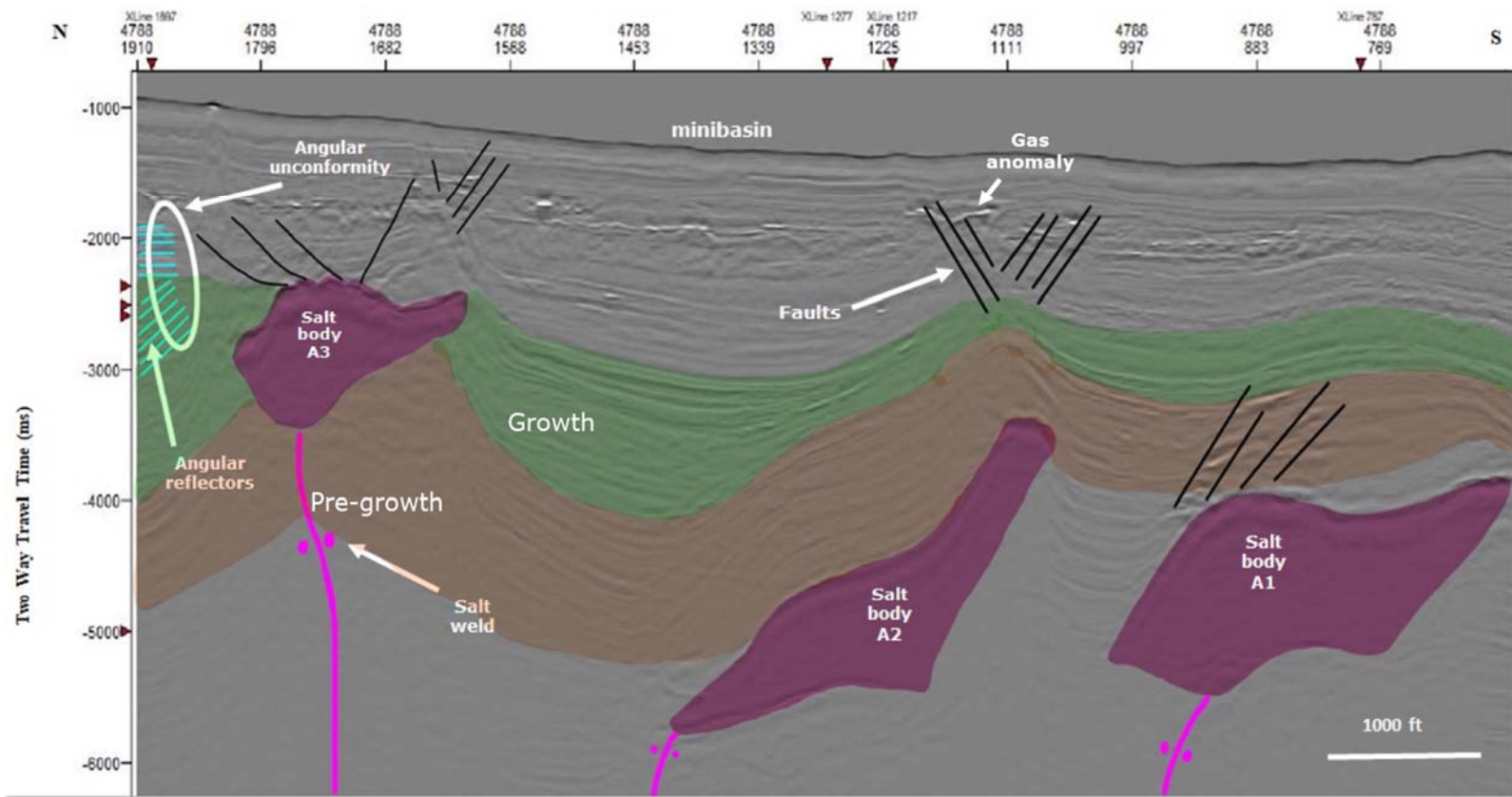


Figure 17. Seismic profile (seismic amplitude) through inline 4708 illustrating salt body A1, salt body A2 and salt body A3.

II. *Distribution of salt bodies within study area B*

Salt is present in the southwest (salt body B1), southeast (salt body B2), upper north (salt body B3) and lower southern (salt body B4) (Fig. 18) parts of study area B. The tops of the salt bodies are shallower than 15,000 feet. Deep salt bodies in this area are present but not readily defined or mappable. The salt mapped may be associated with large composite salt bodies that are not well imaged in the seismic survey. The structural geometry and morphology of the three salt bodies is presented below. The salt bodies mapped within this study area are within the tabular salt minibasin objective (Diegel, 1995).

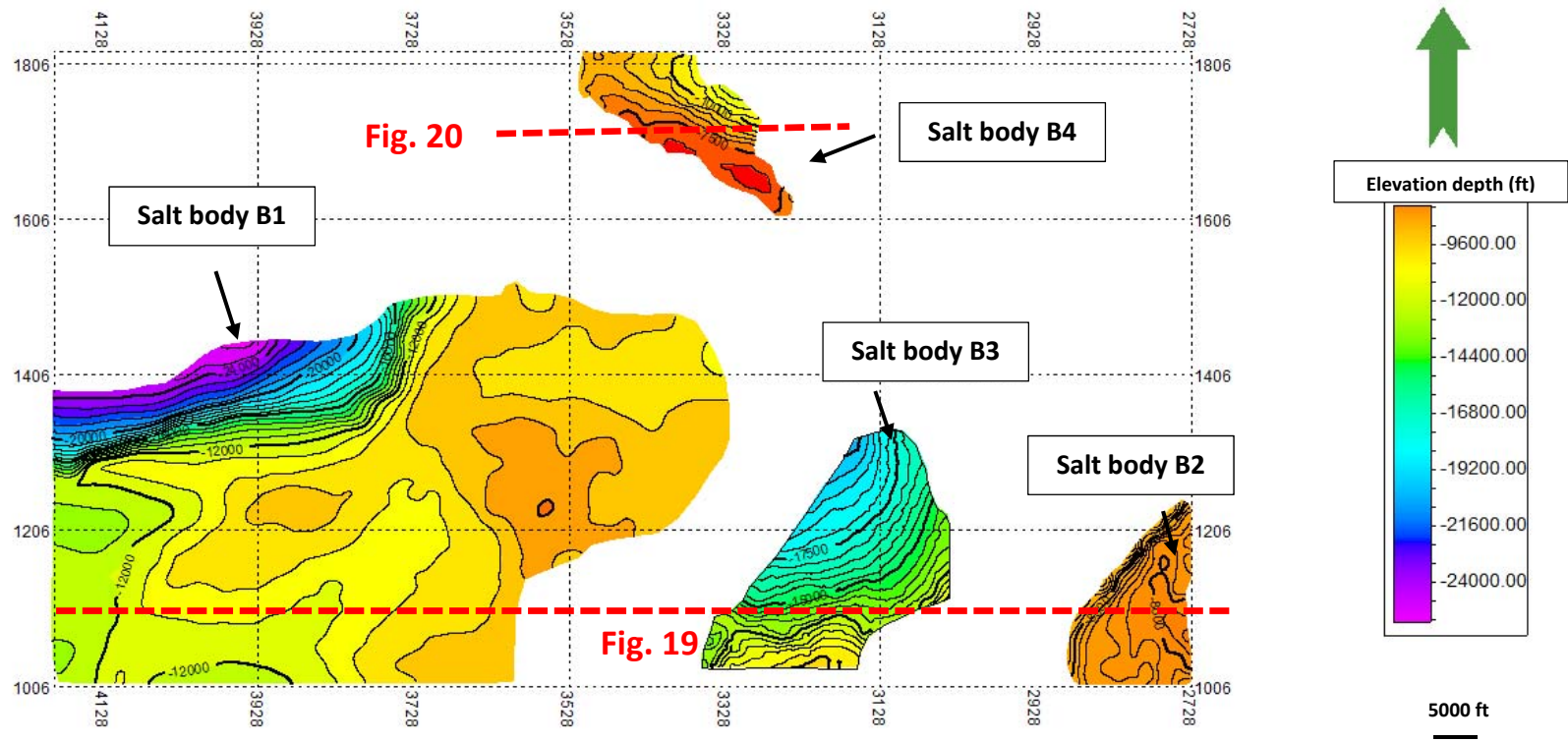


Figure 18. Distribution of shallow salt within study area B.

a. Salt body B1 morphology

Salt body B1 is located in the southwest section of study area B (Fig. 18). Within the study area, Salt body B1 spans approximately 9 mi². The top of salt body B1 is at depths ranging from approximately 7,500 to 10,500 ft, and the thickness of sediment overlying salt body B1 ranges from approximately 3,500 to 4,500 ft. Arbitrary seismic line A illustrates the canopy structural geometry of salt body B1 (Fig. 19).

b. Salt body B2 morphology

Salt body B2 is located in the southwest part of study area B (Fig. 18). It encompasses an area of approximately 22 mi². Figure 19 shows the structural geometry of salt body B2 and its associated suprasalt cover. The top of salt body B2 is at depths ranging from approximately 8,000 to 10,500 ft below sea level, and the thickness of sediment overlying the salt body ranges from approximately 3,100 to 5,000 ft.

c. Salt body B3 morphology

Salt body B3 is located along the northern boundary of study area B (Fig. 18), and it spans approximately 9 mi². The top of salt body B3 is at depths ranging from approximately 7,000 to 11,000 ft, and the thickness of sediment overlying salt body 3 ranges from approximately 3,500 to 4,500 ft. Arbitrary seismic line C illustrates the structural geometry of Salt body B3 (Fig. 19).

d. Salt body B4 morphology

Salt body B4 is located along the southern boundary of study area B (Fig. 18). It covers approximately 15 mi². The top of salt body B4 is at depths ranging from approximately 6,500 to 10,000 ft, and the thickness of sediment overlying salt body 4 ranges from approximately 3,000 to 4,300 ft. Arbitrary seismic line D illustrates the structural geometry of Salt body B4 (Fig. 20).

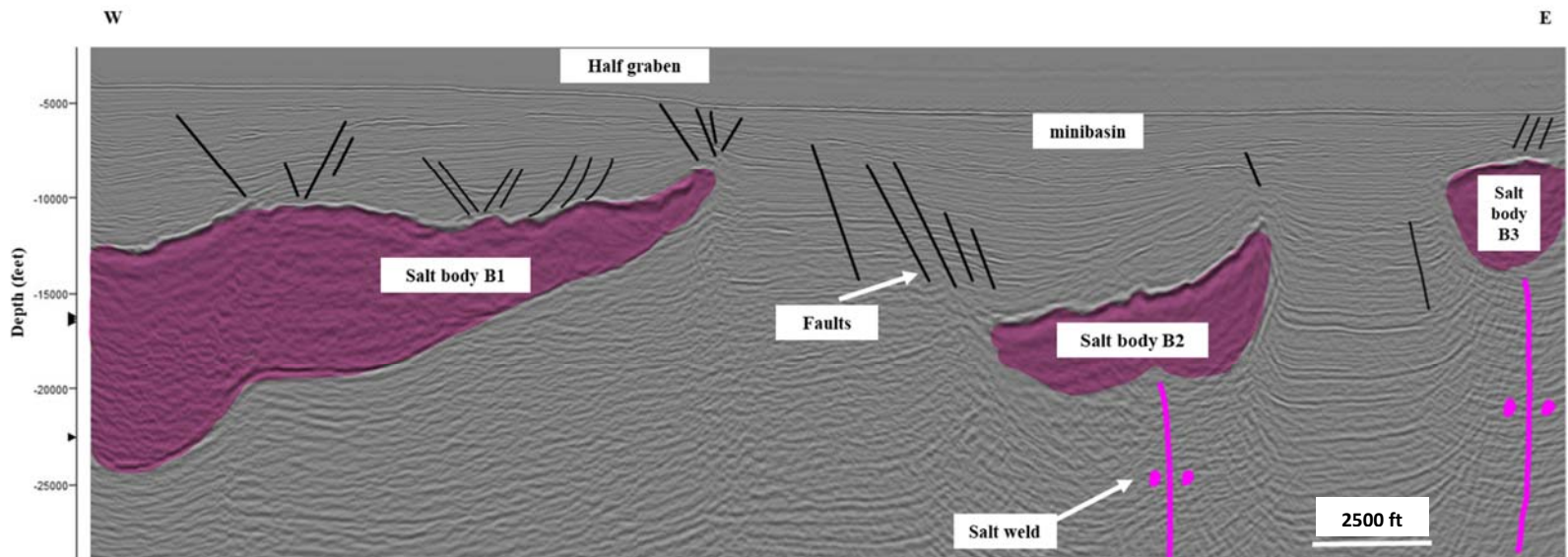


Figure 19. Seismic profile through crossline 1136 illustrating salt bodies B1, B2 and B3.

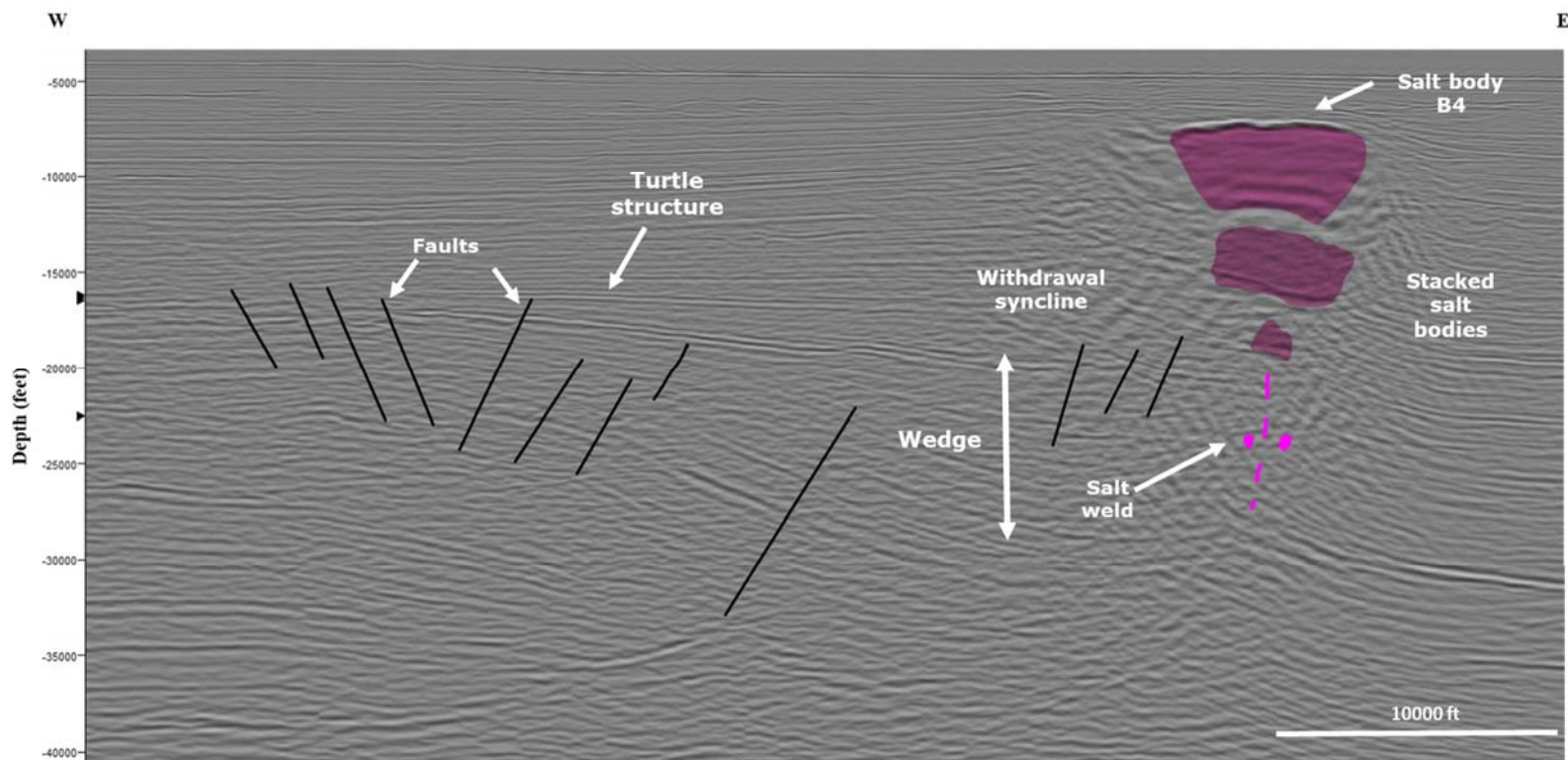


Figure 20. Seismic profile through crossline 1680 illustrating salt body B4.

Observed structural styles of salt minibasins

A variety of structural styles are observed in the basins (Fig. 21): A) relatively symmetric basins; B) basins with highly asymmetrical growth stratigraphy; C) expulsion roll-over basins

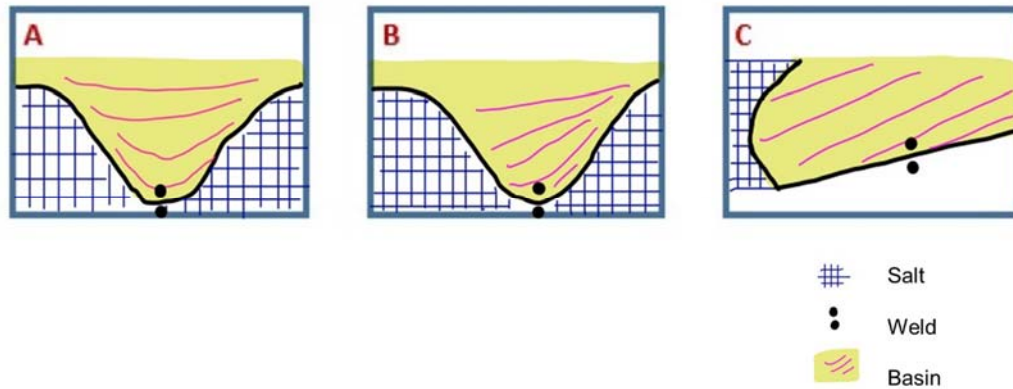


Figure 21. Structural styles of minibasins observed in the Mississippi Canyon protraction area.

The mobilization and re-mobilization of salt and resulting associated sediment deformation, has led to the development of numerous minibasins within the study area. Primarily suprasalt basins, that is, basins overlying salt bodies have been observed within the study area. Subsiding sediment above salt bodies is the primary structural control for the development of minibasins in the northern Gulf of Mexico (Spindler, 1977).

Major fault distribution

Faults are easily observed, identified and interpreted in seismic surveys by the offset of reflectors across the fault (Rowan et al., 1999). Study area A (Fig. 22) and study area B (Fig. 23) are characterized by extensional and contractional faults. Many of the faults are present along the rims of diapiric uplifts, along the margins of salt withdrawal basins, at the crest of anticlinal structures, and close to the top of salt bodies.

I. Major fault distribution within study area A

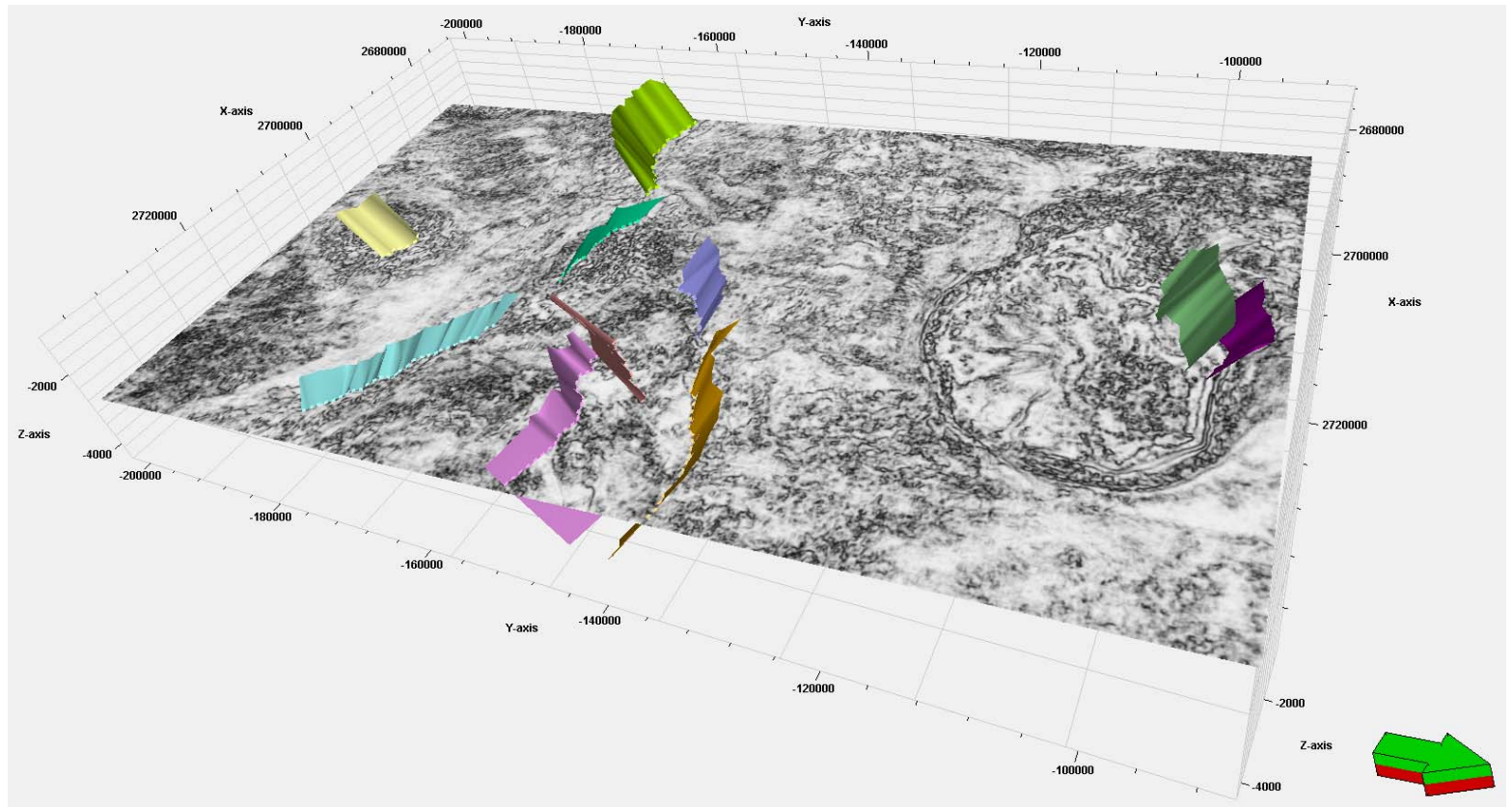


Figure 22. 3-D visualization of major faults in study area A.

II. Major fault distribution within study area B

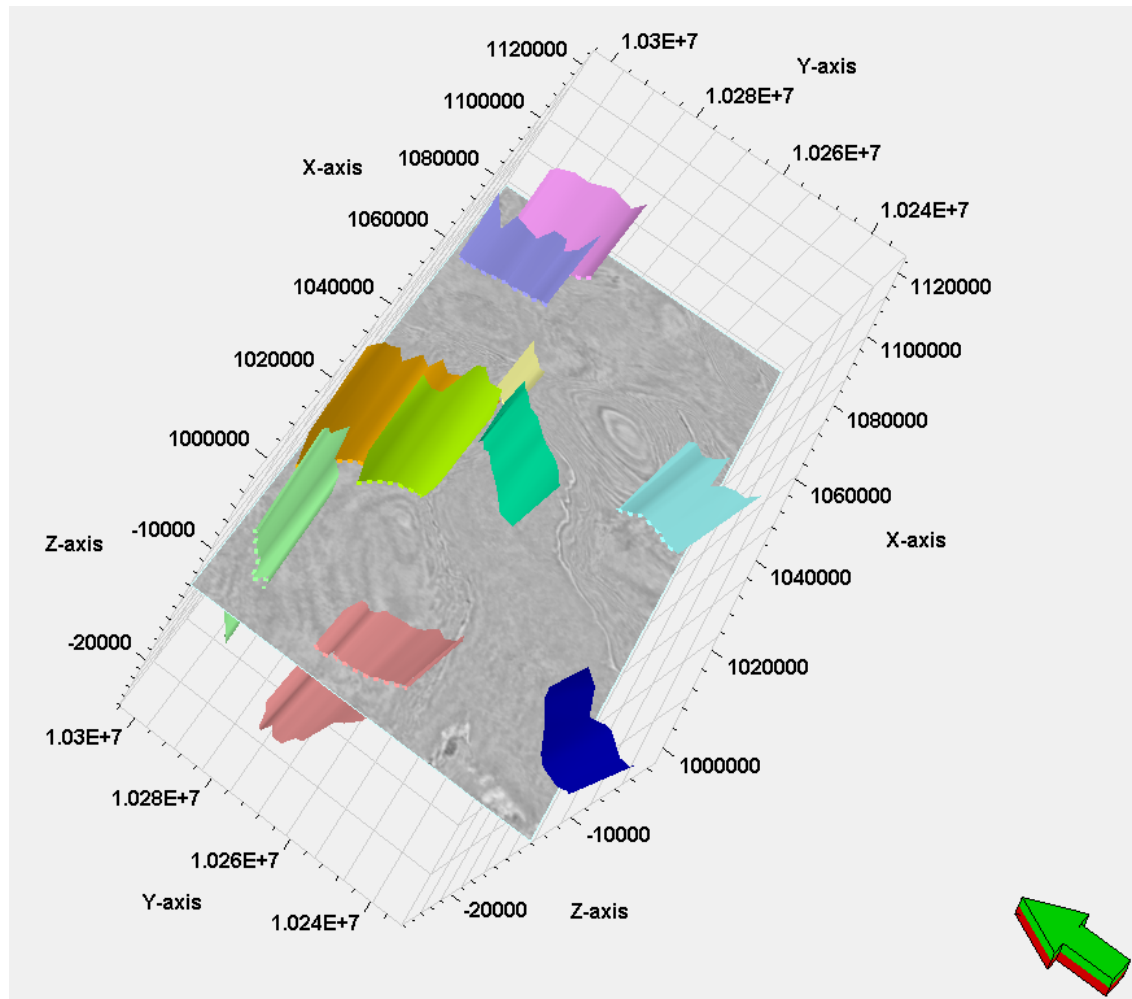


Figure 23. 3-D visualization of major faults in study area B.

Identification of fields for potential tertiary hydrocarbon recovery/carbon sequestration projects

Four oil fields were identified and evaluated in study area A(Fig. 24).

I. Fields identified within Study area A

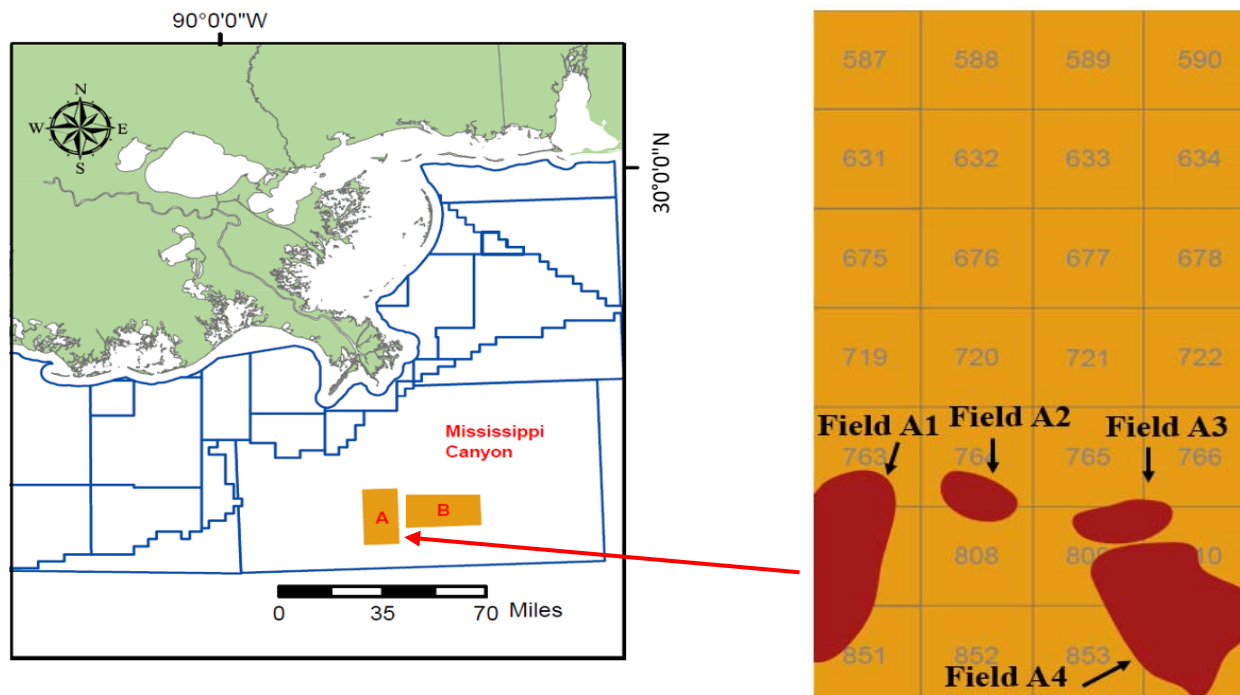


Figure 24. Map of study area A illustrating oil fields (red bubbles) that have been evaluated.

II. Fields evaluated within study area B

Six oil and gas fields were identified and evaluated in study area B (Fig. 25).

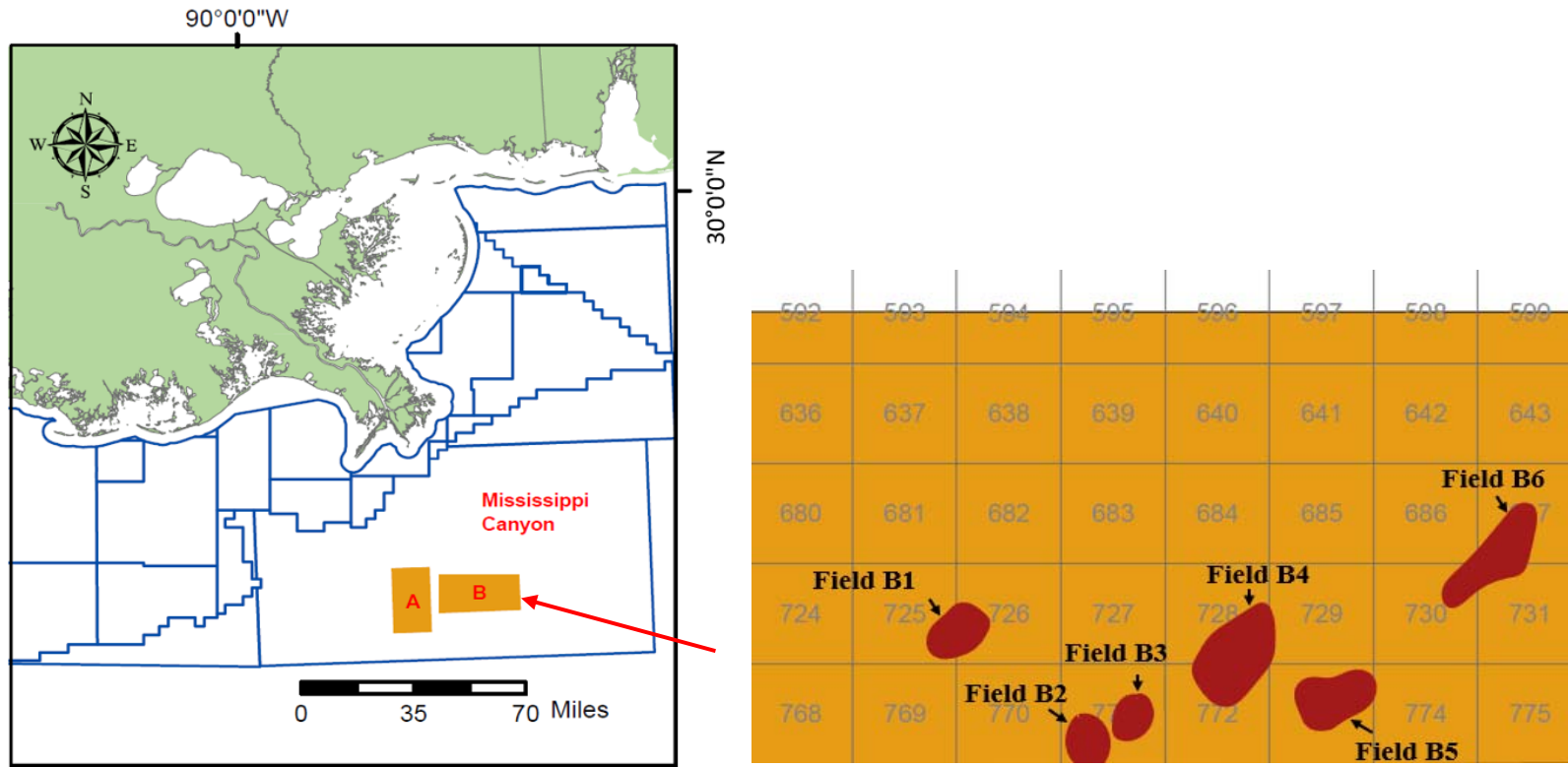


Figure 25. Map of study area B illustrating oil fields (red bubbles) that have been evaluated.

The identification of oil and gas fields in the study areas were facilitated by the signatures within the well log data. Four wells were used in study area A (Table 1, Fig. 26), and five wells were used in study area B (Table 2, Fig. 26). Most of the identified fields are emplaced within withdrawal synclines adjacent to salt bodies (Fig. 27-36)

Table 1: List of fields evaluated and associated well logs used within study area A.

Fields	Well logs used for reservoir evaluation
A1	MC 807-1
A2	MC 764-1
A3	MC 765-1
A4	MC 809-1

Table 2: List of fields evaluated and associated well logs used within study area B.

Fields	Well logs used for reservoir evaluation
B1	MC 682-1
B2	MC 771-1
B3	MC 771-1
B4	MC 772-1
B5	MC 773-1
B6	MC 731-1

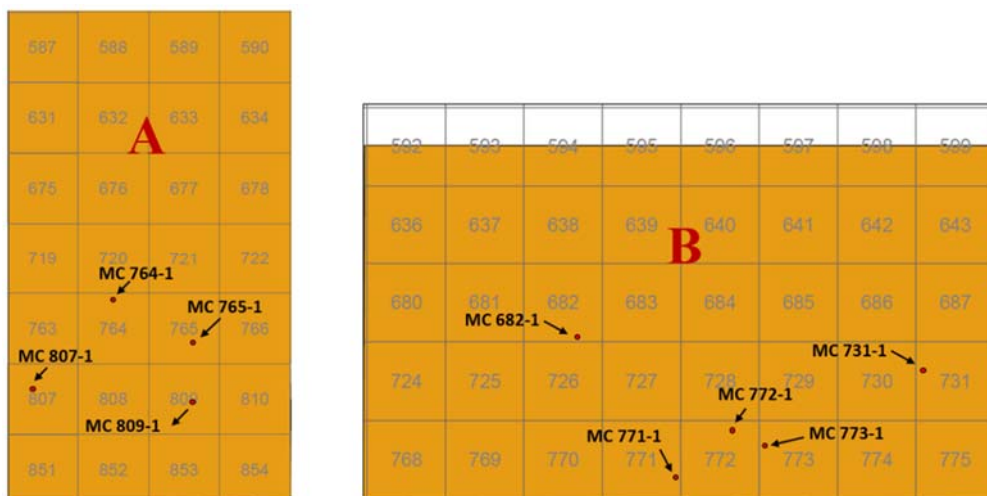


Figure 26. Location of well logs used in this study.

Seismic profiles across identified fields

I. Fields within Study area A

a. Field A1: MC 763-805-851

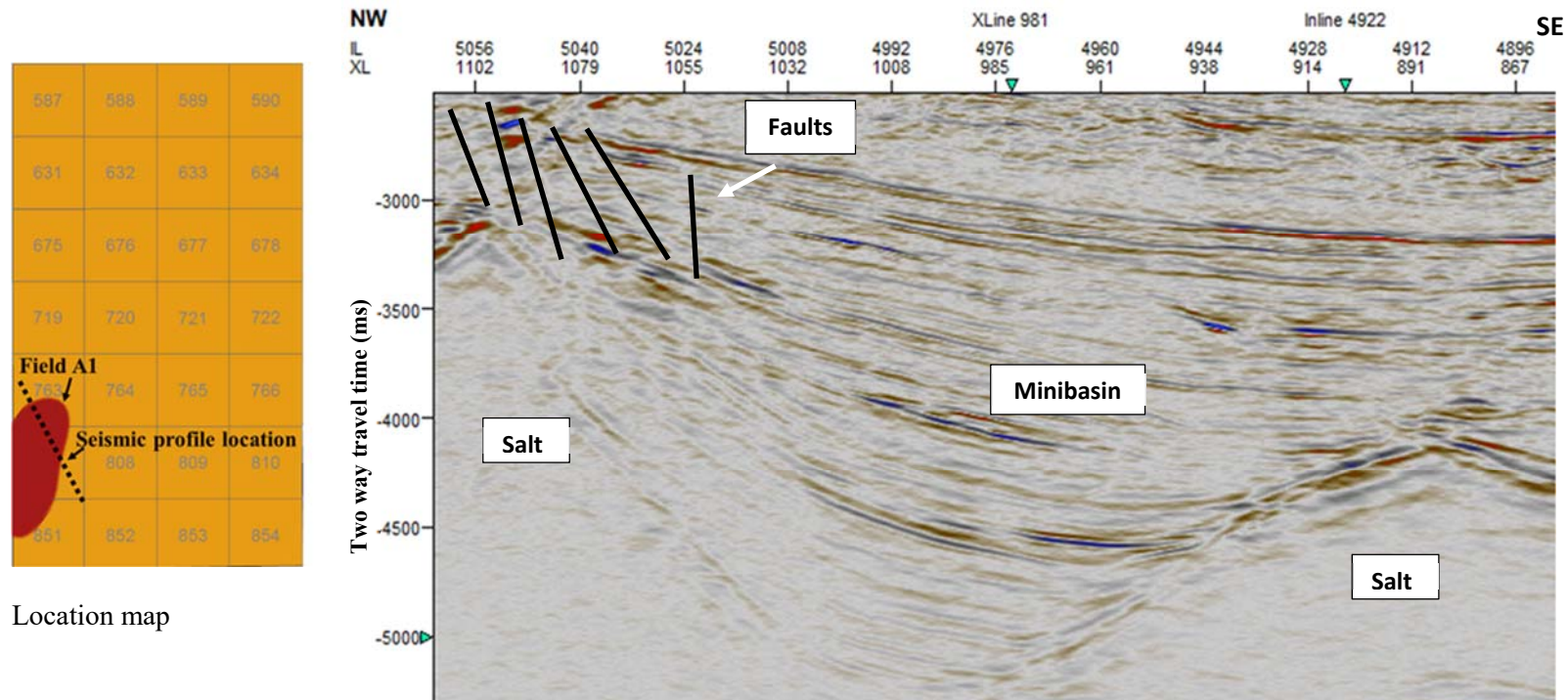


Figure 27. Seismic profile cross-section across field A1: MC 763-805-851. Faults, salt bodies and minibasin are identified.

b. Field A2: MC 764-808

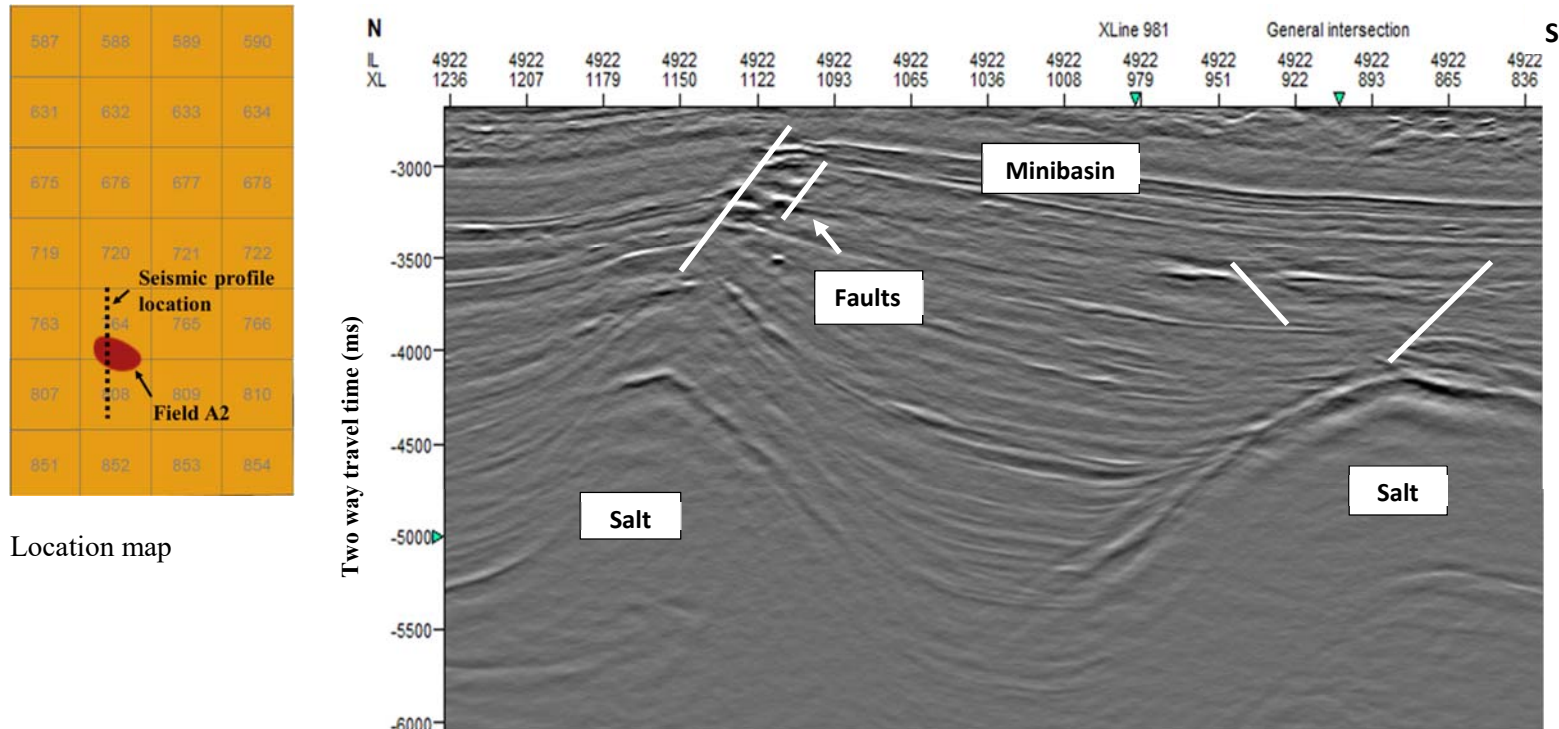


Figure 28. Seismic profile across field A2: MC 764-808. Faults, salt bodies and minibasin are identified.

c. Field A3: MC 809-810

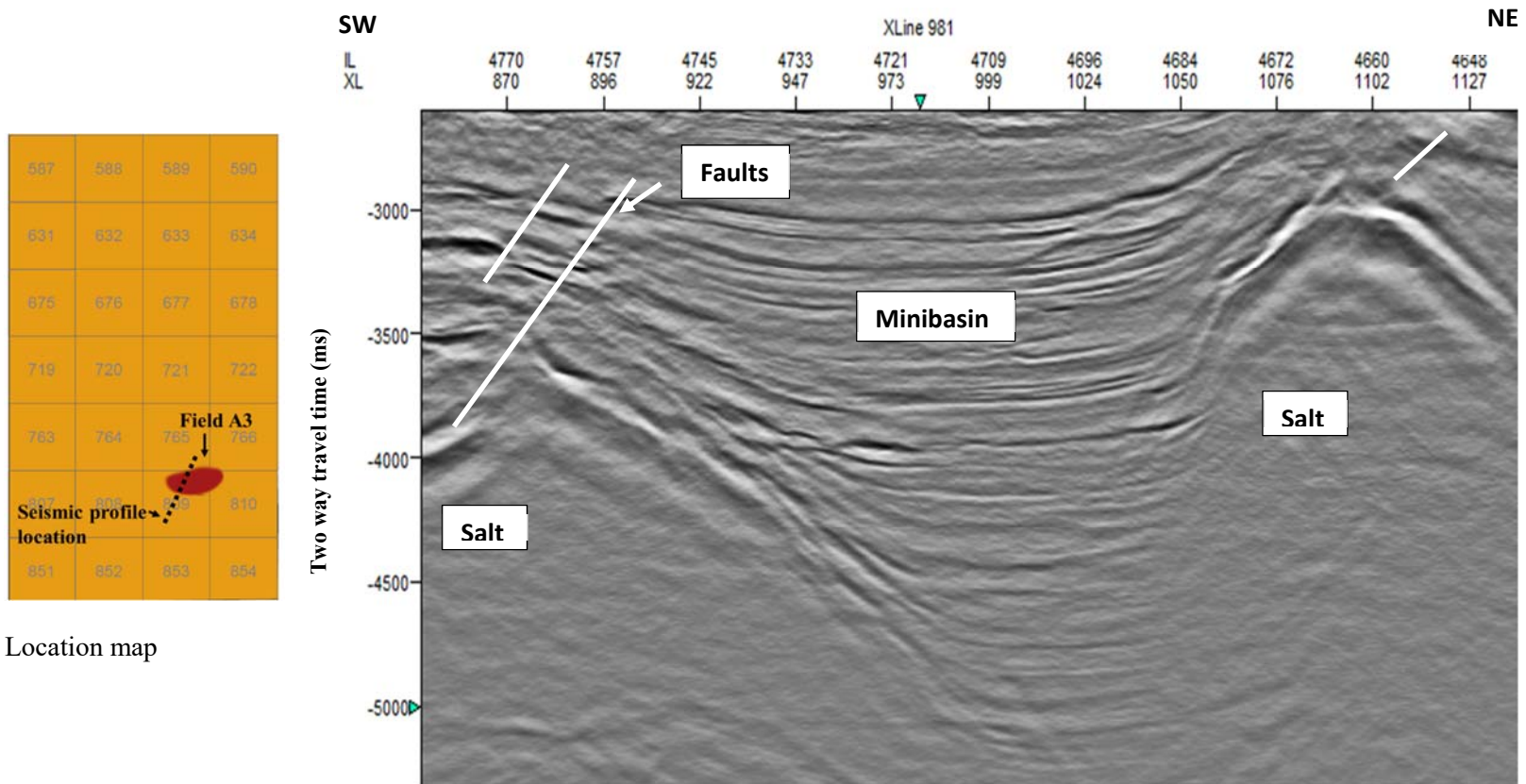


Figure 29. Seismic profile across field A3: MC 809-810. Faults, salt bodies and minibasin are identified.

d. Field A4: MC 809-810-853-854

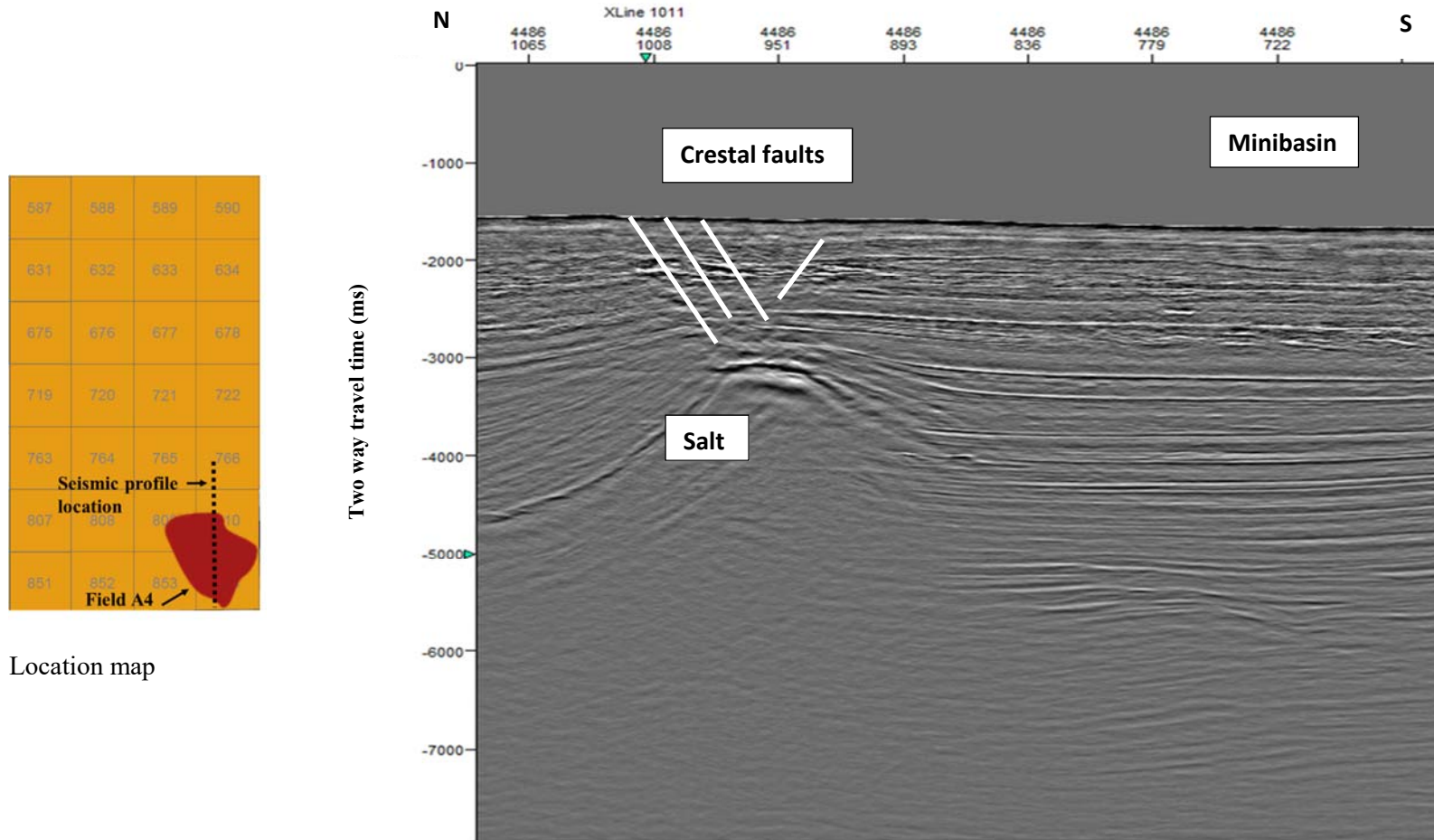


Figure 30. Seismic profile across field A4: MC 809-810-853-854. Crestal faults, salt body and a minibasin are identified.

II. Fields within Study area B

a. Field B1: MC 725-726

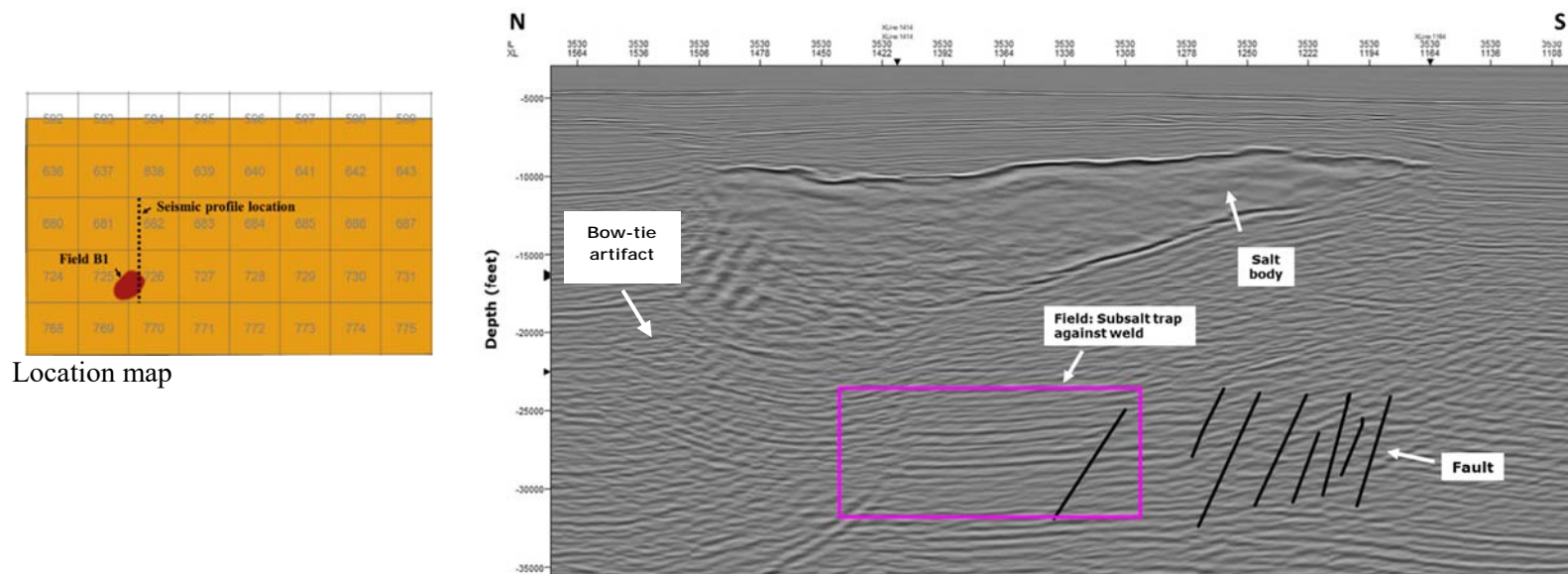
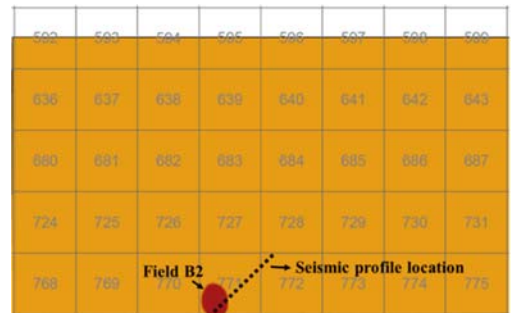


Figure 31. Seismic profile across field B1: MC 725-726. Salt body and faults are identified. Inferred trapping mechanism is indicated. However, bow-tie artifact on the northern part complicates interpretation.

b. Field B2: MC 771a



Location map

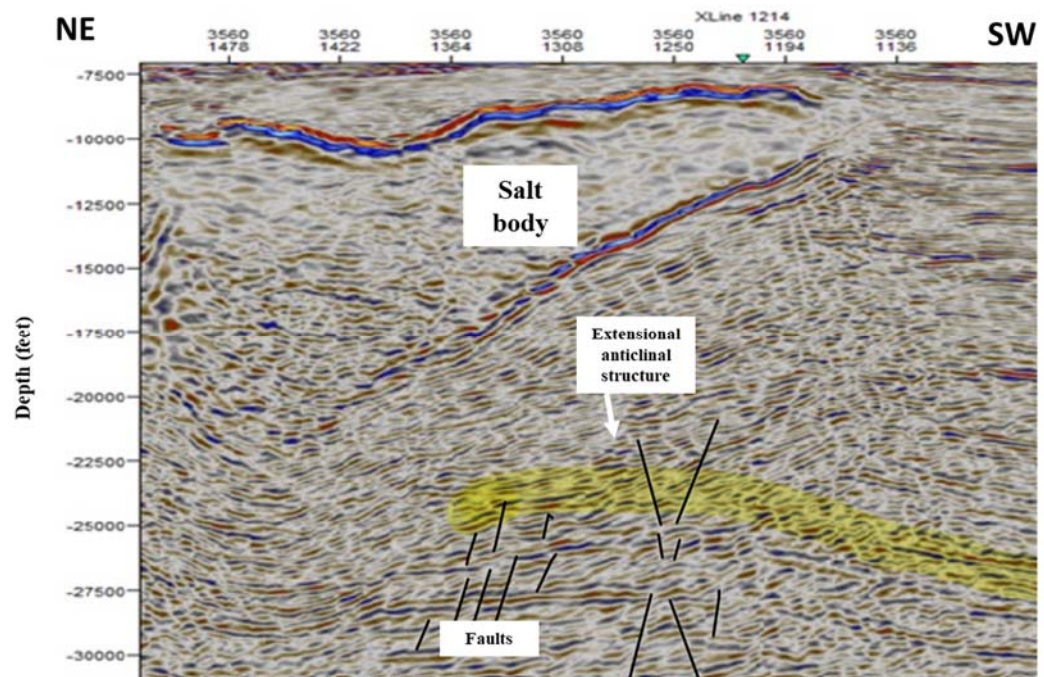
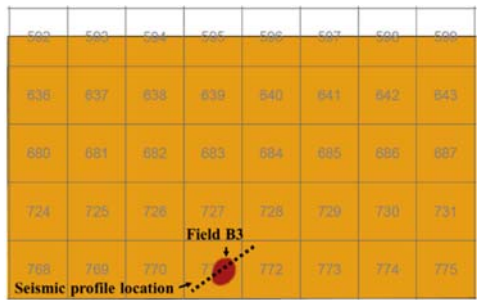


Figure 32. Seismic profile across field B2: MC 771a. Salt body, extensional anticlinal structure and faults are identified.

c. Field B3: MC 771b



Location map

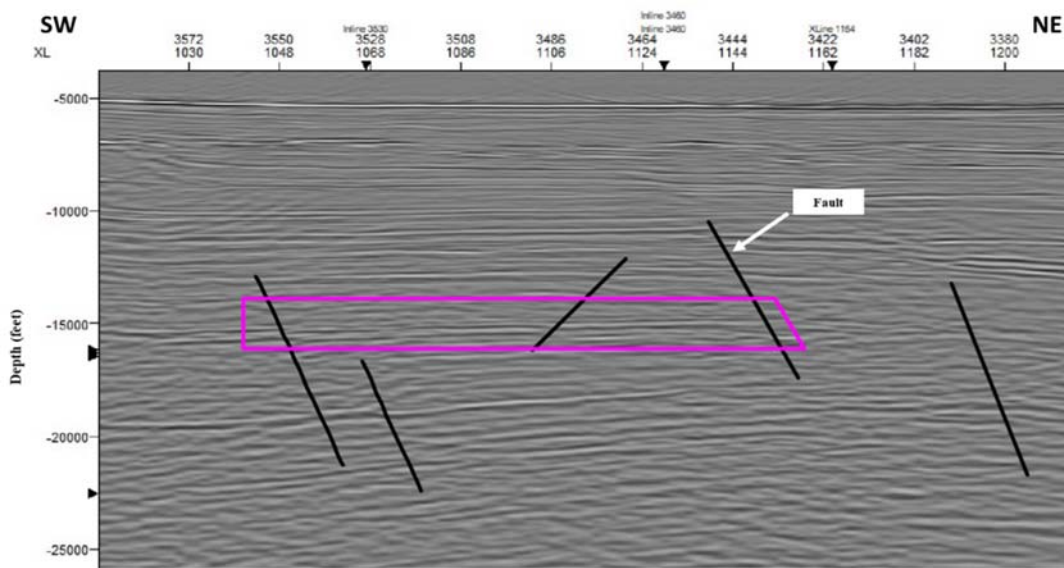
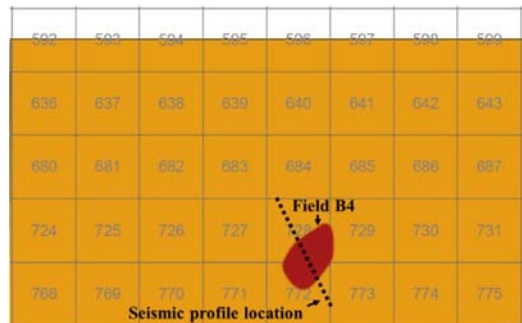


Figure 33. Seismic profile across field B2: MC 771b. Lack of structural trapping mechanism. However, faults are identified. Trapping mechanism is stratigraphic.

d. Field B4: MC 728-772



Location map

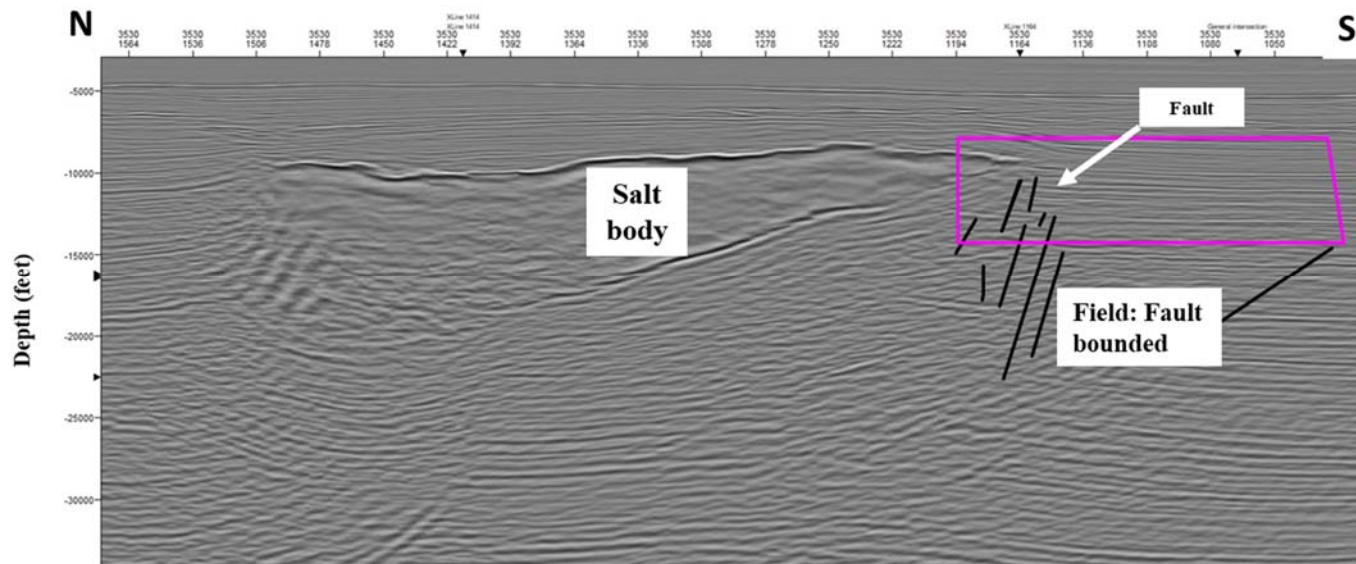


Figure 34. Seismic profile across field B4: MC 728-772. Salt body and faults are identified.

e. Field B5: MC 773

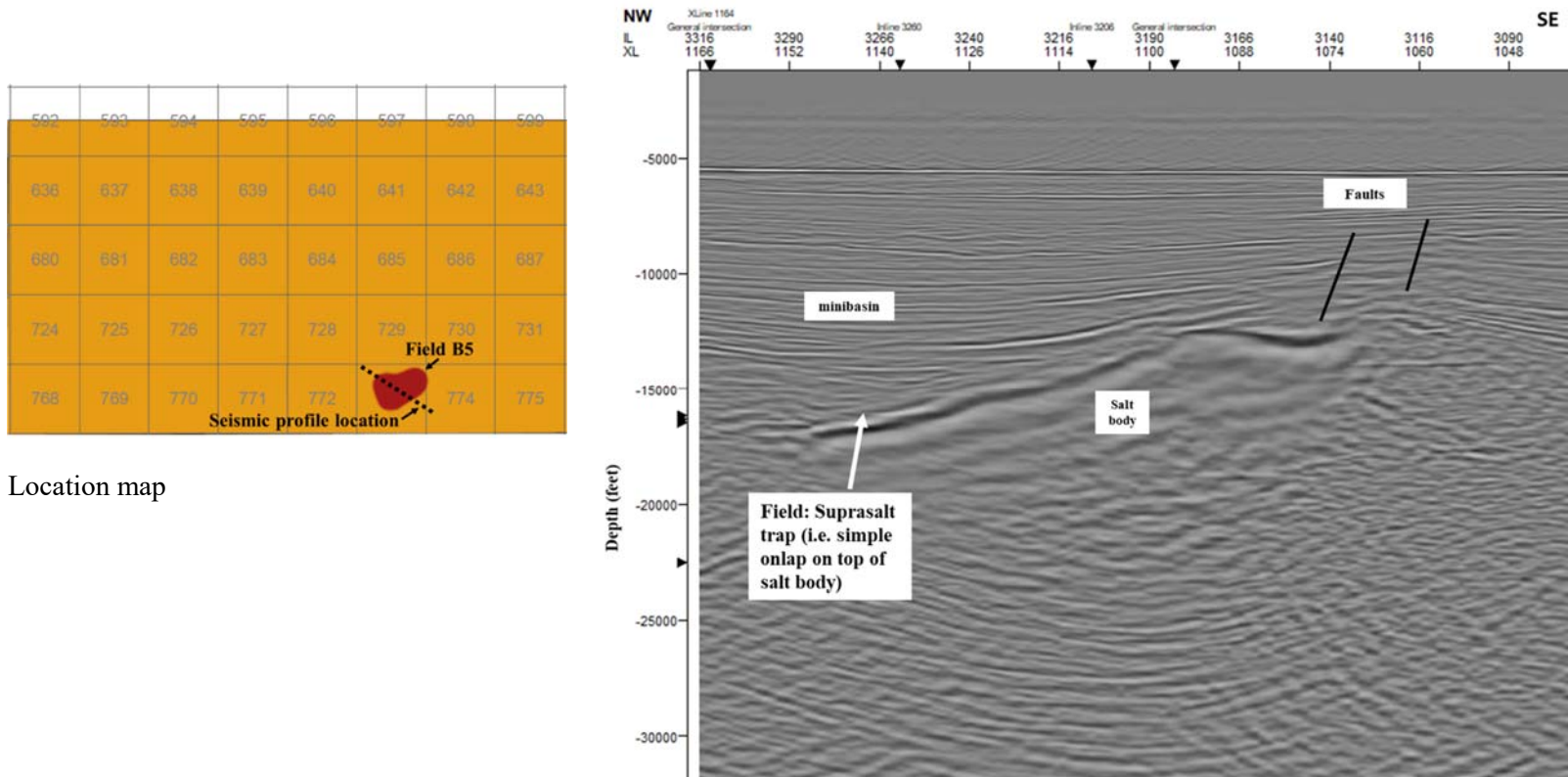
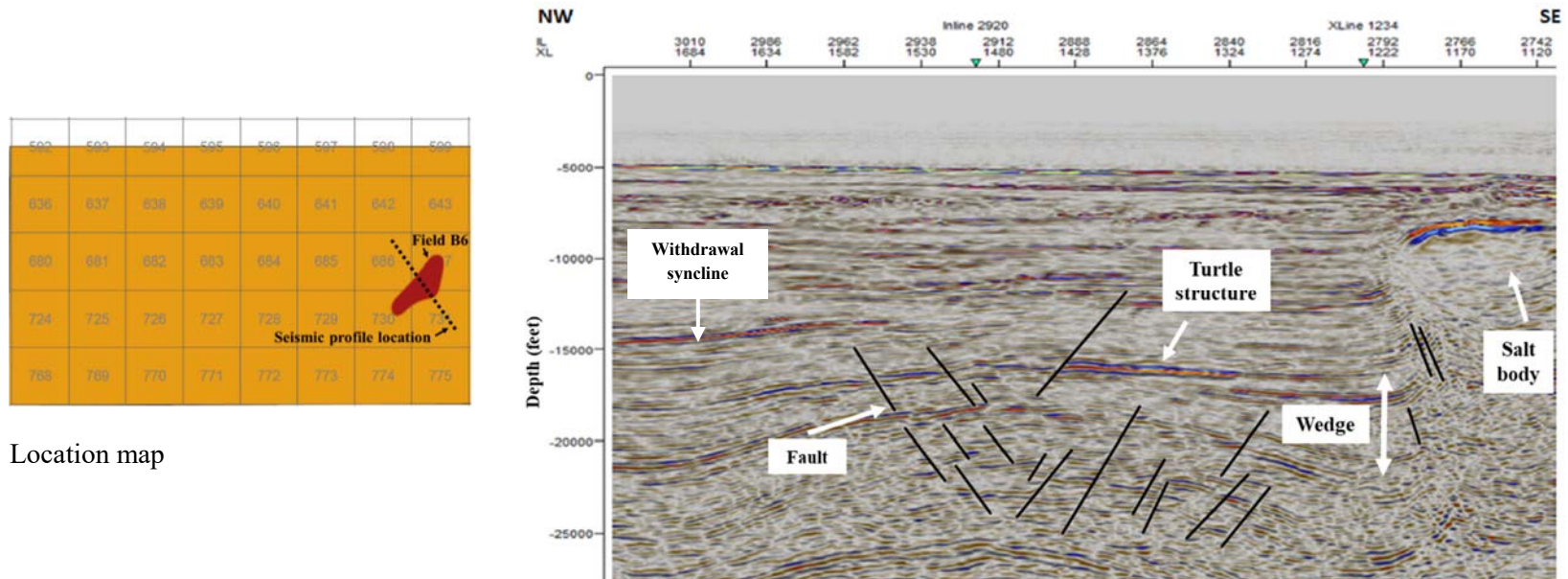


Figure 35. Seismic profile across field B5: MC 773. Salt body, minibasin and faults are identified.

f. Field B6: MC 687-730-731



Location map

Figure 36. Seismic profile across field B6: MC 687-730-731. Withdrawal syncline, faults, turtle structure, stratal wedge geometry and salt body are identified.

Well log (Gamma ray and Resistivity) interpretation

Sediment deposition and reservoir intervals in identified fields were established based on well log Gamma ray signatures (Figs. 37-46). The thick fining-upward successions are interpreted to be channel fills, whereas the thinner serrate to blocky intervals may be lobe deposits.

I. Wells within Study area A

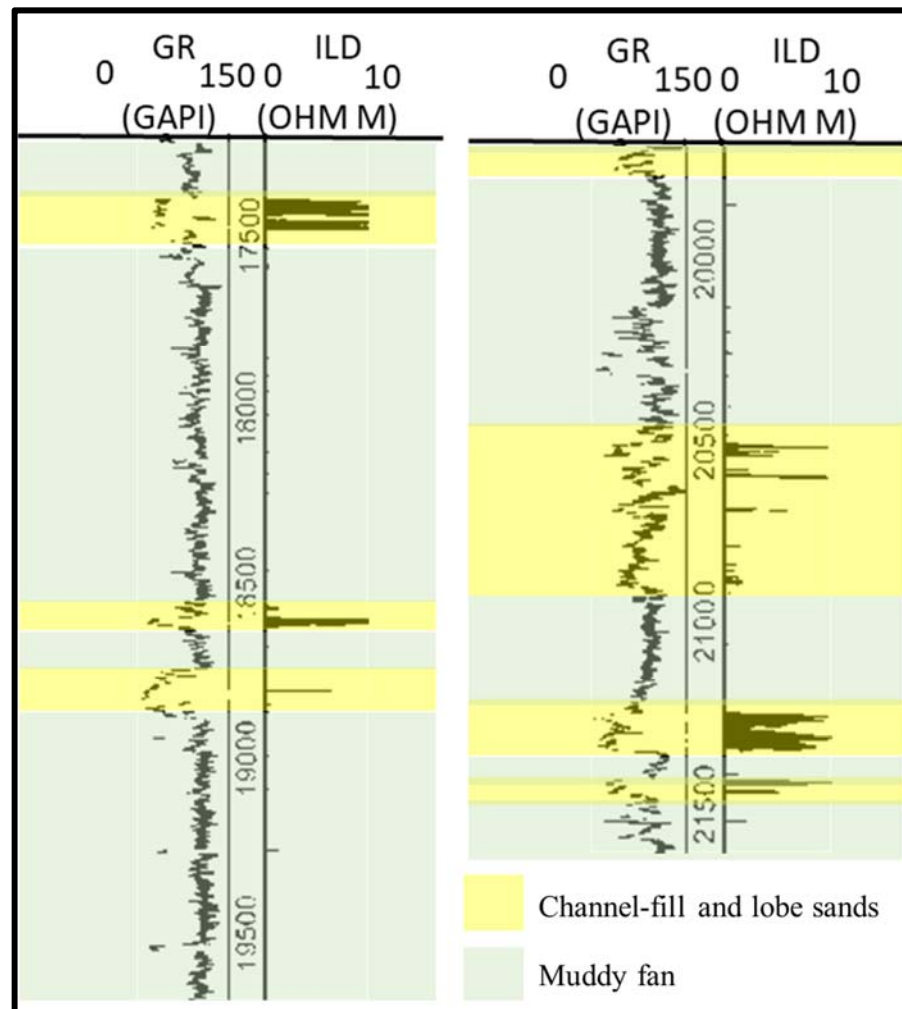


Figure 37: Interpreted geophysical well log from well MC 807-1. Reservoir intervals (yellow) are identified as channel-fill deposits, and occur in field A1: MC 763-805-851. The interbedded log signature is characterized by stacks of increasing and decreasing thicknesses that indicate slope fan deposits made of inter-bedded channel fills and lobe deposits.

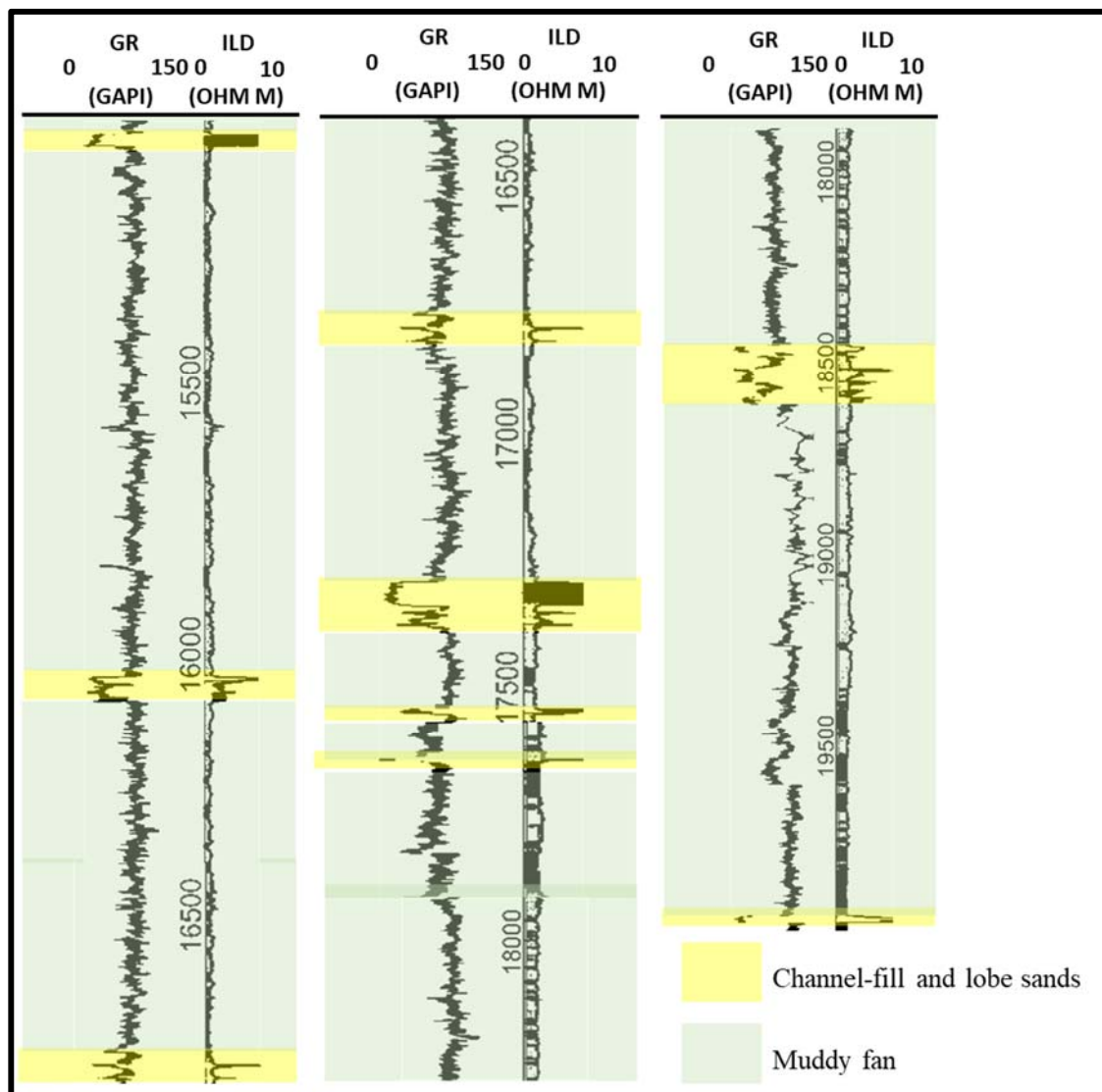


Figure 38: Interpreted geophysical well log from well MC 764-1. Reservoir intervals (yellow) are identified as channel-fill deposits, and occur in Field A2: MC 764-808. The inter-bedded log signature is characterized by thin sandy fans between thicker muddy fans that are indicative of remnant turbidite channels or proximal sea fans.

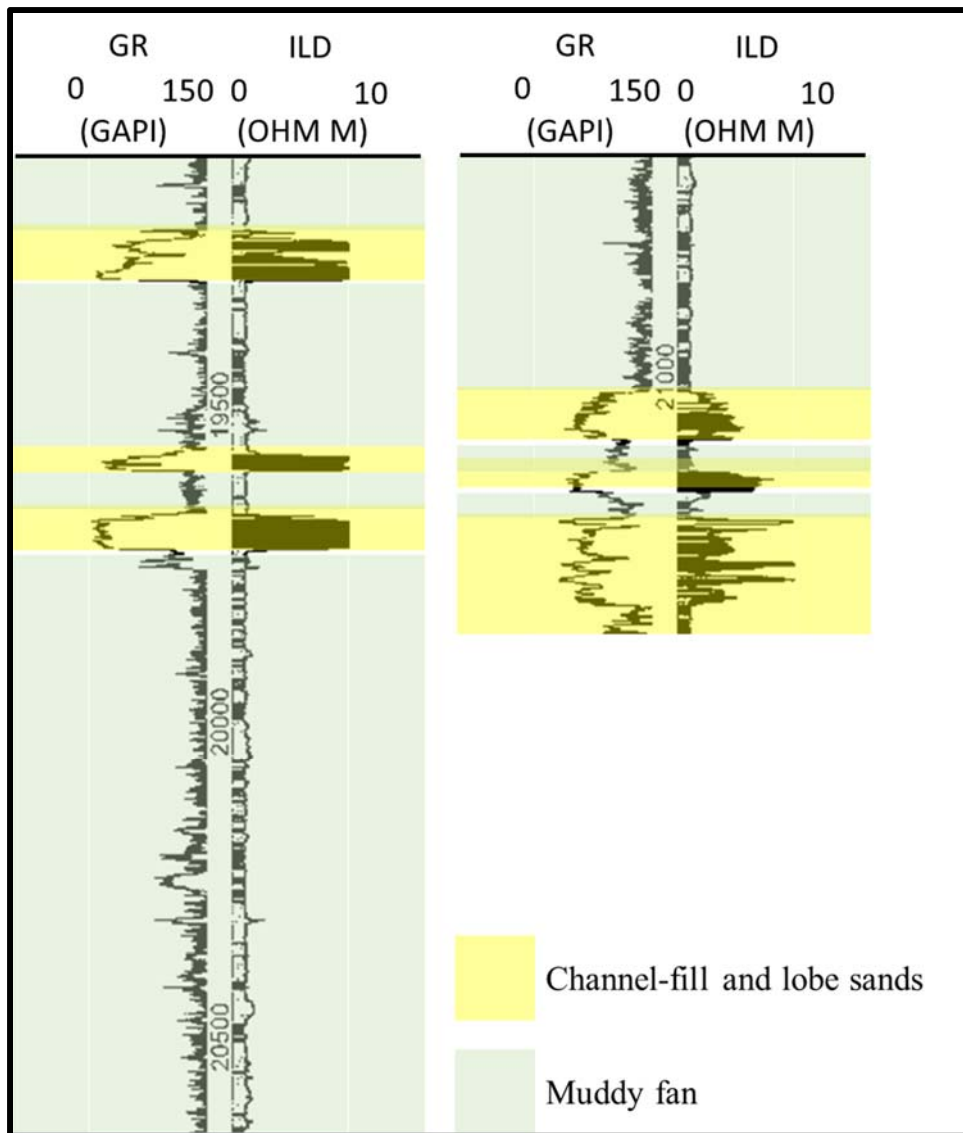


Figure 39: Interpreted geophysical well log from well MC 765-1. Reservoir intervals (yellow) are identified as channel-fill deposits, and occur in field A3: MC 809-810. The serrated well log signature are indicative of deltaic distributaries to turbidite channel complexes.

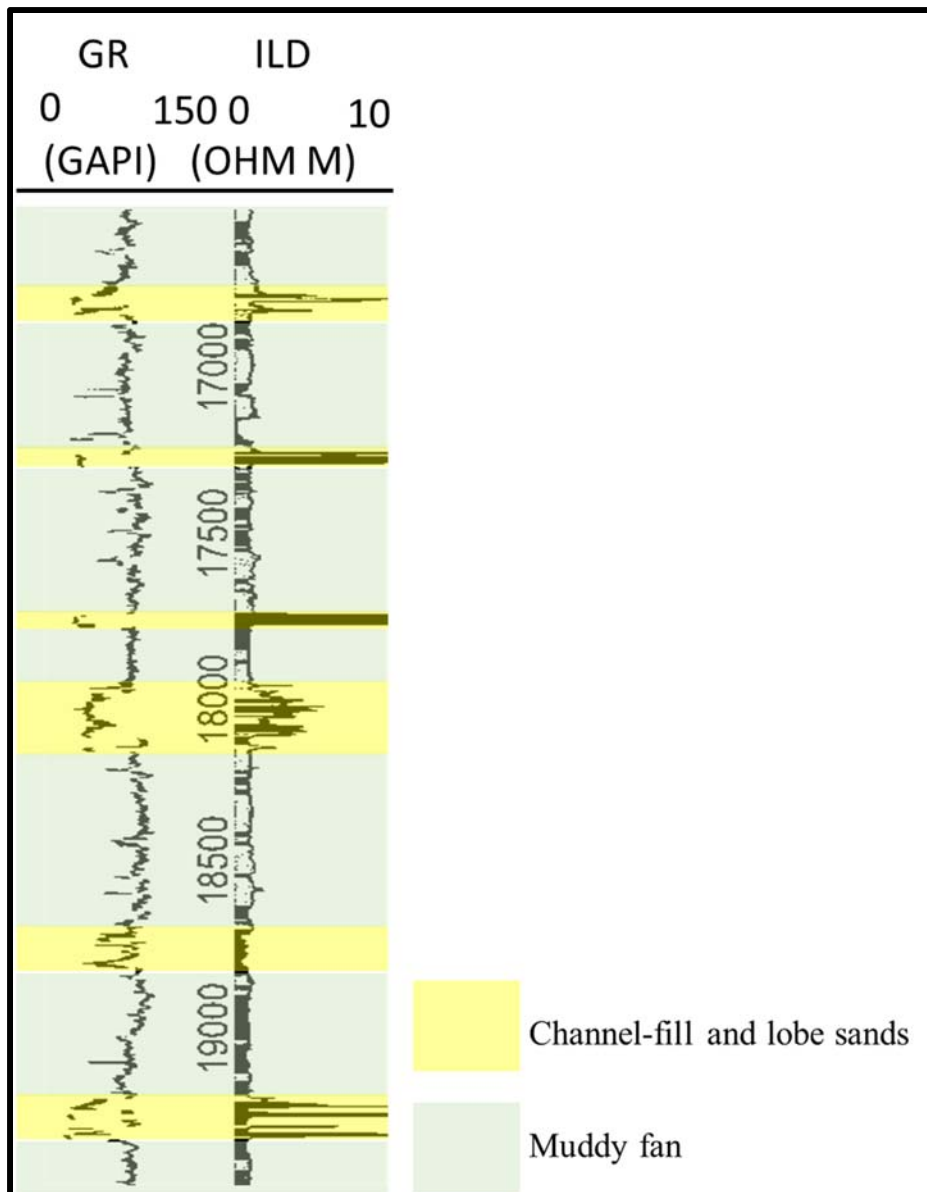


Figure 40: Interpreted geophysical well log from well MC 809-1. Reservoir intervals (yellow) are identified as channel-fill deposits, and occur in field A4: MC 809-810-853-854. The sandy fans indicated above are indicative of a slope fan depositional system as a result of the stacking pattern evident and interbedded character of the well log.

II. Wells within Study area B

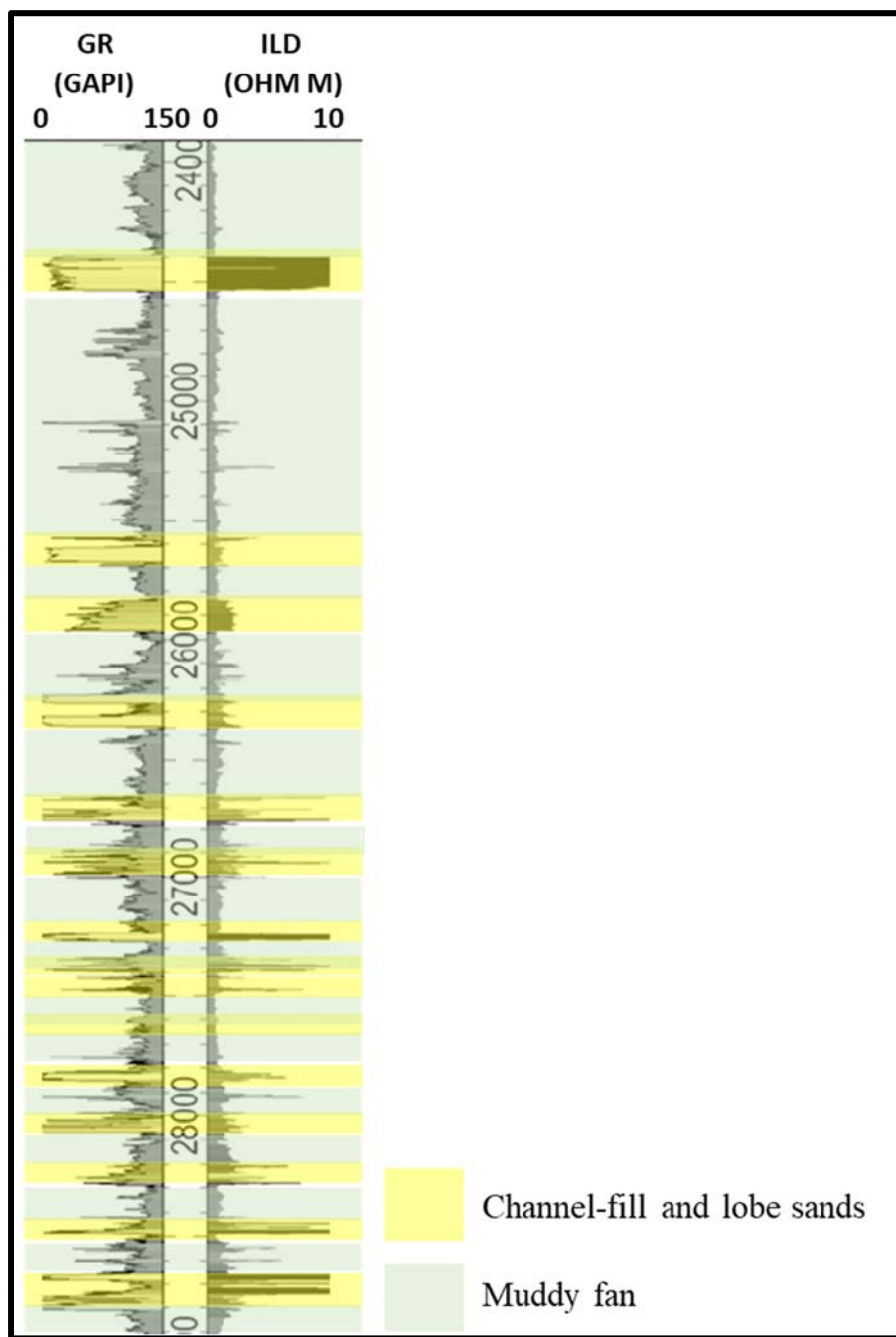


Figure 41: Interpreted geophysical well log from well MC 682-1. Reservoir intervals (yellow) are identified as channel-fill deposits, and occur in field B1: MC 725-726.

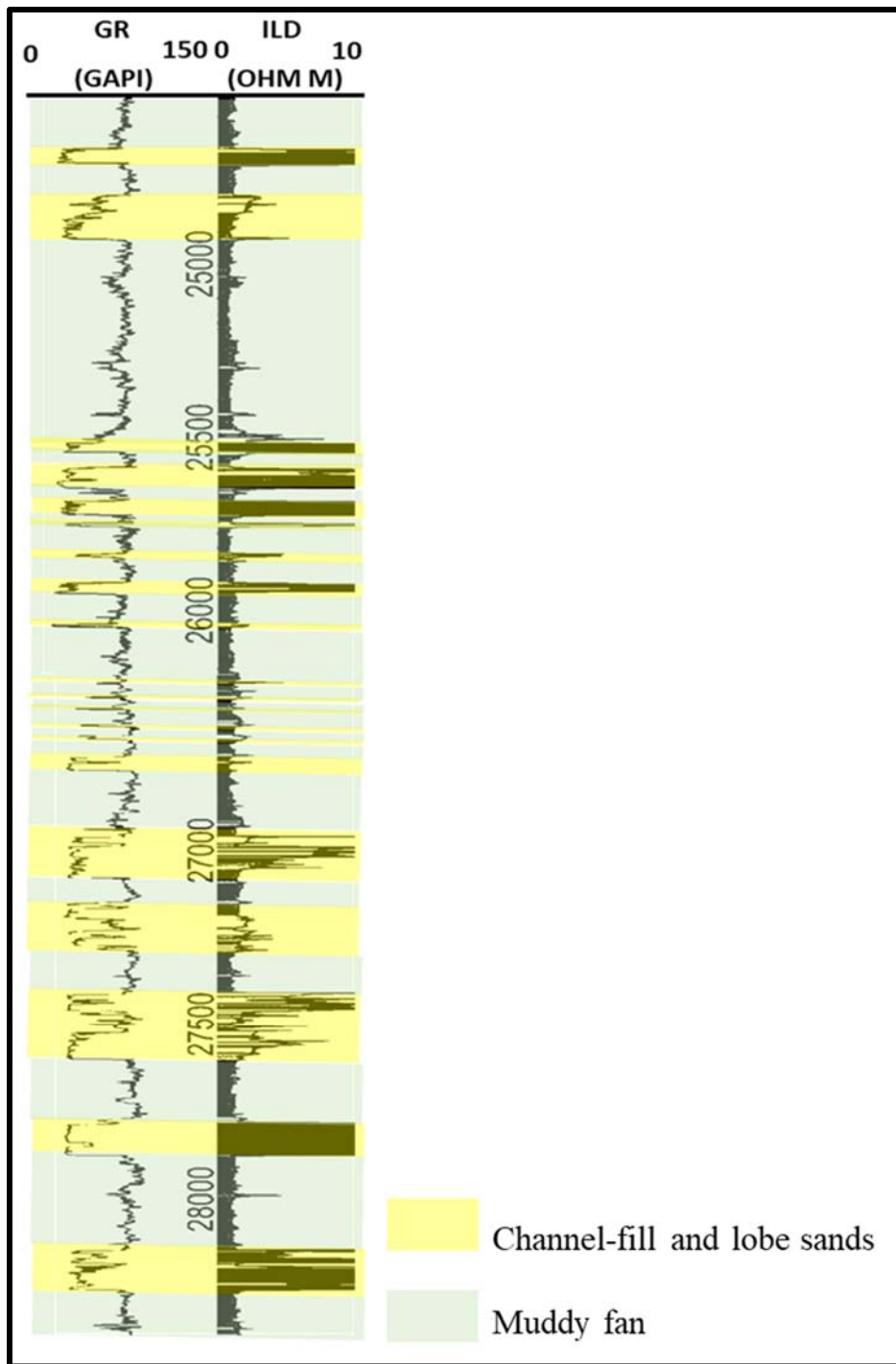


Figure 42: Interpreted geophysical well log from well MC 771-1 (below 24,000 ft). Reservoir intervals (yellow) are identified as channel-fill deposits, and occur in field B2: MC 771a.

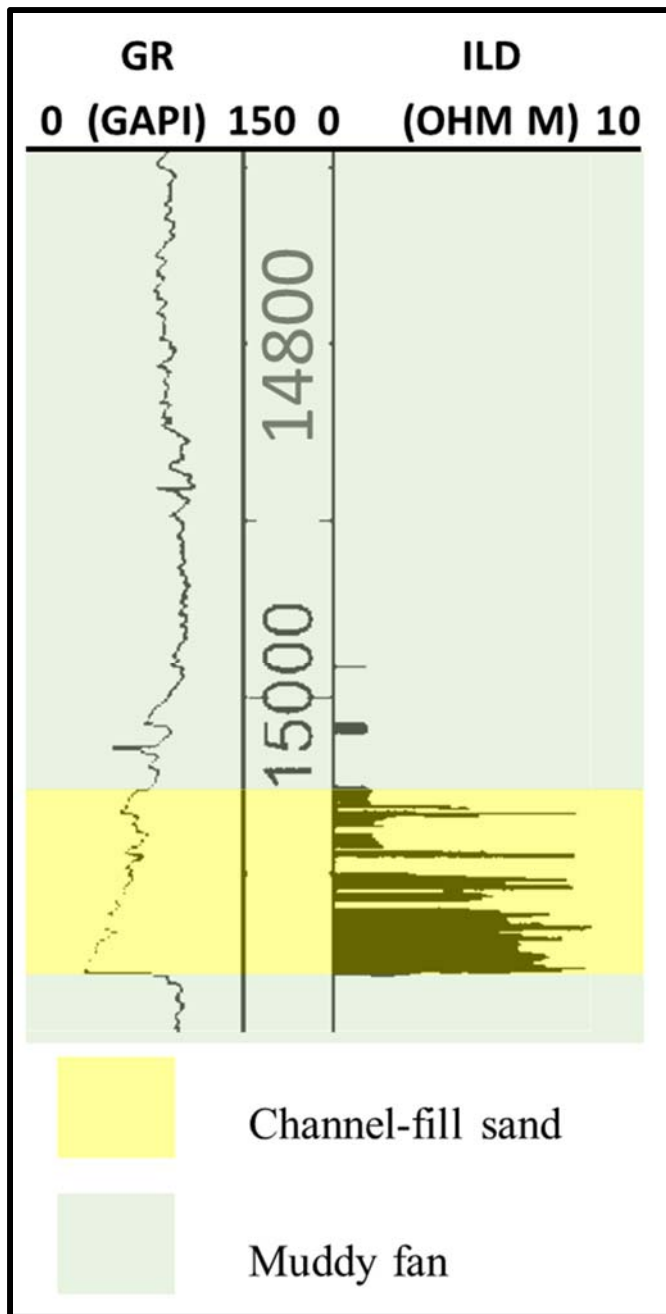


Figure 43: Interpreted geophysical well log from well MC 771-1 (above 15,200 ft). Reservoir interval (yellow) is identified as a channel-fill deposit, and occurs in field B3: MC 771b.

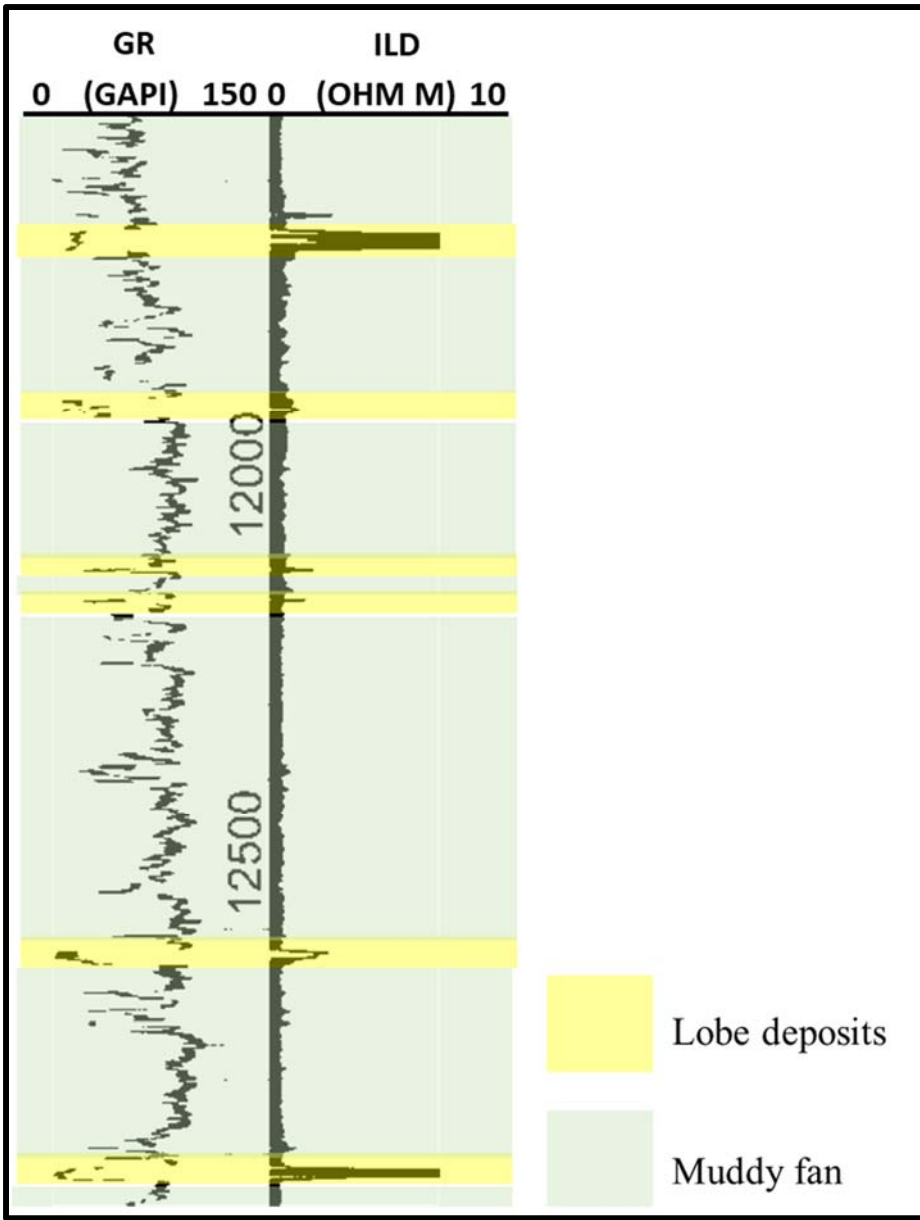


Figure 44: Interpreted geophysical well log from well MC 772-1. Reservoir intervals (yellow) are identified as channel-fill deposits, and occur in field B4: MC 728-772.

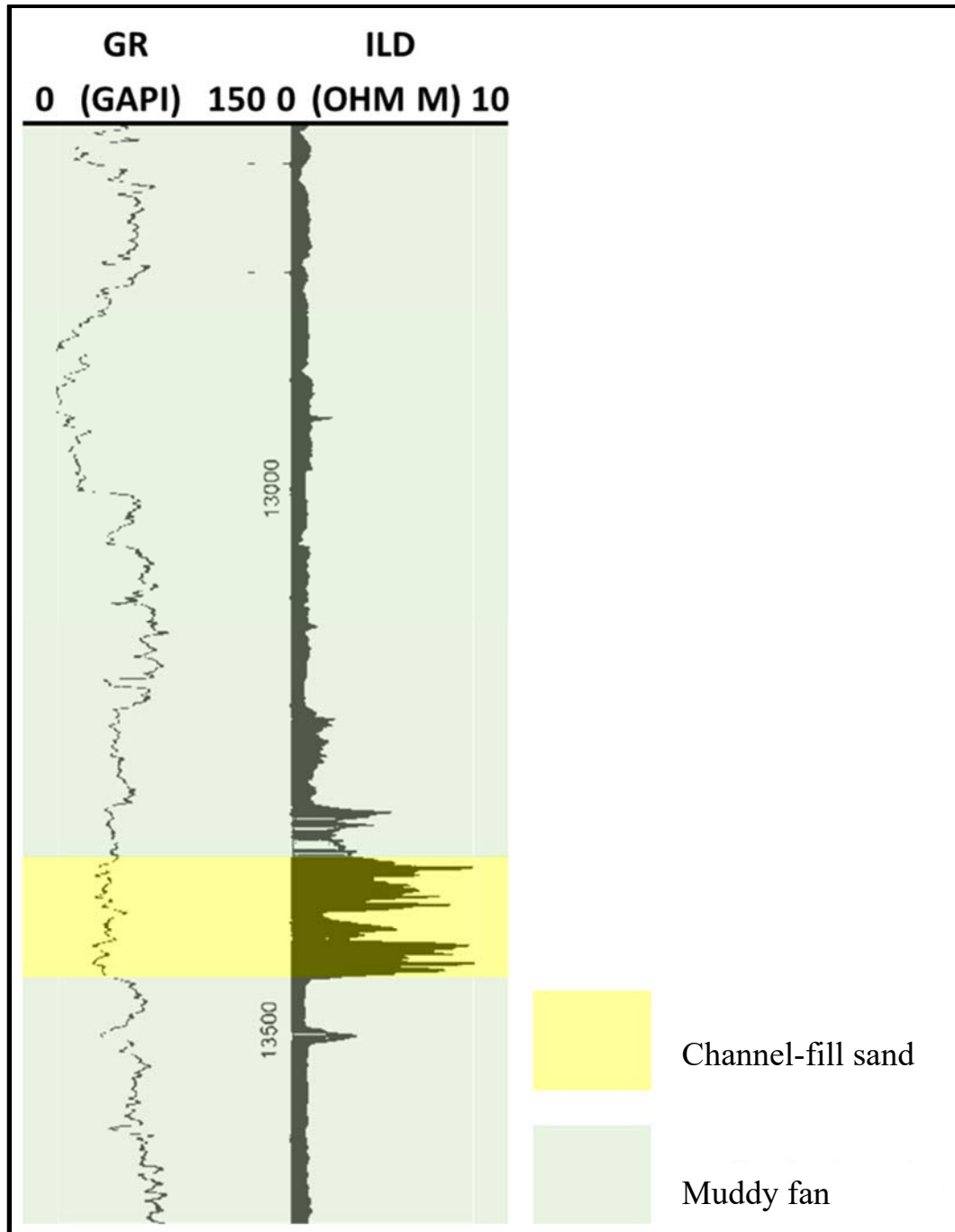


Figure 45: Interpreted geophysical well log from well MC 773-1. Reservoir interval (yellow) is identified as a channel-fill deposit, and occurs in field B5: MC 773.

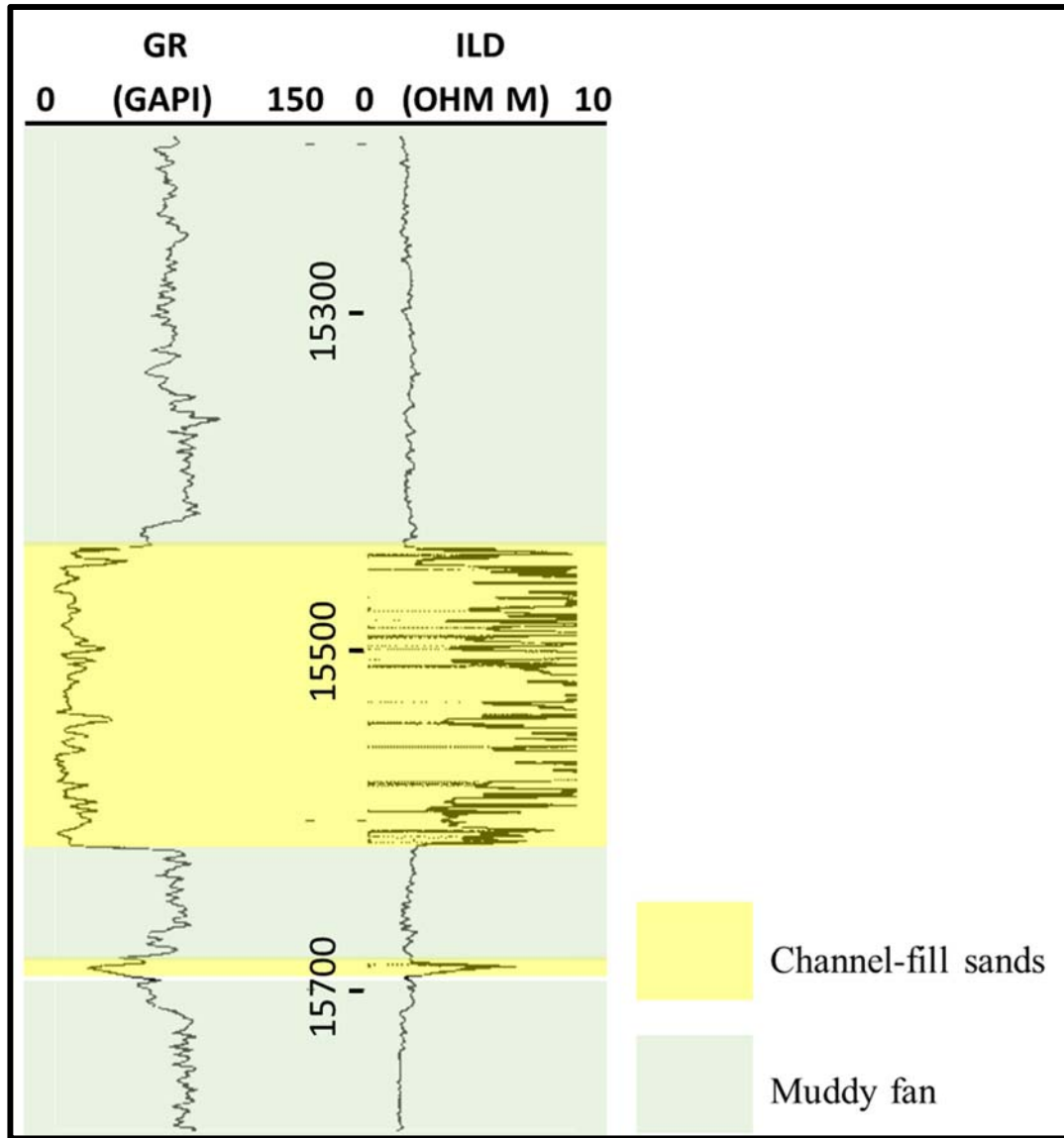


Figure 46: Interpreted geophysical well log from well MC 731-1. Reservoir intervals (yellow) are identified as channel-fill deposits, and occur in field B6: MC 687-730-731. The sand package indicated above indicates an aggradational fill.

Field analysis summary information – Study area A

The fields in study area A are characterized by turbidite sand deposits, and salt-related trapping mechanisms (Table 3). Reservoirs in study area A are relatively thick, have average porosities greater than 20%, and are Miocene to Pliocene in age.

Table 3. Field analysis summary: Study area A.

Field	Reservoir age	Sediment Deposition of reservoir	Trapping mechanism	Porosity (%)	Seal lithology above reservoir	Reservoir thickness (feet)	Well used for analysis	Water Depth (feet)
A1	Late Miocene	Turbidite sands (wedge geometry)	Subsalt trap against salt/weld; Fault-bounded trap	20-30	Salt and secondary laterally extensive shale	850	MC 807-1	2980
A2	Late Miocene	Turbidite sands (sheet geometry)	Subsalt trap against base of salt/weld	20-30	Salt and secondary laterally extensive shale	550	MC764-1	2950
A3	Late Miocene	Turbidite sands (sheet and wedge geometry)	Subsalt trap against base of salt/weld	25-29	Salt and secondary laterally extensive shale	750	MC765-1	3650
A4	Late Miocene to Early Pliocene	Turbidite sands (sheet and wedge geometry)	Subsalt trap against base salt/weld	24-29	Salt and secondary laterally extensive shale	500	MC809-1	3900

Field analysis summary information – Study area B

The fields in study area A are characterized by channel-fill deposits (Table 4). The reservoirs have variable porosities and are Miocene to Pliocene in age.

Table 4. Field analysis summary: Study area B.

Field	Reservoir age	Sediment Deposition and geometry of reservoir	Trapping mechanism	Porosity (%)	Seal lithology above reservoir	Reservoir intervals based on well logs (feet)	Well used for analysis	Water Depth (feet)
B1	Middle Miocene	Channel-fill sands (bowl geometry)	Subsalt trap against base of salt/weld	16-28	Salt and secondary laterally extensive shale	800 (cumulative)	MC 682-1	4300
B2	Middle Miocene	Channel-fill sands (bowl geometry)	extensional anticlinal fold-turtle	Very poor porosity data	Shale	Highly variable	MC771-1	5000
B3	Late Miocene	Channel-fill sands (wedge geometry)	Stratigraphic	Very poor porosity data	Shale	150	MC771-1	5420
B4	Late Miocene – Early Pliocene	Channel-fill sands (wedge geometry)	Fault-bounded trap	Very poor porosity data	Shale	Highly variable intervals	MC772-1	5630
B5	Late Miocene – Early Pliocene	Channel-fill sands(wedge geometry)	Subsalt trap against salt/weld	27-30	Shale	200	MC773-1	5607
B6	Late Miocene	Channel-fill sands (wedge geometry)	Faulted extensional anticlinal trap-turtle	30	Shale	550	MC731-1	5300

CO₂ storage assessment

Under normal hydrostatic and geothermal gradient, reservoirs have to capability to store CO₂ in a supercritical state at approximately 2,470 ft. For this reason, Storage objectives considered for this project are deep enough and plot in the supercritical envelope of the CO₂ temperature-pressure phase diagram (Fig. 47). The CO₂ storage objective assessment for this study focuses on two minibasins located in the south east section of study area A. Both storage objectives, Alpha and Beta are characterized by closure mechanisms influenced by salt tectonics. The CO₂ density used for the CO₂ storage resource assessment was derived from the pressure-temperature chart designated for CO₂ (Fig. 48) under various hydrostatic and lithostatic pressure conditions (Bachu, 2003). The efficiency factors of Goodman et al., 2011 and NETL 2012 were incorporated into calculating the storage estimates. The average reservoir pressure and temperature data used for the calculations were based on associated reservoir pressure data within MC 731 block (Razi and Balinski, 2012).

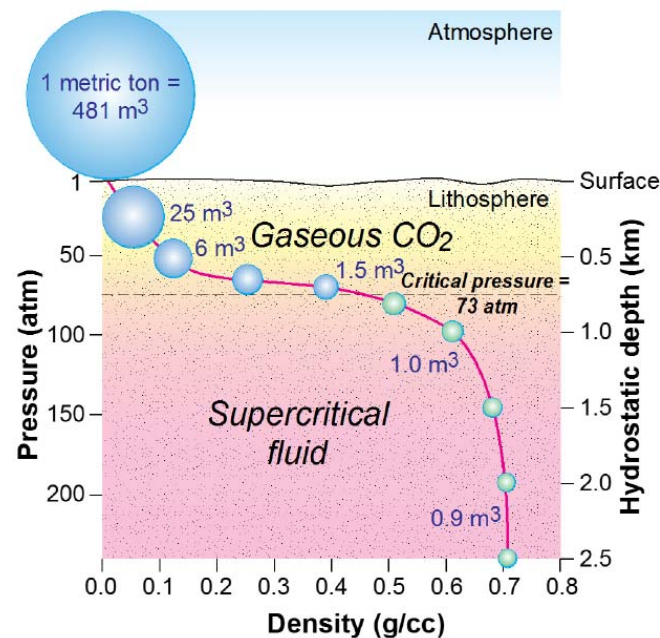


Figure 47: Effect of burial depth on CO₂ density (Pashin, 2016)

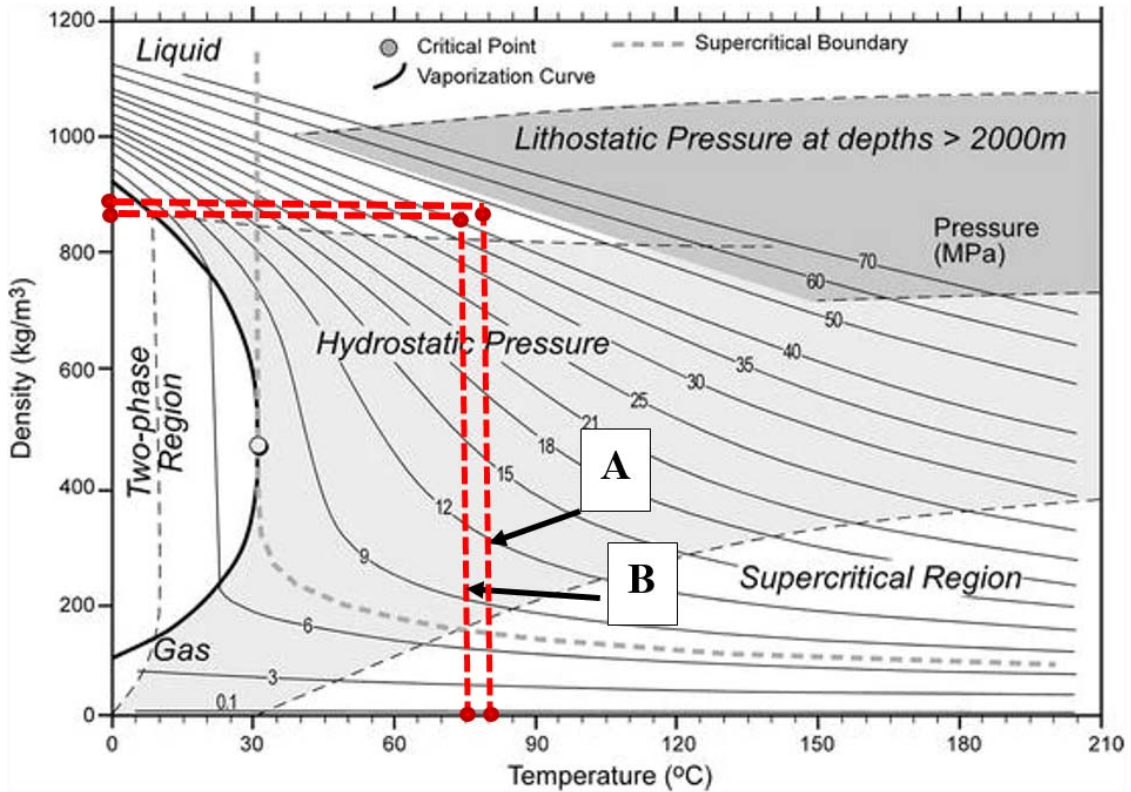


Figure 48. CO₂ density as a function of temperature and pressure (after from Bachu, 2003). Average estimates for storage objectives Alpha (A) and Beta (B) are plotted.

I. Storage objective Alpha

Well log signatures within storage objective Alpha (Fig. 45) are characterized by channel sands. The reservoir is adjacent to allochthonous salt and is emplaced within the salt-minibasin province in the Mississippi Canyon protraction area. The trapping mechanism is a faulted closure (Fig. 49). The reservoir porosity ranges from 27 to 33% and, the net sand thickness is approximately 200 ft. The reservoir permeability is up to 1 Darcy. The reservoir structure spans Mississippi Canyon blocks 729, 772, and 773, and is present at depths shallower than 14,000 ft. The reservoir pressure is approximately 45 MPa. Based on seismic

interpretation, in combination with the petrophysical data, the reservoir sands are interpreted to be part of turbiditic successions.

II. Storage objective Beta

Well log signatures within storage objective Beta (Fig. 46) are characterized by sands that exhibit blocky signatures with aggradational depositional patterns. Generally, such Gamma ray signatures are associated with fine-grained sands. Additionally, these sands generate good reservoir quality as a result of low shale content, and associated high energy depositional conditions Furthermore, the Gamma ray signature can be associated with channel-fill sands deposited the distal sections of turbidite sequences.

The reservoir structure within storage objective Beta covers Mississippi Canyon blocks 686, 687, 730, 731, 744, and 745, (Fig. 49) and is present at depths of 15,200 to 15,790 ft. The average porosity is 30% and the permeability is up to 1 Darcy. The reservoir pressure is approximately 40 MPa. Based on the seismic interpretation of the aggradational sand fill in well MC 730-1, the reservoir sands are interpreted to be amalgamated turbidite sands. The trapping mechanism is a faulted closure (Fig. 49).

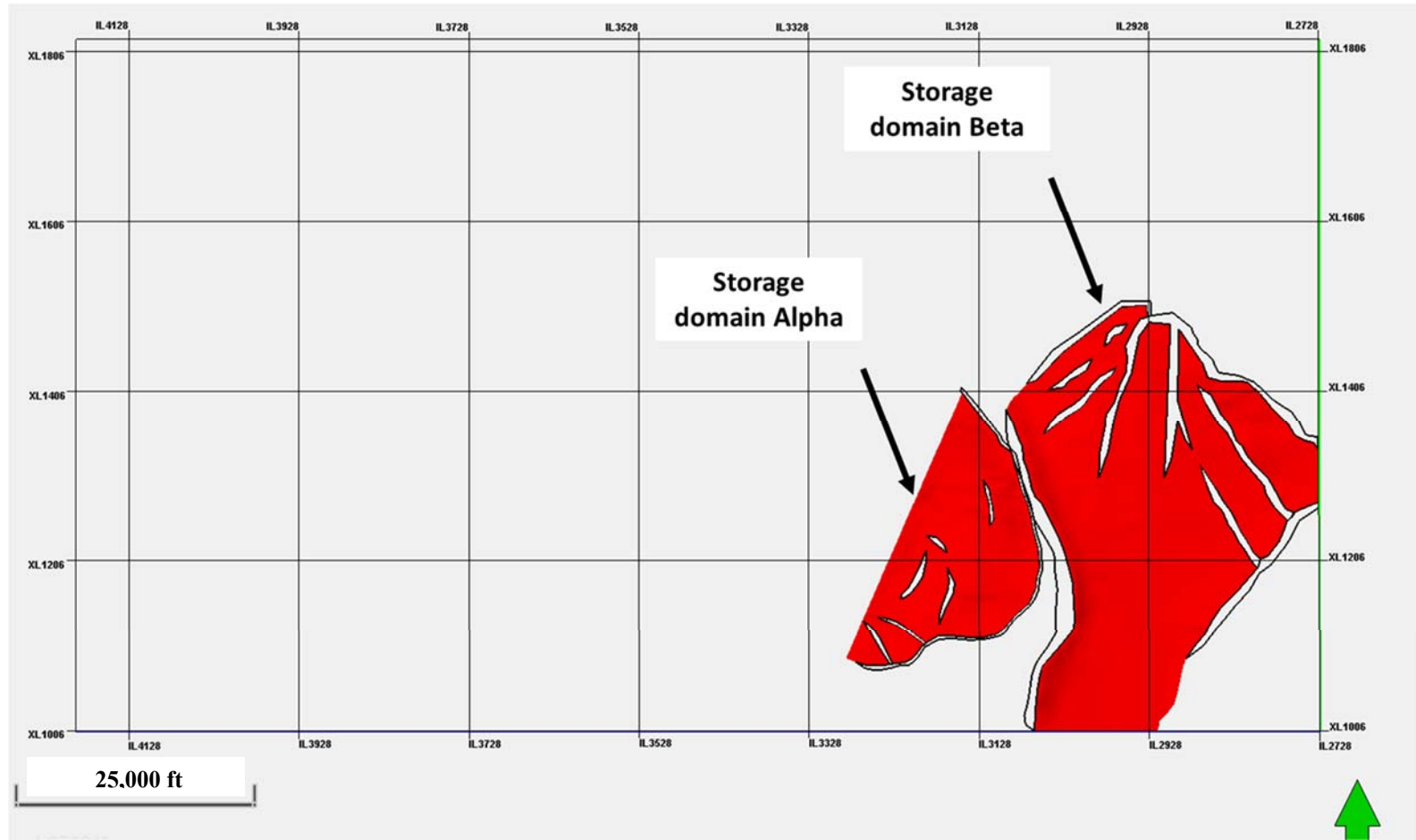


Figure 49. Location of assessed storage objectives within study area B.

Storage objective Alpha: Structure

The potential storage areas in storage objective Alpha (A and B), are bounded by faults, and are emplaced at relatively shallower depths. The general structural geometry is a syncline fault-bounded to the East (Fig. 50). Additionally, at the eastern boundary, an overhanging salt body is present (Fig. 51).

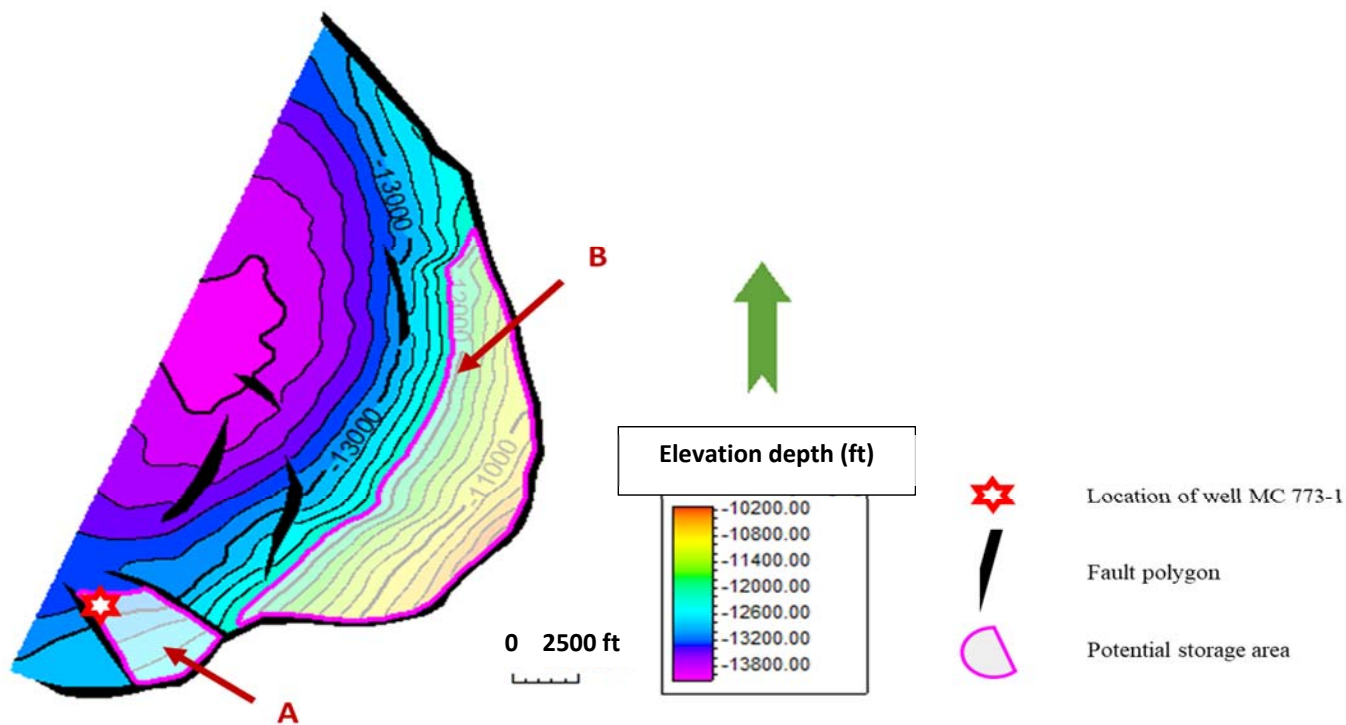


Figure 50. Depth structure map of reservoir horizon (channel sands in well MC 773-1) within storage objective Alpha. Potential storage areas (A and B) are indicated with pink polygons.

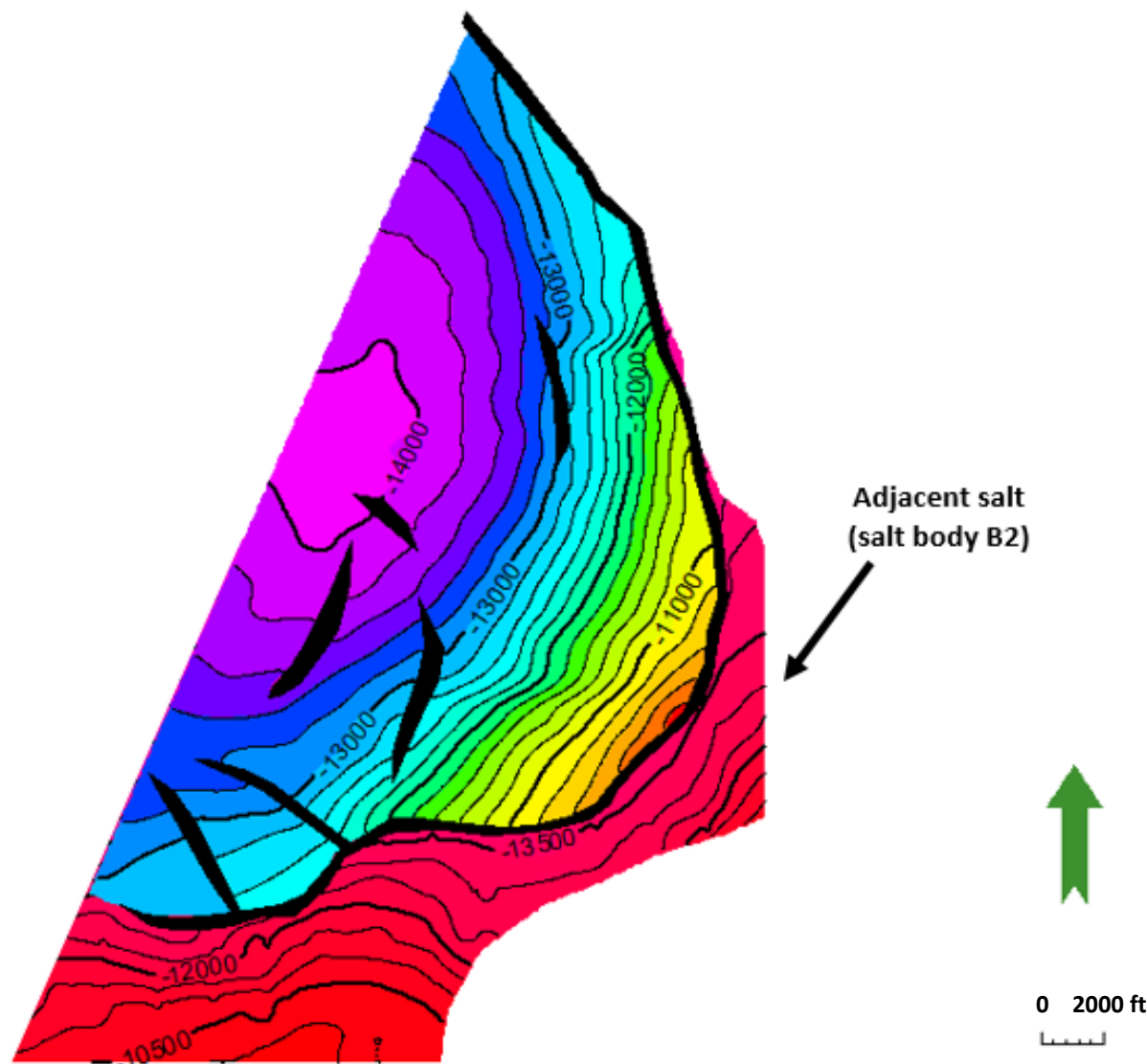


Figure 51. Depth structure map of reservoir horizon (channel sands in well MC 773-1) within storage objective Alpha, with adjacent overhanging salt body. Black solid polygons indicate fault polygons.

Storage objective Alpha: Hydrocarbon indicator

The RMS amplitude is suppressed below salt overhangs. Based on structural position, continuity of imaging, and proven production, the reservoir areas extend under overhangs. RMS seismic attributes amplifies regions that house hydrocarbons for potential further production. Based on hydrocarbon accumulation signatures in the RMS amplitude volume, the plausible position for potential CO₂-EOR target will be within potential storage area A (Fig. 52). Potential storage area A is approximately 12 km², whereas potential storage area B is approximately 67 km² (Table 5). CO₂ storage resource estimates based on efficiency factors from Goodman et al., (2011) range from approximately 90 to 293 Mt (Table 6).

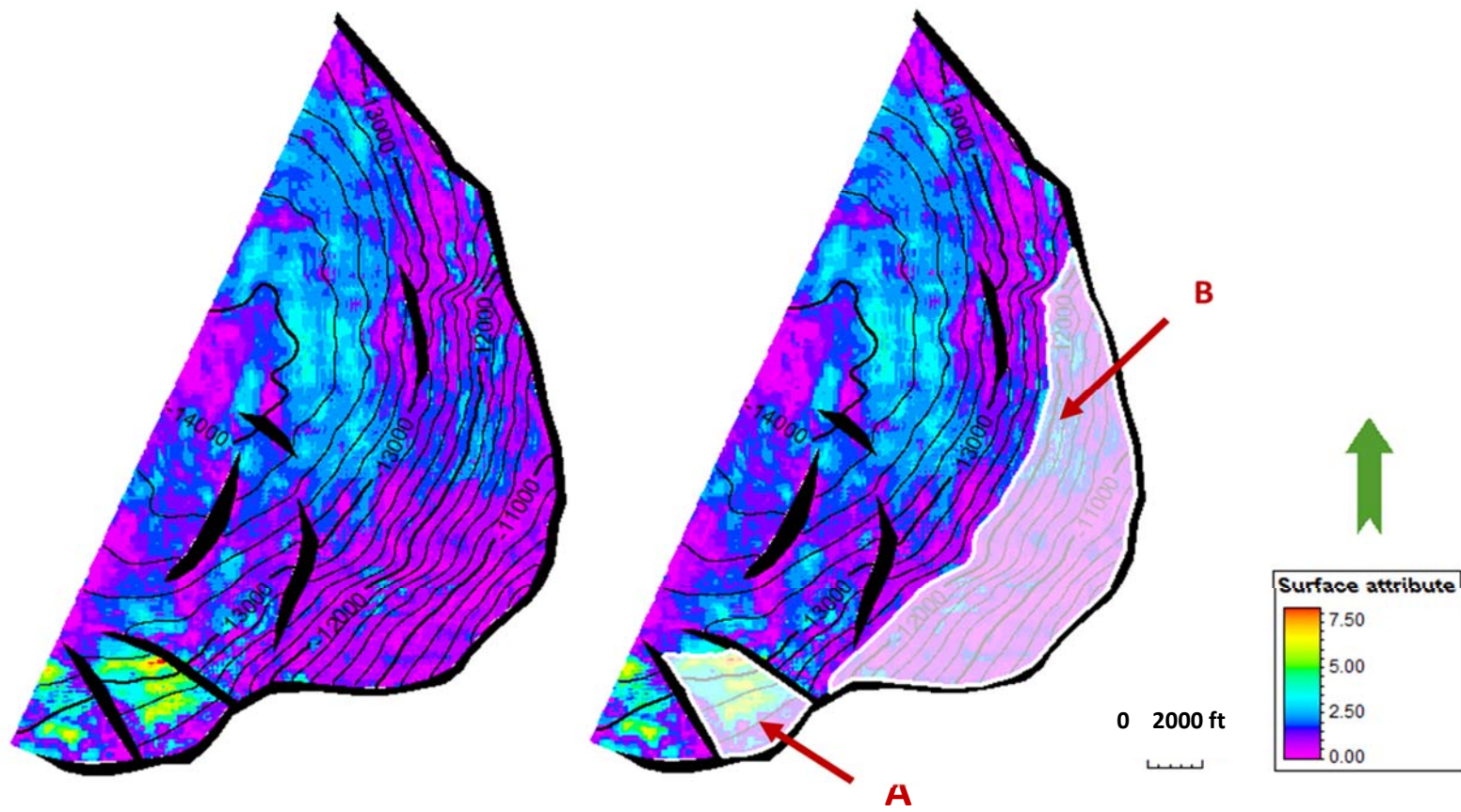


Figure 52. RMS attribute map of reservoir horizon (channel sands in well MC 773-1) within storage objective Alpha to identify hydrocarbon indicators like bright spots.

Reservoir properties: Storage objective Alpha

- Age: Late Miocene to early Pliocene
- Depositional character: Channel sands
- Average porosity: 28.5%; Permeability: up to 1 Darcy
- Mississippi Canyon protraction area blocks covered: MC 729, MC 772, MC 773
- Sandstone thickness: 200 ft
- Reservoir temperature (Celsius): 80 °C
- Average reservoir pressure: 45 MPa
- CO₂ density at reservoir depth: 890 kg/m³

Table 5: Potential storage areas: Storage objective Alpha

Potential storage area	Area (km ²)
A	12.0649
B	66.8548
Total	78.9197

Table 6: CO₂ Storage resource: Storage objective Alpha.

CO ₂ Storage resource (Mt) (Efficiency factors from Goodman et al., 2011)	Alpha		Total (Mt)
	A	B	
P10 (CO ₂ Efficiency factor = 7.4 %)	13.80	76.50	90.30
P50 (CO ₂ Efficiency factor = 14 %)	26.12	144.72	170.84
P90 (CO ₂ Efficiency factor = 24 %)	44.77	248.10	292.87

Storage objective Beta: Structure

The potential storage areas in storage objective Beta, are bounded by faults , and are emplaced at relatively structural high. The general structural geometry is an extensional anticlinal fault-bounded framework (Fig. 53). Additionally, at the western boundary, a deeper salt body is present (Fig. 54). However, an overhanging salt body is emplaced at the eastern boundary (Fig. 54).

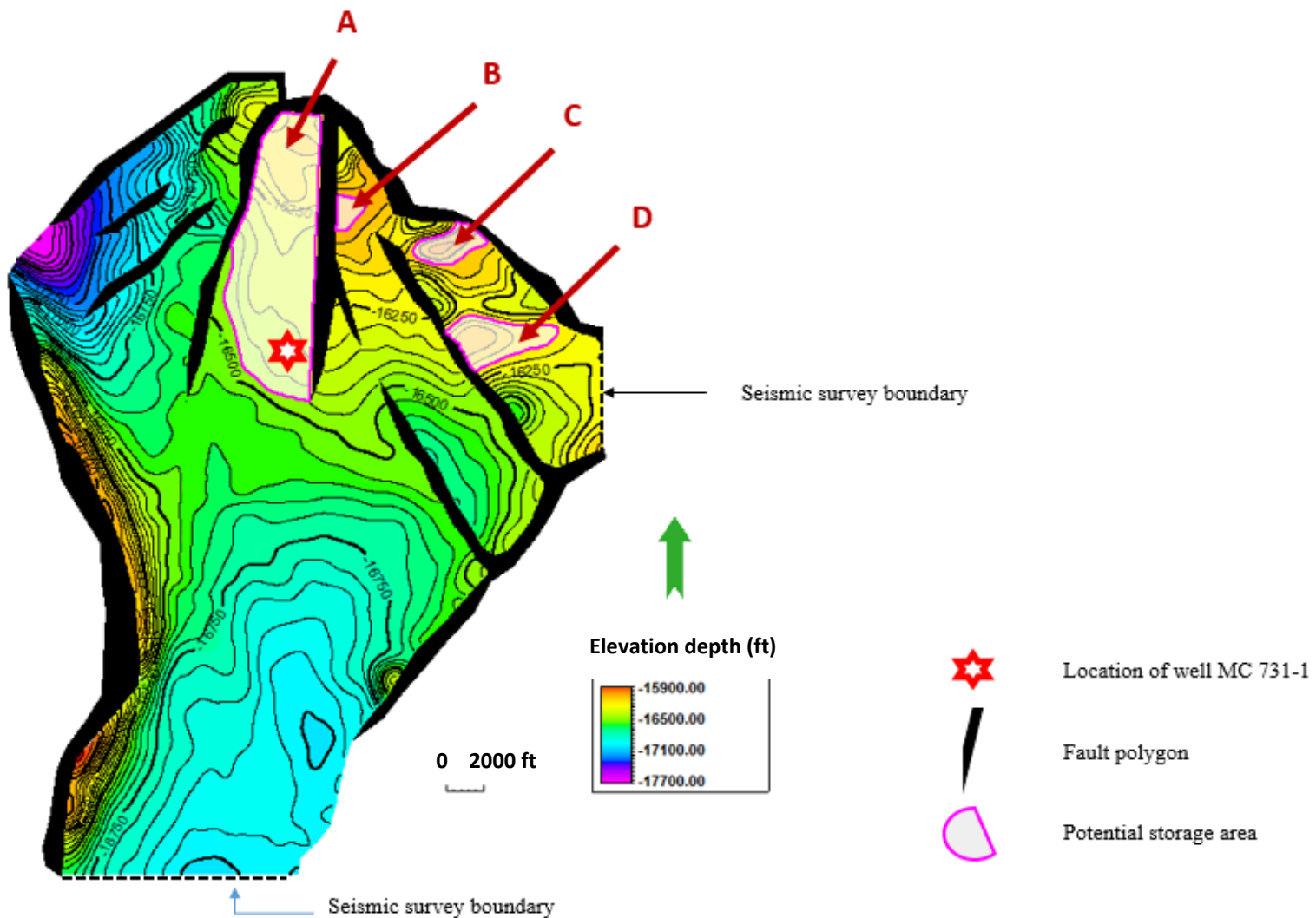


Figure 53. Depth structure map of reservoir horizon (amalgamated sands in well MC 731-1) within storage objective Beta. Potential storage areas (A to D) are indicated with pink polygons. The potential storage areas are bounded by faults and structural highs.

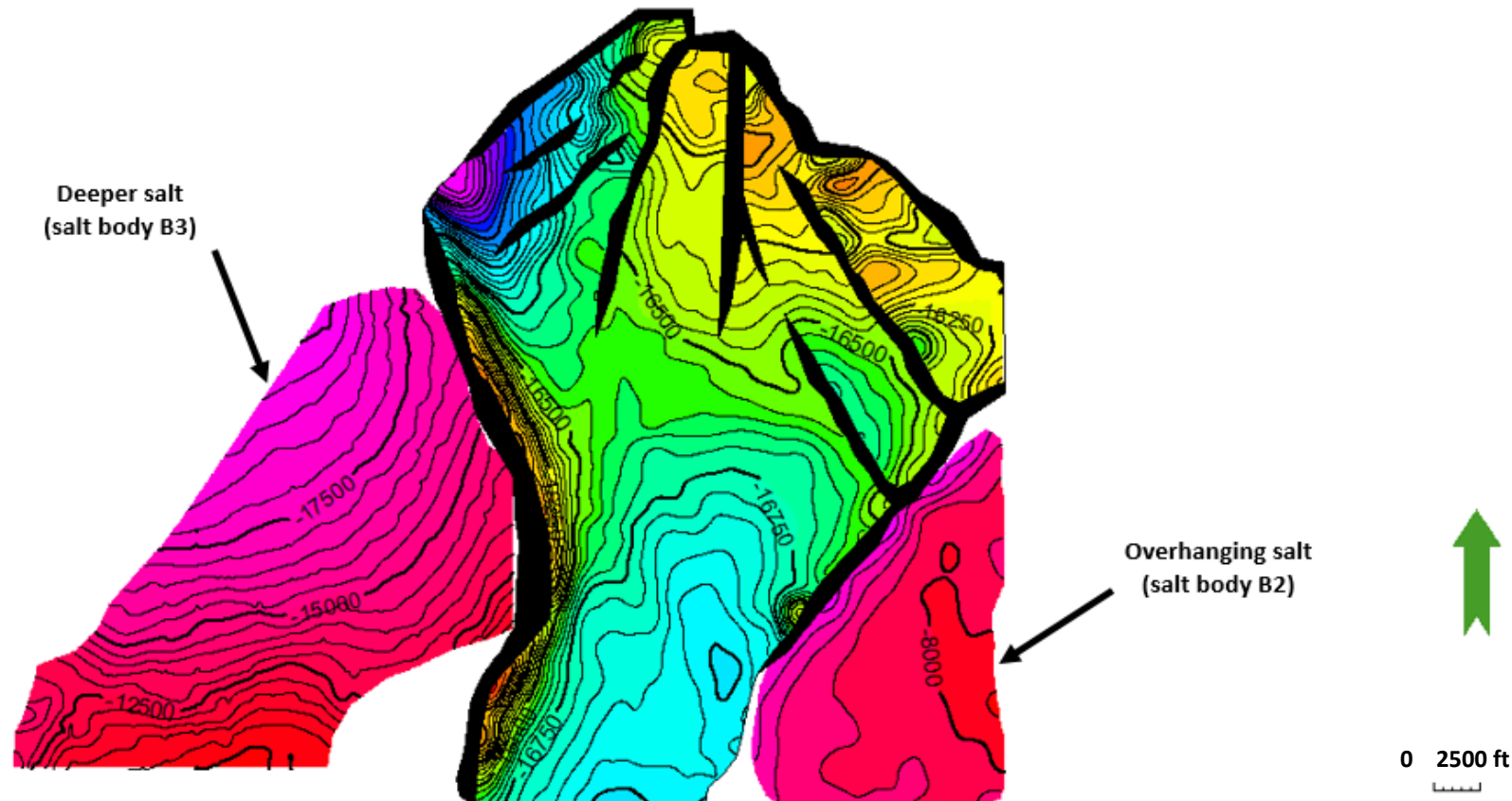


Figure 54. Depth structure map of reservoir horizon (amalgamated sands in well MC 731-1) within storage objective Beta, with adjacent salt bodies. Black solid polygons indicate fault polygons.

Storage objective Beta: Hydrocarbon indicator

The RMS amplitude is suppressed below salt overhangs. Based on structural position, continuity of imaging, and proven production, the reservoir areas extend under overhangs. RMS seismic attributes amplifies regions that house hydrocarbons for potential further production. Based on hydrocarbon accumulation signatures in the RMS amplitude volume, the plausible position for potential CO₂-EOR target will be within potential storage area A (Fig. 55). Potential storage area A, B, C and D are approximately 59, 2, 5 and 10 km² respectively (Table 7). CO₂ storage resource estimates based on efficiency factors from Goodman et al., (2011) range from approximately 252 to 817 Mt (Table 8).

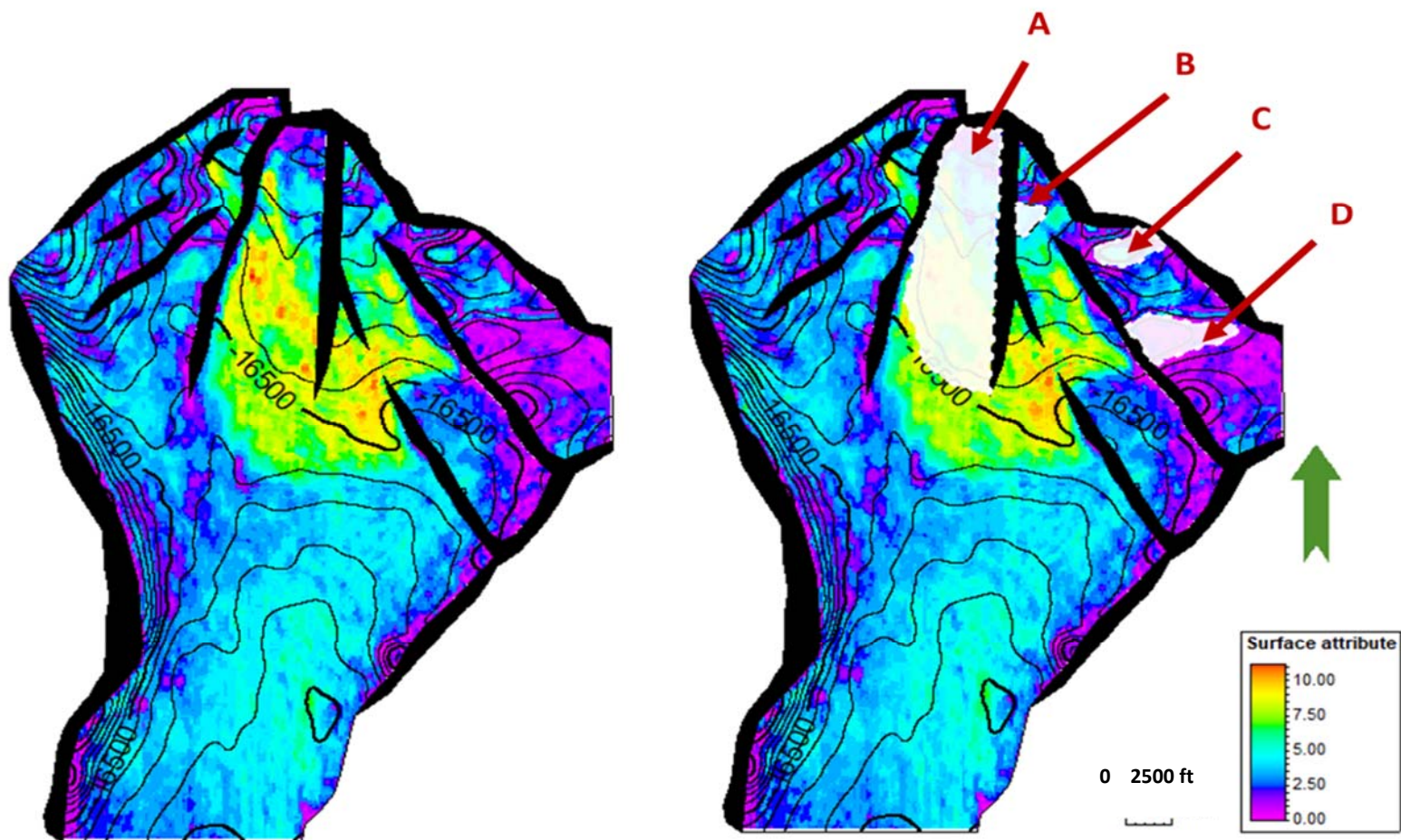


Figure 55. RMS attribute map of reservoir horizon (amalgamated sands in well MC 731-1) within storage objective Beta to identify hydrocarbon indicators like bright spots.

Reservoir properties: Storage objective Beta

- Age: Upper Miocene
- Turbidite sands
- Average porosity: 30%; Permeability: up to 1 Darcy
- Mississippi protraction area blocks covered: MC 686, MC 687, MC 730, MC 731
- Sandstone thickness: 550 ft
- Reservoir temperature: 75 °C
- Average reservoir pressure: 40 MPa
- CO₂ density at reservoir depth: 880 kg/m³

Table 7: Potential storage areas: Storage objective Beta

Potential storage area	Area (km ²)
A	59.3700
B	2.1762
C	5.2509
D	10.1079
Total	76.9041

Table 8: CO₂ Storage resource: Storage objective Beta

CO ₂ Storage resource (Mt)	Beta				Total (Mt)
	A	B	C	D	
P10 (CO ₂ Efficiency factor = 7.4 %)	194.43	7.13	17.20	33.10	251.86
P50 (CO ₂ Efficiency factor = 14 %)	367.86	13.48	32.53	62.63	476.5
P90 (CO ₂ Efficiency factor = 24 %)	630.61	23.11	55.77	107.36	816.85

The assessed storage objectives, Alpha and Beta, are approximately 78.9 km² and 76.90 km². Within storage objective A, there are the two potential storage area mapped. Within storage objective B, four potential storage objectives were mapped. The estimated total P50 CO₂ storage resource for storage objective Alpha is 171 Mt, while that of storage objective Beta is 476 Mt. The combined CO₂ storage resource is approximately 647 Mt. Sandstone units within storage objective Alpha and Beta are relatively continuous and laterally extensive within the strata and structural geometries. However, signatures within gamma ray signatures suggest a possibility for vertical stacking of similar sandstone bearing formations.

Storage objective Alpha has a synclinal geometry bounded by a fault on its eastern boundary. However, potential storage areas within the objective rely on the free upward migration of fluids and the sealing potential of bounding faults. Very high amplitude within a part of storage objective Alpha, show promise for potential CO₂ enhance recovery. Reservoirs in storage objective Alpha are characterized by channel sands and sheet sands that have an average porosity of 28.5%. By utilizing the NETL CO₂ storage assessment approach, efficiency factors of 7.40%, 14.00% and

24.00%, were implemented in calculations. Thus for P10, P50 and P90, the estimated storage capacities are 90 Mt, 171 Mt and 293 Mt respectively.

Storage objective Beta has a turtle anticlinal geometry bounded by faults on its boundaries and within the anticlinal crests. However, potential storage areas within the objective focus on the reliability of the in-place sealing zones within faults that bound areas characterized by high RMS amplitudes (hydrocarbon indicators). These high amplitude areas show promise for potential CO₂ enhanced oil recovery as well. The depositional character within storage objective Beta is characterized by turbidite channel sheet sands that have an average porosity of 30%. By utilizing the NETL CO₂ storage assessment approach, efficiency factors of 7.40 %, 14.00 % and 24.00 %, were implemented in calculations. Thus for P10, P50 and P90, the estimated storage capacities are 252 Mt, 476 Mt and 817 Mt respectively. Limitations to this potentially secure storage objectives include but are not limited to leaking windows in faults, fractures, and even cracks in wellbores. However, the presence of shale regional beds, and adjacent salt bodies, help to minimize the risk of potential leakage of CO₂ from storage complexes.

CHAPTER V

CONCLUSION

The geology of the study area within the Mississippi Canyon protraction area comprises a thick Cenozoic sedimentary fill (>15,000 m; 50,000 ft) containing varied allochthonous salt systems, extensional and contractional faults, and fold belts (Rowan et al., 1999). Structural features that form a complex structural setting in the study area include basement faults, allochthonous salt systems, anticlines, shallow faults, growth fault families, and decollements that separate structural and depositional objectives and Salt welds. Welds form where nearly complete evacuation of salt has occurred. (Rowan et al., 1999). Major fault distribution, including crestal faults were mapped within study area A and study area B. Thus, caution is needed when delineating potential CO₂ storage objectives and sinks, because some faults could be a risk for storage targets, and subsequent CO₂ plume migration pathways.

Subsurface geologic storage of carbon dioxide CO₂ has potential to help alleviate the adverse effects of greenhouse gas emissions on the environment (Baines and Worden, 2004). This project identifies potential storage objectives within the Mississippi Canyon protraction area for carbon sequestration/enhanced oil recovery. With the study area having large amounts of oil remaining in place, the potential for EOR, and existing pipeline infrastructure in place, it is an ideal geological province to which CO₂ can be transported for CO₂-enhanced oil recovery (EOR) or carbon sequestration projects. The study area is characterized by strata highly impacted by salt-

related structural geometry. Results show that the Mississippi Canyon area is characterized by laterally continuous sandstone reservoirs that are overlain by thick and regionally correlated sections of tight mudrock that form effective seals. In addition, salt seals along salt flanks, and at the base of salt bodies, are very common in this area, and oil reservoirs include major subsalt accumulations in the Pliocene-Pleistocene sections.

Fields identified within the study area contain multiple saline, and hydrocarbon-filled sandstone formations that are thought to be under normal pressure. All observed reservoir units are below 12,000 ft and are thicker than 30 ft, thus meeting the criteria for carbon sequestration and CO₂-EOR projects. The reservoirs range in age from late Miocene to early Pliocene, and are characterized by minibasins with channel fill and sheet sands deposited in a wedge, sheet or bowl geometry. The recognized trapping mechanisms observed in seismic surveys range from subsalt traps against the base of salt, traps associated with salt flanks or welds, fault bounded traps, to stratigraphic traps. Favorably, seals are present above and below all reservoirs observed. Primary seals include salts, faults, and salt seals. However, most secondary seals are regional shales present within the Mississippi Canyon protraction area.

The volumetric assessment of two promising potential storage objectives reveals that the P50 storage resource for CO₂ is about 646 Mt. Fundamental parameters for considering promising injection sites include storage resource, reservoir homogeneity character, major trapping mechanisms, and reservoir depths. The structure maps in combination with the RMS amplitude maps delineate major structural geometry characterized by promising hydrocarbon accumulations and sand-bearing formations. All potential storage areas within storage objectives Alpha and Beta are bounded optimally by faults and adjacent salt bodies for carbon sequestration related projects. Trapping mechanisms observed in seismic range from subsalt trap against salt base, salt flanks or weld, to fault bounded traps, to stratigraphic traps. Favorably, seals are present above and below

all reservoirs observed. Primary seals include salts, faults, and salt seals. However, most secondary seals are regional shales present within the Mississippi Canyon protraction area.

REFERENCES

- Alberty, M. W., M. E. Hafle, and J. C. Minge, 1997, Mechanisms of Shallow Waterflows and Drilling Practices for Intervention: Offshore Technology Conference, 7 p.
- Alexander, L. L., and J. W. Handschy, 1998, Fluid flow in a faulted reservoir system: Fault trap analysis for the Block 330 field in Eugene Island, South Addition, offshore Louisiana: AAPG Bulletin, v. 82, p. 387–411.
- Asquith, G. B., D. Krygowski, and C. R. Gibson, 2004, Basic Well Log Analysis: Tulsa, AAPG, 216 p.
- Azevedo, L., and G.R. Pereira, 2009, Seismic Attributes in Hydrocarbon Reservoir Characterization, Universidade de Aveiro, Departamento de Geociências, 165 p.
- Bachu, S., 2001, Geologic sequestration of anthropogenic carbon dioxide; applicability and current issues, in L.C. Gerhard, W.E. Harrison, and B.M. Hanson, eds., Geological perspectives of global climate change: AAPG Studies in Geology 47, p. 285-303.
- Bachu, S., 2003, Screening and ranking of sedimentary basins for sequestration of CO₂ in geological media in response to climate change: Environmental Geology, v. 44, p. 277-289.
- Baines, S.J., and R. H. Worden, 2004, Geological storage of carbon dioxide: London, Geological Society Special Publication 233, 255 p.
- Beard, J. H., J. B. Sangree, and L. A. Smith, 1982, Quaternary chronology, paleoclimate, depositional sequences, and eustatic cycles: AAPG Bulletin, v. 66, p. 158-169.
- Behrens, E. W., 1985, Unifite muds in intraslope basins, northwest Gulf of Mexico: Geo-Marine Letters, v. 4, p. 227-233.

- Bouma, A. H., 1981, Depositional sequences in clastic continental slope deposits, Gulf of Mexico: *Geo-Marine Letters*, v. 1, p. 115-121.
- Bouvier, J. D., C. H. Kaarslijpestein, D. F. Kluesner, C. C. Onyejekwe, and R. C. Vanderpal, 1989, 3-dimensional seismic interpretation and fault sealing investigations, Nun River Field, Nigeria: *AAPG Bulletin*, v. 73, p. 1397–1414.
- Brown, A. R., 2011, Interpretation of Three-Dimensional Seismic Data: The American Association of Petroleum Geologists and the Society of Exploration Geophysicists, AAPG Memoir 42, SEG Investigations in Geophysics v. 9, 665 p.
- Buffler, R. T., and D. S. Sawyer, 1985, Distribution of crust and early history, Gulf of Mexico basin: *Gulf Coast Association of Geological Societies Transactions*, v. 35, p. 333-344.
- Buffler, R. T., 1989, Distribution of crust, distribution of salt, and the early evolution of the Gulf of Mexico basin: SEPM Gulf Coast Section Tenth Annual Research Foundation Conference, p. 25-27.
- Buffler, R. T., 1991, Seismic stratigraphy of the deep Gulf of Mexico basin and adjacent margins: *The Gulf of Mexico Basin: Geological Society of America, Decade of North American Geology*, p. 353-387.
- Bureau of Ocean Energy Management (BOEM), 2014, Deep water Gulf of Mexico, Outer Continental Shelf Report: BOEM 2016-057, U.S. Department of the Interior 88 p.
- Burman, S. S., and S. J. Norton, 1998, Mensa project: well drilling and completion: *Proceedings of the Offshore Technology Conference*, paper 8578, 12 p.
- Byrd, T. M., J. M. Schneider, D. J. Reynolds, M. W. Alberty, and M. E. Hafle, 1996, Identification of flowing water sand drilling hazards in the deep water Gulf of Mexico: *Proceedings of the Offshore Technology Conference*, paper 7971, p. 137-142.
- Chopra, S., and K. J. Marfurt, 2007, Seismic attributes for prospect identification and reservoir characterization: *Tulsa, Oklahoma Society of Exploration Geophysicists*, 11, 481 p.
- Chopra, S., and K. J. Marfurt, 2008, Emerging and future trends in seismic attributes: *The Leading Edge*, v. 27, no. 3, p. 298–318, doi:10.1190/1.2896620.
- Coleman, J. M., D. B. Prior, and J. F. Lindsay, 1983, Deltaic influences on shelf edge stability processes: *SEPM Special Publication* 33, p. 121-137.
- Davies, R. K., L. J. An, P. Jones, A. Mathis, and C. Cornette, 2003, Fault-seal analysis South Marsh Island 36 field, Gulf of Mexico: *AAPG Bulletin*, v. 87, p. 479–491.

- Deangelo, M. V., and L. J. Wood, 2001, 3-D seismic detection of undrilled prospective areas in a mature province, South Marsh Island, Gulf of Mexico: *The Leading Edge*, v. 20, no. 11, p. 1282–1292, doi:10.1190/1.1487261.
- Diegel, F. A., Karlo, J. F., D. C., Schuster, R. C. Shoup, and P. R. Tauvers, 1995, Cenozoic structural evolution and tectonostratigraphic framework of the northern Gulf Coast continental margin: AAPG Memoir 65, p. 109–151.
- Dixon, B. T., and P. Weimer, 1994, Regional sequence stratigraphic setting of the Mississippi Fan complex, northern deep Gulf of Mexico: implications for evolution of the northern Gulf basin margin, *Gulf of Mexico Salt Tectonics, Associated Processes and Exploration Potential: GCSSEPM Foundation Fifteenth Annual Research Conference Programs and Abstracts*, p. 373-381.
- Dixon, B. T. and P. Weimer, 1998, Sequence Stratigraphy and Depositional History of the Eastern Mississippi Fan (Pleistocene), Northeastern Deep Gulf of Mexico: AAPG Bulletin, v. 82, p. 1207-1232.
- Fletcher, R. C., M. R. Hudec, and I. A. Watson, 1995, Salt glacier and composite sediment-salt glacier models for the emplacement and early burial of allochthonous salt sheets, in M. P. A. Jackson, D. G. Roberts, and S. Snellson, eds., *Salt tectonics: a global perspective*: AAPG Memoir 65, p. 77-108.
- Galloway, W. E., 1989, Genetic stratigraphic sequences in the basin analysis I: Architecture and genesis of flooding-surface bounded depositional units: AAPG Bulletin, v. 73, p. 125-142.
- Galloway, W. E., P. E. Ganey-Curry, X. Li, and R. T. Buffler, 2000, Cenozoic depositional history of the Gulf of Mexico basin: AAPG Bulletin, 84, 1743–1774.
- Galloway, W.E., 2008, Depositional evolution of the Gulf of Mexico sedimentary basin, in K.J. Hsu, ed., *Sedimentary Basins of the World*, v. 5, *The Sedimentary Basins of the United States and Canada*, Miall, A.D., ed.: The Netherlands, Elsevier, p. 505-549.
- Gentzis, T., 2000, Subsurface sequestration of carbon dioxide — an overview from an Alberta (Canada) perspective: *International Journal of Coal Geology*, v. 43, p. 287-305.
- Gibson, R. G., 1994, Fault-zone seals in siliciclastic strata of the Columbus Basin, offshore Trinidad: AAPG Bulletin, v. 78, p. 1372–1385.
- Goodman, A., Hakala, A., Bromhal, G., Deel, D., Rodosta, T., Frailey, S., Small, M., Allen, D., Romanov, V., and Fazio, J., 2011, US DOE methodology for the development of geologic storage potential for carbon dioxide at the national and regional scale: *International Journal of Greenhouse Gas Control*, v. 5, p. 952-965.

Hudec, M. R., R. A. Fletcher, and I. A. Watson, 1995, The composite salt glacier: extension of the salt glacier model to post-burial conditions: AAPG Annual Convention Official program, p. 45a.

Jenyon, M. K., 1986, Salt tectonics: London, Elsevier, 191 p.

Kim, Y. J., S. Cheong, J. H. Chun, D. Cukur, S. P. Kim, J. K. Kim, and B. Y. Kim, 2020, Identification of shallow gas by seismic data and AVO processing: Example from the southwestern continental shelf of the Ulleung Basin, East Sea, Korea: Marine and Petroleum Geology, v. 117, p. 104346, doi:10.1016/j.marpetgeo.2020.104346.

Lehner, P., 1969, Salt tectonics and Pleistocene stratigraphy on continental slope of northern Gulf of Mexico: AAPG Bulletin, v. 53, p. 2431-2479.

Lopez, J. A., 1989, Distribution of structural styles in the northern Gulf of Mexico and Gulf Coast, Gulf of Mexico Salt Tectonics, Associated Processes and Exploration Potential: GCSSEPM Foundation Tenth Annual Research Conference Programs and Abstracts, p. 101-108.

MacRae, G., and J. S. Watkins, 1993, Basin architecture, salt tectonics, and Upper Jurassic structural styles, DeSoto Canyon salt basin, northeastern Gulf of Mexico: AAPG Bulletin, v. 77, p. 1809-1824.

Martin, R. G., 1978, northern and eastern Gulf of Mexico continental margin: stratigraphic and structural framework, *in* A. H. Bouma, G. T. Moore, and J. M. Coleman eds., Framework, facies and oil-trapping characteristics of the upper continental margin: AAPG Studies in Geology, v. 7, p. 21-48.

McGuinness, D. B., and J. R. Hossack, 1993, The development of allochthonous salt sheets as controlled by rates of extension, sedimentation, and salt supply: GCSSEPM Foundation 14th Annual Research Conference-Rates of Geological Processes, p. 127-139.

McKee, B., 2003, CO₂ capture and storage in geological formations: International Energy Agency (IEA), 14 p.

Nelson, T. H., 1991, Salt tectonics and listric-normal faulting, *in* A. Salvador ed., The geology of North America; the Gulf of Mexico basin: GSA Decade of North American Geology, v. J, p. 73-89.

Nelson, T. H., and L. Fairchild, 1989, Emplacement and evolution of salt sills in the northern Gulf of Mexico: Houston Geological Society Bulletin, v. 31, p. 6-7.

NETL, 2012, The United States 2012 Carbon Utilization and Storage Atlas, 4th Edition, 130 p.

- Pashin, J. C., Guohai Jin, and Hills, D. J., 2016, Mesozoic petroleum systems and structure in the Mobile, Pensacola, Destin Dome, and Viosca Knoll Areas of the MAFLA Shelf, in Lowery, C., Snedden, J. W., and Blum, M. D., eds., Mesozoic of the Gulf Rim and Beyond: New Progress in Science and Exploration of the Gulf of Mexico Basin: GCSSEPM Perkins-Rosen Special Publication, p. 416-449.
- Peel, F.J., C.J. Travis, and J.R. Hossack, 1995, Genetic structural provinces and salt tectonics of the Cenozoic offshore U.S. Gulf of Mexico: a preliminary analysis, in M. P. A. Jackson, D.G. Roberts, and S. Snell, eds., Salt Tectonics: A Global Perspective: AAPG Memoir 65, p. 153-175.
- Pindell, J. L., 1985, Alleghenian reconstruction and subsequent evolution of the Gulf of Mexico, Bahamas, and Proto-Caribbean: Tectonics, v. 4, p. 1-39.
- Razi, M., and P. W. Bilinski, 2012, Mensa Field, Deep water Gulf of Mexico (GOM) – Case Study: SPE Annual Technical Conference and Exhibition, SPE-159741-MS, 11 p.
- Redini, N. A., A. M. Bakr, and S. M. Dahroug, 2017, Seismic data interpretation for hydrocarbon potential, for Safwa/Sabbar field, East Ghazalat onshore area, Abu Gharadig basin, Western Desert, Egypt: NRIAG Journal of Astronomy and Geophysics, v. 6, no. 2, p. 287–299, doi:10.1016/j.nrjag.2017.01.003.
- Roberts, H. H., and J. M. Coleman, 1988, Sedimentary development of the Louisiana continental shelf related to sea level cycles, part 2: seismic response: Geo-Marine Letters, v. 8, p. 109-119.
- Rowan, M. G., M. P. Jackson, and B. D. Trudgill, 1999, Salt-related fault families and fault welds in the northern Gulf of Mexico. AAPG Bulletin, v. 83, p. 1454-1484.
- Salvador, A., 1987, Late Triassic-Jurassic paleogeography and origin of Gulf of Mexico basin: AAPG Bulletin, v. 71, p. 419-451
- Salvador, A., 1991, Origin and development of the Gulf of Mexico, in A. Salvador ed., The Geology of North America, v. J, p. 389-444.
- Sandwell, D. T., R. D. Müller, W. H. F. Smith, E. Garcia, and R. Francis, 2014, New global marine gravity model from CryoSat-2 and Jason-1 reveals buried tectonic structure: Science, v. 346, no. 6205, p. 65–67, doi:10.1126/science.1258213.
- Sangree, J. B., P. R. Vail, and R. M. Sneider, 1988, Evolution of facies interpretation of the shelf-slope: application of the new eustatic framework to the Gulf of Mexico: Proceedings of the 1988 Offshore Technology Conference, v. 2, p. 133-144.

- Satyavani, N., K. Sain, M. Lall, and B. J. P. Kumar, 2008, Seismic attribute study for gas hydrates in the Andaman Offshore India: Marine Geophysical Researches, v. 29, no. 3, p. 167–175, doi:10.1007/s11001-008-9053-x.
- Schuster, D. C., 1995, Deformation of allochthonous salt and evolution of related salt structural systems, eastern Louisiana Gulf Coast, *in* M. P. A. Jackson, D. G. Roberts, and S. Snellson eds., Salt tectonics: a global perspective: AAPG Memoir 65.
- Seni, S. J., 1994, Salt Tectonics on the Continental Slope, Northeast Green Canyon Area, Northern Gulf of Mexico: Evolution of Stocks and Massifs from Reactivation of Salt Sheets: The University of Texas at Austin, Bureau of Economic Geology, Report of Investigations v. 212, 102 p.
- Spindler, W. M., 1977, Structure and stratigraphy of a small Plio-Pleistocene depocenter, Louisiana continental shelf: Gulf Coast Association of Geological Societies Transactions, v. 27, p. 180-196.
- Stuart, C. J., and C. A. Caughey, 1977, Seismic facies and sedimentology of terrigenous Pliocene-Pleistocene depocenters, outer continental shelf, Louisiana and Texas: AAPG Memoir 26, p. 249-275.
- Swiercz, A. M., 1992, Seismic stratigraphy and salt tectonics along the Sigsbee Escarpment, southeastern Green Canyon region, *in* R. A. Geyer ed., CRC Handbook of Geophysical Exploration at Sea: 2nd ed., p. 227-294.
- Talbot, C. J., 1994, Spreading of salt structures in the Gulf of Mexico: Tectonophysics, v. 228, p. 151-166.
- Vav Bemmel, P., and R. E. F. Pepper, 2000, Seismic signal processing method and apparatus for generating a cube of Variance values, U.S. Patent Number 6, 151, 555.
- Vidas, H., B. Hugman, A. Chikkatur, and B. Venkatesh, 2012, Analysis of the Costs and Benefits of CO₂ Sequestration on the U.S. Outer Continental Shelf, Bureau of Ocean Energy Management (BOEM) Herndon, Virginia: OCS Study BOEM 2012-100, U.S. Department of the Interior, 129 p.
- Waterman, A. S., 2000, Gulf of Mexico chronostratigraphic correlation chart: PaleoData, Inc. (<http://www.paleodata.com>).
- Weber, K. J., G. Mandl, W. F. Pilaar, F. Lehner, and R. G. Precious, 1978, The role of faults in hydrocarbon migration and trapping in Nigerian growth fault structures: Annual Offshore Technology Conference Proceedings, p. 2643–2653.

- Weimer, P., 1989, Sequence stratigraphy of the Mississippi Fan (Plio-Pleistocene), Gulf of Mexico: *Geo-Marine Letters*, v. 9, p. 185-272.
- Weimer, P., and T. L. Davis, 1996, Applications of 3-D seismic data to exploration and production: *AAPG Studies in Geology*, v. 42, 270 p.
- Weimer, P., and R. Bouroullec, 2012, Petroleum Geology of the Mississippi Canyon, Atwater Valley, Western Desoto Canyon, and Western Lloyd Areas, Northern Deep Gulf of Mexico: Traps, Reservoirs, and Their Timing: New Understanding of the Petroleum Systems of Continental Margins of the World: 32nd Annual, p. 110–132.
- Woodbury, H. O., J. H. Spotts, and W. H. Akers, 1978, Gulf of Mexico Continental slope sediments and sedimentation, in A. H. Bouma, G. T. Moore, and J. M. Coleman eds., Framework, facies and oil-trapping characteristics of the upper continental margin: *AAPG Studies in Geology*, v. 7, p. 117-137.
- Worall, D. M., and S. Snelson, 1989, Evolution of the northern Gulf of Mexico, with emphasis on Cenozoic growth faulting and the role of salt, in A. W. Bally and A. R. Palmer eds., *The geology of north America-an overview: The Geology of North America*: Boulder, CO, v. A, p. 97-138.
- Wu, S., A. W. Bally, and C. Cramez, 1990a, Allochthonous salt, structure, and stratigraphy of the northeastern Gulf of Mexico; part I, stratigraphy: *Marine and Petroleum Geology*, v. 7, p. 318-333.
- Wu, S., A. W. Bally, and C. Cramez, 1990b, Allochthonous salt, structure, and stratigraphy of the northeastern Gulf of Mexico; part II, structure: *Marine and Petroleum Geology*, v. 7, p. 334-370.
- Yorston, H. J., and J. F. Fox, 1985, Practical application of subsurface and seismic methods to prospecting in salt provinces with emphasis on the Gulf Coast Tertiary: an exploration workshop: *Houston Geological Society Continuing Education Series*, 33 p.
- Zhang, Q., L. Geiger, C. Reta-Tang, S. Hightower, S. Yang, and W. Gao, 2013, New views on salt tectonics and salt modeling using the latest seismic imaging technologies, for subsalt and presalt exploration in the Mississippi Canyon, Gulf of Mexico: *Gulf Coast Association of Geological Societies Transactions*, v. 63, p. 637–639.

VITA

Seyi Dupe Sholanke

Candidate for the Degree of

Master of Science

Thesis: STRUCTURAL FRAMEWORK ANALYSIS IN THE MISSISSIPPI CANYON PROTRACTION AREA, CENTRAL CULF OF MEXICO: IMPLICATIONS FOR AND CO₂ SEQUESTRATION

Major Field: Geology

Biographical:

Education:

Completed the requirements for the Master of Science in Geology at Oklahoma State University, Stillwater, Oklahoma in July, 2020.

Completed the requirements for the Bachelor of Science in Geology at Texas A&M University, College Station, Texas in 2017.

Experience:

Virtual Geoscience Intern, EVOLVE by SEG (Jan – May 2020).

Team Participant, AAPG IBA Program, Mid-Continent Section (Jan – Mar 2019).

Student Worker, Berg-Hughes Center at Texas A&M University (Jul – Aug 2016).

Geology & Asset Management Intern, Addax Petroleum Nigeria (Jul – Aug 2015).

Geology Intern, ExxonMobil Nigeria (Jun – Aug 2014).

Professional Memberships:

Association for Women Geoscientists (AWG), American Association of Petroleum Geologists (AAPG), Geological Society of American (GSA), and Society of Exploration Geophysicist (SEG).